



รายงานวิจัยฉบับสมบูรณ์

โครงการการสร้างทรงกลมของไหลไม่สม่ำเสมอแบบมีประจุ
สำหรับพิกัดแบบต่าง ๆ ในทฤษฎีสัมพัทธภาพทั่วไป

โดย ผศ.ดร. เพชรอาภา บุญเสริม

เดือน ปี ที่เสร็จโครงการ

2 มิถุนายน 2561

สัญญาเลขที่ RSA5980038

รายงานวิจัยฉบับสมบูรณ์

โครงการการสร้างทรงกลมของไหลไม่สม่ำเสมอแบบมีประจุ
สำหรับพิกัดแบบต่าง ๆ ในทฤษฎีสัมพัทธภาพทั่วไป

ผู้วิจัย ผศ.ดร. เพชรอาภา บุญเสริม
สังกัดภาควิชาคณิตศาสตร์และวิทยาการคอมพิวเตอร์
คณะวิทยาศาสตร์ จุฬาลงกรณ์มหาวิทยาลัย

สนับสนุนโดยสำนักงานกองทุนสนับสนุนการวิจัย

(ความเห็นในรายงานนี้เป็นของผู้วิจัย
สกว.ไม่จำเป็นต้องเห็นด้วยเสมอไป)

รูปแบบ Abstract (บทคัดย่อ)

Project Code : RSA5980038

(รหัสโครงการ)

Project Title : การสร้างทรงกลมของไหลไม่สม่ำเสมอแบบมีประจุสำหรับพิกัดแบบต่าง ๆ ในทฤษฎีสัมพัทธภาพทั่วไป

(ชื่อโครงการ)

Investigator : ผศ.ดร. เพชรอาภา บุญเสริม จุฬาลงกรณ์มหาวิทยาลัย

(ชื่อนักวิจัย)

E-mail Address : Petarpa.Boonserm@gmail.com

Project Period : 2 ปี

(ระยะเวลาโครงการ)

บทคัดย่อ

Anisotropic fluid spheres are the solutions to the Einstein field equation. The difference between anisotropic fluid and perfect fluid is that the radial pressure in the anisotropic fluid is not equal to the transverse pressure, while the pressures are the same in every direction for the perfect fluid. One way in which anisotropic fluids are generated is through the presence of charge. In this project, we will obtain a new class of charged anisotropic fluid solutions by developing solution generating theorems for the charged anisotropic fluid spheres, using pressure and density as parameters. We will express these theorems in the form of general diagonal coordinates, Gaussian polar coordinates, Synge isothermal coordinates, Buchdahl coordinates, generalized Buchdahl coordinates, and isotropic coordinates. Charged anisotropic fluid solutions will be classified into seed and non-seed solutions. The regularity conditions at the center of the fluid spheres will be investigated. The solutions will be expressed in terms of

pressure, while the central red shift and the surface red shift will also be calculated. Additionally, the compactness of stars will also be studied.

Keywords : anisotropic fluid, charge, pressure and density, seed and non-seed,

(คำหลัก) solution generating theorem

วัตถุประสงค์

1) To develop solution generating theorems for charged anisotropic fluid spheres in general diagonal coordinates, Gaussian polar coordinates, Synge isothermal coordinates, Buchdahl coordinates, generalized Buchdahl coordinates, and isotropic coordinates, using pressure and density as parameters.

2) To classify charged anisotropic fluid solutions into seed and non-seed solutions.

3) To investigate the regularity conditions at the center of fluid spheres.

4) To calculate the central red shift, the surface red shift, and the compactness of stars.

5) To compare with observational data.

วิธีดำเนินงานวิจัย

1) Review related literatures.

In Bayin's work [5], he discussed how anisotropy in stars can exist. For a neutron star, the anisotropy occurs as a result of two perfect fluid spheres combining with each other to form a neutron star. Generally, a neutron is not stable because it can decay to an electron and a proton. Therefore, in a stable neutron star, one of the two perfect fluids is a fluid of neutrons, while the other is a fluid of electrons and protons. This anisotropy can increase the neutron star mass limit. Furthermore, the surface red-shift can also be explained by the anisotropy.

Lattimer and Prakash [18] studied the physics of neutron stars. In general, a neutron star is usually referred to as a star with a mass of order 1.5 times the solar mass (M_{\odot}), and a radius of approximately 12 km. Neutron stars are formed by the gravitational collapse of a dead star of initial mass greater than $8M_{\odot}$. The maximum mass limit of a neutron star lies between $1.44M_{\odot}$ and $3M_{\odot}$, while the minimum mass of a stable neutron star is $0.1M_{\odot}$. A neutron star consists of five sections; the inner core, the outer core, the crust, the envelope, and the atmosphere. Most neutron stars emit photons and are observed as pulsars.

Pant, Pradhan, and Singh [7] presented a class of charged anisotropic fluids in the form of isotropic coordinates. The presence of charge can be explained by the Einstein-Maxwell

equation rather than the usual Einstein field equation. They solved the Einstein-Maxwell equation by assuming a seed solution as a particular case of Haji-Boutros [19] and Murad-Pant [20]. They found that the radial pressure, the transverse pressure, and the density are maximum at the center, and monotonically decrease with the increase in the radial distance. Neutron stars and quark stars can be modeled by these solutions. They obtained the maximum mass of $M = 1.53M_{\odot}$ and radius of $R = 11.48$ km for a neutron star of the density $2.7 \times 10^{14} \text{ g/cm}^3$, and the maximum mass of $M = 1.16M_{\odot}$ and radius of $R = 8.71$ km for a strange quark star of density $4.6888 \times 10^{14} \text{ g/cm}^3$.

Boonserm, Visser, and Weinfurter [13] developed solution generating theorems for perfect fluid spheres. We worked with Schwarzschild (curvature) coordinates in the development. We found that these theorems sometimes generate new perfect fluid solutions, but sometimes provide the known perfect fluid solutions. We also classified perfect fluid solutions into seed and non-seed metrics.

We also developed solution generating theorems for the TOV equation [15]. We found the conditions under which a physically reasonable solution to the TOV equation can transform into a new solution with its physical reasonableness preserved. By physical reasonableness, we mean that the pressure and the density of a star are finite and positive at the center of the star.

Sulaksono [8] studied the properties of neutron stars with hyperons inside, which are influenced by the anisotropic pressure. He found that the anisotropic pressure increases the stiffness of the neutron star's equation of state. This effect can be balanced by the presence of hyperons, which softens the equation of state. The maximum mass limit of a neutron star is increased by the anisotropic pressure, while the minimum mass limit remains quite unchanged.

Maurya et al. [9] found the anisotropic fluid solutions to the Einstein field equation using the Herrera et al. algorithm [21]. The spacetime exterior to these anisotropic fluid spheres is the Schwarzschild spacetime. Most of these solutions satisfy reality and true physical conditions, and can be used as models for neutron stars and pulsars. One of the anisotropic fluid spheres has been determined to have a maximum mass of $1.7609M_{\odot}$ and a radius of 16.0780 km, while another solution renders the maximum mass as $0.8672M_{\odot}$ and the radius as 3.1274 km.

Lastowiecki et al. [22] studied quark matter in a neutron star and derived an equation of state for matter in beta equilibrium. They modeled a neutron star using the Nambu–Jona-Lasinio (NJL) effective model. They found that for neutron stars with mass in the range of $2M_{\odot}$, it is possible for deconfined quark matter to exist within the core of the neutron star.

Riazi et al. [23] derived the generalized Tolman-Oppenheimer-Volkoff (TOV) equation for anisotropic fluid. They solved the generalized TOV equation by assuming a bi-polytropic

equation of state, which consists of two terms, one being a linear term and the other being a power-law term. The exact solutions are regular at the origin and asymptotically flat. These solutions can either have no horizon, one horizon, or two horizons. In the case of two horizons, the solutions are similar to the non-extremal Reissner-Nordstrom black holes.

In this project, solution generating theorems for charged anisotropic fluid spheres in general relativity, in terms of their pressure and density profiles, will be established. We will work with general diagonal coordinates, Gaussian polar coordinates, Synge isothermal coordinates, Buchdahl coordinates, generalized Buchdahl coordinates, and isotropic coordinates. We will classify the charged anisotropic fluid solutions into seed and non-seed solutions. We will investigate the regularity conditions at the center of the fluid spheres. The central red shift and the surface red shift will also be calculated. Furthermore, the compactness of stars will be studied as well.

2) Write down the generalized TOV equation for charged anisotropic spheres.

The energy momentum tensor for perfect fluid spheres is

$$T_f^{\mu\nu} = (\rho_f + p_f) V^\mu V^\nu + p_f g^{\mu\nu}.$$

The energy momentum tensor for electromagnetic field is

$$T_{em}^{\mu\nu} = F^{\mu\alpha} g_{\alpha\beta} F^{\nu\beta} - \frac{1}{4} g^{\mu\nu} (F_{\alpha\beta} F^{\alpha\beta}).$$

The energy momentum tensor for massless scalar field is

$$T_s^{\mu\nu} = \phi^{;\mu} \phi^{;\nu} - \frac{1}{2} g^{\mu\nu} (g^{\alpha\beta} \phi_{;\alpha} \phi_{;\beta}).$$

Using the conservation of energy, $T^{\mu\nu}_{;\nu} = 0$, we obtain

$$\frac{dp_f}{dr} = - \frac{(\rho_f + p_f) [m(r) + 4\pi p_f r^3]}{r^2 [1 - 2m(r)/r]} - \frac{\sigma_{em} E}{\sqrt{1 - 2m(r)/r}} - \sigma_s \frac{d\phi}{dr}.$$

This is the generalized TOV equation.

3)-5) Deform a solution to the generalized TOV equation. Derive the conditions under which the new solution still satisfies the generalized TOV equation. Establish solution generating theorems and classify solutions into seed and non-seed solutions.

Theorem P3. Let $p_1(r)$, $p_2(r)$, and $m_1(r)$ solve the generalized TOV equation. Then, the deformed solutions $p(r) = p_0(r) + \delta p_0(r)$ and $m(r) = m_1(r) + \delta m_1(r)$ also solve the generalized TOV equation, where

$$\begin{aligned}
p_0(r) &= \frac{\lambda \mu_1(r) p_1(r) + (1-\lambda) \mu_2(r) p_2(r)}{\lambda \mu_1(r) + (1-\lambda) \mu_2(r)}, \\
\mu_1(r) &= \exp \left[- \int \frac{4\pi r^2}{r - 2m_1(r)} p_1(r) dr \right], \\
\mu_2(r) &= \exp \left[- \int \frac{4\pi r^2}{r - 2m_1(r)} p_2(r) dr \right], \\
\delta p_0(r) &= - \frac{\delta m_1(r)}{4\pi r^2} \frac{1 + 8\pi r^2 p_0(r)}{r - 2m_1(r)}, \\
\delta m_1(r) &= \frac{4\pi r^3 \delta \rho_c}{3[1 + r g_0(r)]^2} \exp \left[2 \int_0^r g_0(t) \frac{1 - t g_0(t)}{1 + t g_0(t)} dt \right],
\end{aligned}$$

and

$$g_0(r) = \frac{m_1(r) + 4\pi r^3 p_0(r)}{r[r - 2m_1(r)]}.$$

Theorem P4. Let $p_1(r)$, $p_2(r)$, $m_1(r)$, and $m_2(r)$ solve the generalized TOV equation. Then, the deformed solutions $p_0(r)$, $m_0(r) = m_1(r) + \delta m_1(r)$ and $m_2(r) = m_2(r) + \delta m_2(r)$ also solve the generalized TOV equation, where

$$\begin{aligned}
p_0(r) &= \frac{\lambda \mu_1(r) \theta_1(r) + (1-\lambda) \mu_2(r) \theta_2(r)}{\lambda \mu_1(r) + (1-\lambda) \mu_2(r)}, \\
\mu_1(r) &= \exp \left[- \int \frac{4\pi r^2}{r - 2m_1(r)} \theta_1(r) dr \right], \\
\mu_2(r) &= \exp \left[- \int \frac{4\pi r^2}{r - 2m_2(r)} \theta_2(r) dr \right], \\
\theta_1(r) &= p_1(r) + \delta p_1(r), \\
\theta_2(r) &= p_2(r) + \delta p_2(r), \\
\delta p_1(r) &= - \frac{\delta m_1(r)}{4\pi r^2} \frac{1 + 8\pi r^2 p_1(r)}{r - 2m_1(r)}, \\
\delta p_2(r) &= - \frac{\delta m_2(r)}{4\pi r^2} \frac{1 + 8\pi r^2 p_2(r)}{r - 2m_2(r)}, \\
\delta m_1(r) &= \frac{4\pi r^3 \delta \rho_c}{3[1 + r g_1(r)]^2} \exp \left[2 \int_0^r g_1(t) \frac{1 - t g_1(t)}{1 + t g_1(t)} dt \right],
\end{aligned}$$

$$\delta m_2(r) = \frac{4\pi r^3 \delta \rho_c}{3[1 + r g_2(r)]^2} \exp \left[2 \int_0^r g_2(t) \frac{1 - t g_2(t)}{1 + t g_2(t)} dt \right],$$

$$g_1(r) = \frac{m_1(r) + 4\pi r^3 p_1(r)}{r[r - 2m_1(r)]},$$

and

$$g_2(r) = \frac{m_2(r) + 4\pi r^3 p_2(r)}{r[r - 2m_2(r)]}.$$

ผลการทดลอง

In this section, we will show you the effect of charge on density [24]. We develop solution generating theorems for charged anisotropy both in terms of the generalized TOV equation [25, 26] and in terms of spacetime geometry [27]. We will also show the difference between the use of inappropriate coordinates and the use of appropriate coordinates in expressing velocity and acceleration of test particles near the Schwarzschild black hole [28]. Moreover, we will show that the exponential metric characterize a worm hole [29]. Finally, we will show how we can obtain the rigorous bounds on the greybody factors for black holes in dRGT massive gravity [30].

1. The effect of charge on density [24]

a) Special case: when p_f and ρ_{em} is constant and σ_s is zero

In this case, the generalized TOV equation becomes

$$0 = -\frac{[\rho_f(r) + p_f][m(r) + 4\pi r^3 p_f]}{r[r - 2m(r)]} - \frac{\sigma_{em} E \sqrt{r}}{\sqrt{r - 2m(r)}} \quad (1.1)$$

with

$$\frac{dm(r)}{dr} = 4\pi r^2 [\rho_f(r) + \rho_{em}]. \quad (1.2)$$

Solving equation (1.1), we obtain

$$\rho_f(r) = -\frac{\sigma_{em} E r \sqrt{r[r - 2m(r)]}}{m(r) + 4\pi r^3 p_f} - p_f. \quad (1.3)$$

Substitution in equation (1.2) gives

$$\frac{dm(r)}{dr} = 4\pi r^2 \left[-\frac{\sigma_{em} E r \sqrt{r[r - 2m(r)]}}{m(r) + 4\pi r^3 p_f} - p_f + \rho_{em} \right]. \quad (1.4)$$

By numerically solving equation (1.4) and substituting in equation (1.3), we get the fluid density as shown in Figure 1.

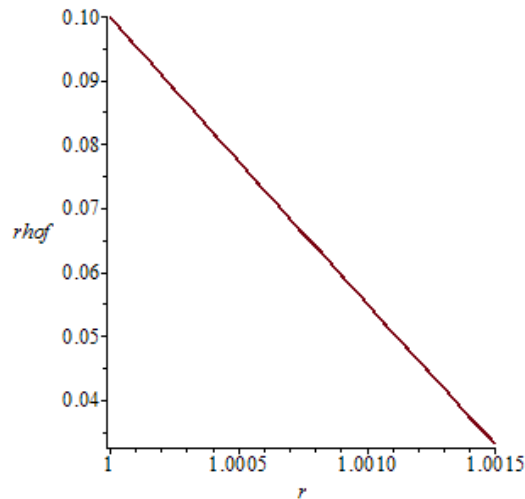


Figure 1. The fluid density as a function of radius with $\sigma_{em} = 1$, $E = 2$, $p_f = 3$, and $\rho_{em} = 4$.

Figure 1 shows that the fluid density decreases as the radius increases. That is, the fluid dilutes away from the center of a charged fluid sphere.

b) The effect between charge and density

From equation (1.3) and equation (1.4), the effect of charge on fluid density can be investigated. The results are shown in TABLE I.

Charge density (σ_{em})	Fluid density (ρ_f)
1	0.077
2	0.089
3	0.093
4	0.095
5	0.097

Table I. The effect of charge on fluid density with $E = 2$, $p_f = 3$, and $\rho_{em} = 4$.

2. Generating theorems for charged anisotropy in general relativity [25, 26]

A static and spherically symmetric spacetime can be written as

$$ds^2 = -\zeta_0^2(r)dt^2 + \frac{dr^2}{B_0(r)} + r^2 d\Omega^2.$$

The Einstein tensors in this spacetime are given by

$$G_{\tilde{r}\tilde{r}} = \frac{4B\zeta'r - 2\zeta + 2\zeta B}{2r^2\zeta} \text{ and } G_{\hat{\theta}\hat{\theta}} = \frac{B'\zeta r + 2B\zeta' + 2r^2\zeta''B + r^2\zeta'B'}{2r^2\zeta}.$$

The condition for being charged fluid sphere is

$$G_{\tilde{r}\tilde{r}} - G_{\hat{\theta}\hat{\theta}} = 8\pi\Delta,$$

where Δ is the difference between the radial pressure and the transverse pressure. This condition leads to a first order linear non-homogeneous differential equation

$$(r^2\zeta' + r\zeta)B' + (2r^2\zeta'' - 2r\zeta' - 2\zeta)B + (2 + 16\pi\Delta r^2)\zeta = 0.$$

Theorem 1. Suppose $\{\zeta_0(r), B_0(r)\}$ represents a charged fluid sphere. Define

$$\Delta_0 = \left(\frac{\zeta_0(r)}{\zeta_0(r) + r\zeta_0'(r)} \right)^2 r^2 \exp \left[2 \int \frac{\zeta_0'(r) \zeta_0(r) - r\zeta_0'(r)}{\zeta_0(r) \zeta_0(r) + r\zeta_0'(r)} dr \right].$$

Then for all λ , the geometry defined by holding $\zeta_0(r)$ fixed and setting

$$ds^2 = -\zeta_0^2(r)dt^2 + \frac{dr^2}{B_0(r) + \lambda\Delta_0(r)} + r^2 d\Omega^2$$

is also a charged fluid sphere. That is, the mapping of

$$T_1(\lambda) : \{\zeta_0, B_0\} \mapsto \{\zeta_0, B_0 + \lambda\Delta_0(\zeta_0)\}$$

takes charged fluid spheres into charged fluid spheres.

Corollary 1. Let $\{\zeta_0, B_a\}$ and $\{\zeta_0, B_b\}$ both represent charged fluid spheres, then for all p

$$\{\zeta_0, pB_a + (1-p)B_b\}.$$

is also a charged fluid sphere.

Theorem 2. Suppose $\{\zeta_0(r), B_0(r)\}$ represents a charged fluid sphere. Define

$$Z_0(r) = \sigma + \varepsilon \int \frac{rdr}{\zeta_0^2(r)\sqrt{B_0(r)}}.$$

Then for all σ and ε , the geometry defined by holding $B_0(r)$ fixed and setting

$$ds^2 = -\zeta_0^2(r)Z_0^2(r)dt^2 + \frac{dr^2}{B_0(r)} + r^2 d\Omega^2$$

is also a charged fluid sphere. That is, the mapping of

$$T_2(\sigma, \mathcal{E}) : \{\zeta_0, B_0\} \text{ a } \{\zeta_0 z_0(\zeta_0, B_0), B_0\}$$

takes charged fluid spheres into charged fluid spheres.

Corollary 2. Let $\{\zeta_a, B_0\}$ and $\{\zeta_b, B_0\}$ both represent charged fluid spheres, then for all p and q

$$\{p\zeta_a + q\zeta_b, B_0\}.$$

is also a charged fluid sphere.

We can classify charged fluid spheres into seed and non- seed metrics based on the following definitions.

Definition (seed metric): Take a metric g and apply theorem 1 or theorem 2 to it. If each of the applications supplies us with a new solution, the metric is defined as a seed metric.

Definition (non-seed metric): Take a metric g and apply theorem 1 or theorem 2 to it. If only one of the applications supplies us with a new solution, while the other one gives us the same metric we started with, the metric is defined as a non-seed metric.

3. Generating perfect fluid sphere in isotropic coordinate [27]

The metric of a static, spherically symmetric, perfect fluid sphere in isotropic coordinates takes the form

$$ds^2 = -\zeta^2(r)dt^2 + \frac{1}{\zeta^2(r) + B^2(r)}(dr^2 + r^2 d\Omega^2). \quad (3.1)$$

The condition for a perfect fluid takes the form

$$\left[\frac{\zeta'(r)}{\zeta(r)} \right]^2 = \frac{B''(r) - B'(r)/r}{2B(r)}. \quad (3.2)$$

We can rewrite the above equation in the Riccati form as

$$h'(r) = g^2(r) + \frac{1}{r}h(r) - 2h^2(r), \quad (3.3)$$

where

$$g(r) = \frac{\zeta'(r)}{\zeta(r)} \text{ and } h(r) = \frac{B'(r)}{2B(r)}. \quad (3.4)$$

One property of the Riccati equation is that if we know a particular solution, a general solution can be derived. Let $\{g_0(r), h_0(r)\}$ satisfy equation (3.3). Then

$$h_0'(r) = g_0^2(r) + \frac{1}{r}h_0(r) - 2h_0^2(r). \quad (3.5)$$

We assume that the general solution takes the form

$$h(r) = h_0(r) + \frac{1}{z(r)} \text{ and } g(r) = g_0(r) + \dot{g}(r). \quad (3.6)$$

In order for $h(r)$ to satisfy equation (3.3), $z(r)$ must satisfy

$$z'(r) + \left[\frac{1}{r} - 4h_0(r) \right] z(r) = 2. \quad (3.7)$$

Similarly, in order for $g(r)$ to satisfy equation (3.3), it must satisfy

$$g(r) = -g_0(r). \quad (3.8)$$

That is, if we have $\{g_0(r), h_0(r)\}$ representing a perfect fluid sphere, then

$$\left\{ -g_0(r), h_0(r) + \frac{1}{z(r)} \right\} \quad (3.9)$$

also represents a perfect fluid sphere.

4. Near horizon of the Schwarzschild black hole. [28]

When the anisotropic sphere collapses, a black hole may be formed. The simplest black hole in general relativity is a Schwarzschild black hole which can be expressed as

$$ds^2 = -\left(1 - \frac{2m}{r}\right) dt^2 + \left(1 - \frac{2m}{r}\right)^{-1} dr^2 + r^2 (d\theta^2 + \sin^2 \theta d\phi^2).$$

Consider the motion of a non-zero rest mass particle starting at rest from spatial infinity and then falling into the Schwarzschild black hole. In the Schwarzschild curvature coordinates, which are inappropriate ones, the radial coordinate velocity and the radial coordinate acceleration are given by

$$\dot{r} = -\left(1 - \frac{2m}{r}\right) \sqrt{\frac{2m}{r}} \text{ and } \ddot{r} = -\frac{m}{r^2} \left(1 - \frac{2m}{r}\right) \left(1 - \frac{6m}{r}\right).$$

The radial coordinate velocity and the radial coordinate acceleration for the non-zero rest mass particle are plotted as shown in Figures 2 and 3.

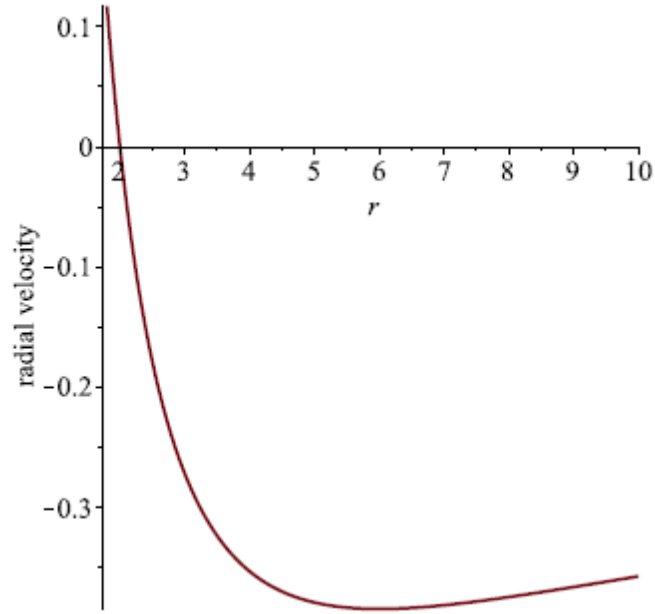


Figure 2. The radial coordinate velocity of a non-zero rest mass particle in the Schwarzschild geometry for $m = 1$. In this case, the horizon is located at $r = 2$.

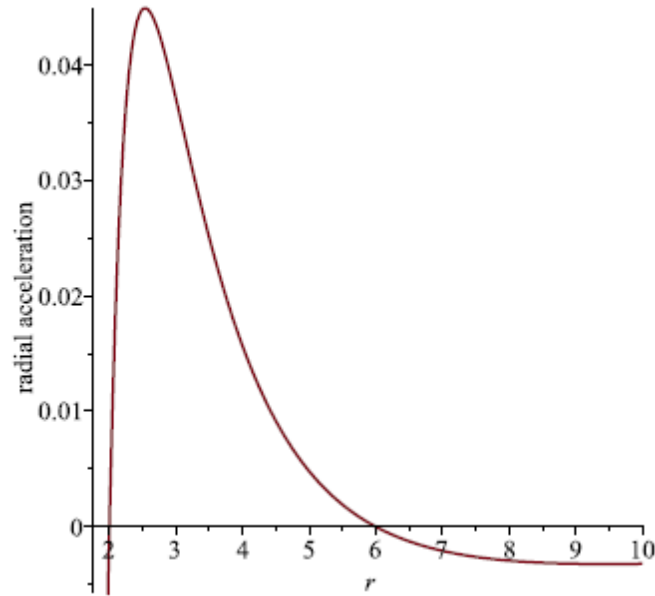


Figure 3. The radial coordinate acceleration of a non-zero rest mass particle in the Schwarzschild geometry for $m = 1$. Again, in this case, the horizon is located at $r = 2$.

For a massless particle such as photon, the radial coordinate velocity and the radial coordinate acceleration in the Schwarzschild curvature coordinates are given by

$$\dot{r} = -\left(1 - \frac{2m}{r}\right) \text{ and } \ddot{r} = 2\frac{m}{r^2}\left(1 - \frac{2m}{r}\right).$$

The radial coordinate velocity and the radial coordinate acceleration for the massless particle are plotted as shown in Figures 4 and 5.

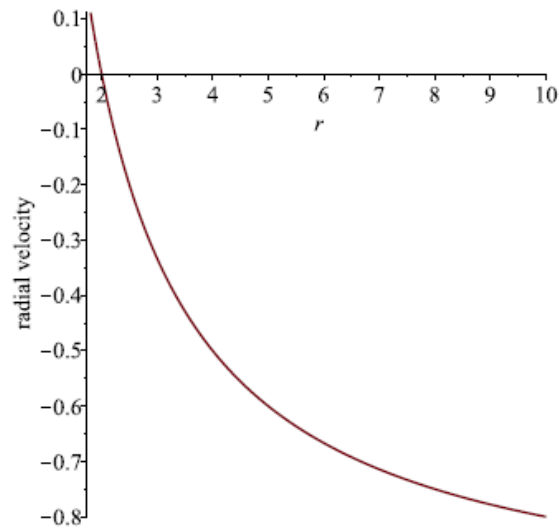


Figure 4. The radial coordinate velocity of a massless particle in the Schwarzschild geometry for $m = 1$. The horizon is located at $r = 2$.

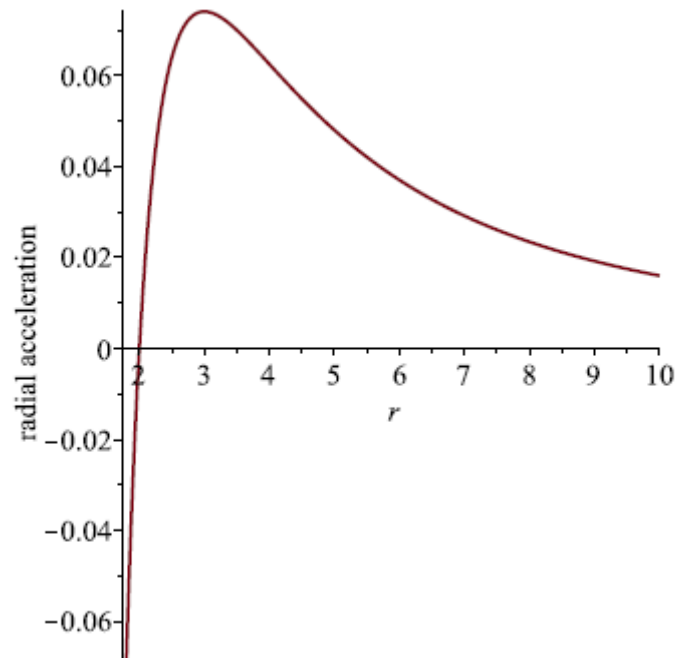


Figure 5. The radial coordinate acceleration of a massless particle in the Schwarzschild geometry for $m = 1$. Again, the horizon is located at $r = 2$.

These graphs show that a particle initially at rest from spatial infinity moves with increasing speed towards the Schwarzschild black hole. The maximum speed is at $r = 6$. After that it

continues to move but with decreasing speed towards the Schwarzschild black hole and finally stop at the horizon. It appears that a particle never crosses the horizon. However, the true situation does not occur like this. This behavior results from the use of inappropriate coordinates. To clarify this, consider the Painleve–Gullstrand coordinates defined by

$$ds^2 = -\left(1 - \frac{2m}{r}\right) dt_{PG}^2 + 2\sqrt{\frac{2m}{r}} dt_{PG} dr + dr^2 + r^2 (d\theta^2 + \sin^2 \theta d\phi^2).$$

In this case, the radial coordinate velocity and the radial coordinate acceleration for a non-zero rest mass particle are given by

$$\dot{r} = -\sqrt{\frac{2m}{r}} \quad \text{and} \quad \ddot{r} = -\frac{m}{r^2}$$

and those for a massless particle are given by

$$\dot{r} = -1 - \sqrt{\frac{2m}{r}} \quad \text{and} \quad \ddot{r} = -\frac{1}{2r} \sqrt{\frac{2m}{r}} \left(1 + \sqrt{\frac{2m}{r}}\right).$$

These results show that a particle initially at rest from spatial infinity moves with increasing speed towards the Schwarzschild black hole until it reaches the singularity. Note that it can cross the horizon.

5. The exponential metric [29]

The exponential metric can be written as

$$ds^2 = -e^{-2m/r} dt^2 + e^{2m/r} \left[dr^2 + r^2 (d\theta^2 + \sin^2 \theta d\phi^2) \right]$$

Note that it contains no horizon. Consider the area of the spherical surfaces of constant r coordinate

$$A(r) = 4\pi r^2 e^{2m/r}$$

With some algebra, we obtain

$$\frac{dA(r)}{dr} = 8\pi(r - m)e^{2m/r}$$

and

$$\frac{d^2 A(r)}{dr^2} = 8\pi e^{2m/r} \left[\left(1 - \frac{m}{r}\right)^2 + \frac{m^2}{r^2} \right] > 0.$$

We see that the area is minimum at $r = m$. Furthermore, all metric components are finite at $r = m$. This sufficiently shows that the surface $r = m$ is a traversable wormhole throat.

To determine the circular orbits, consider the affinely parameterized tangent vector to the worldline of a massive or massless particle

$$g_{\mu\nu} \frac{dx^\mu}{d\lambda} \frac{dx^\nu}{d\lambda} = -e^{2m/r} \left(\frac{dt}{d\lambda} \right)^2 + e^{2m/r} \left[\left(\frac{dr}{d\lambda} \right)^2 + r^2 \left(\frac{d\theta}{d\lambda} \right)^2 + r^2 \sin^2 \theta \left(\frac{d\phi}{d\lambda} \right)^2 \right] = \mathcal{E},$$

where $\mathcal{E} = -1$ for a massive particle orbit and $\mathcal{E} = 0$ for a massless particle orbit. We focus on the equatorial plane where $\theta = \pi / 2$. The above equation reduce to

$$g_{\mu\nu} \frac{dx^\mu}{d\lambda} \frac{dx^\nu}{d\lambda} = -e^{2m/r} \left(\frac{dt}{d\lambda} \right)^2 + e^{2m/r} \left[\left(\frac{dr}{d\lambda} \right)^2 + r^2 \left(\frac{d\phi}{d\lambda} \right)^2 \right] = \mathcal{E}.$$

The Killing symmetries imply two conserved quantities

$$e^{-2m/r} \left(\frac{dt}{d\lambda} \right) = E \text{ and } e^{2m/r} r^2 \left(\frac{d\phi}{d\lambda} \right) = L.$$

Then,

$$\left(\frac{dr}{d\lambda} \right)^2 = E^2 + e^{-2m/r} \left(\mathcal{E} - e^{-2m/r} \frac{L^2}{r^2} \right).$$

Therefore, the effective potential for geodesics orbits is

$$V_{\mathcal{E}}(r) = e^{-2m/r} \left(-\mathcal{E} + e^{-2m/r} \frac{L^2}{r^2} \right).$$

For photon ($\mathcal{E} = 0$), the effective potential is

$$V_0(r) = \frac{e^{-4m/r} L^2}{r^2},$$

where L is the angular momentum of photon. The unstable photon sphere is located at $r = 2m$.

Note that in the Schwarzschild geometry, the unstable photon sphere is located at $r = 3m$. For a massive particle ($\mathcal{E} = -1$), the effective potential is

$$V_1(r) = e^{2W(m/r_s)} \left(1 + \frac{L^2}{r_s^2} \right).$$

This shows that there are circular orbits for a massive particle at any radius down to $r = 2m$.

However, this does not guarantee stability. The stability occurs when L is minimum. Figure 6 shows the angular momentum (L) varying with the radius.

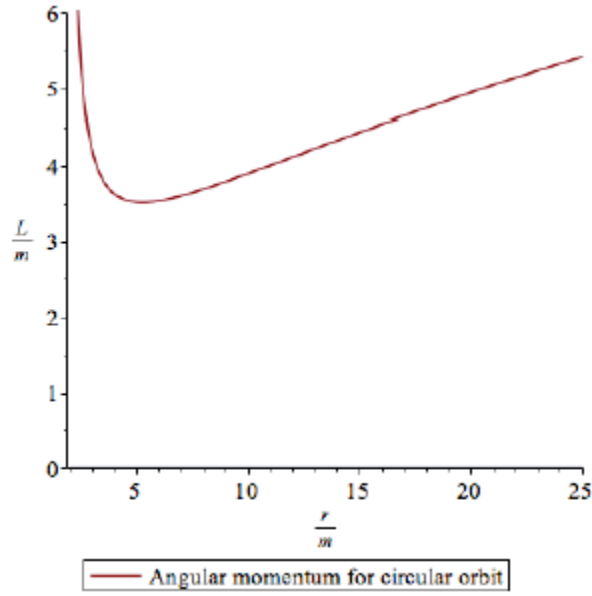


Figure 6. The graph shows the angular momentum L/m required to establish a circular orbit at radius r/m .

From Figure 6, the location of the innermost stable circular orbit is at

$$r_{\text{ISCO}} = \left(3 + \sqrt{5}\right)m \approx 5.236m,$$

whereas it is at $r_{\text{ISCO}} = 6m$ in the Schwarzschild spacetime.

6. The bounds on the greybody factors for black holes in dRGT massive gravity [30]

According to cosmological observations, today's universe is expanding with acceleration. One way to account for the current acceleration of the universe is the assumption that gravity has mass called massive gravity. One of the successful theories of massive gravity is the dRGT massive gravity. The static and spherically symmetric black hole solution satisfying this theory of dRGT massive gravity can be written as

$$ds^2 = -f(r)dt^2 + \frac{dr^2}{f(r)} + r^2 d\Omega^2,$$

where

$$f(r) = 1 - \frac{2M}{r} + \frac{Q^2}{r^2} + \frac{\Lambda}{3}r^2 + \gamma r + \zeta.$$

The radial part of the Klein-Gordon equation is given by

$$\frac{d^2\psi(r)}{dr_*^2} + [\omega^2 - V(r)]\psi(r) = 0,$$

where r_* is the tortoise coordinate defined by

$$\frac{dr_*}{dr} = \frac{1}{f(r)}$$

and the potential produced by the black hole is given by

$$V(r) = f(r) \left[\frac{l(l+1)}{r^2} + \frac{f'(r)}{r} \right].$$

The rigorous bounds on the greybody factors are given by

$$T \geq \text{sech}^2 \left[\frac{1}{2\omega c} \left\{ l(l+1) \left(\frac{1}{\rho_o} - \frac{1}{\rho_H} \right) + M \left(\frac{1}{\rho_o} - \frac{1}{\rho_H} \right) + 2\alpha_g c_2 (\rho_o - \rho_H) - \alpha_g c_1 \ln \left| \frac{\rho_o}{\rho_H} \right| \right\} \right],$$

where $M = M/c$, c is constant,

$$\rho_o = \frac{6M}{\alpha_m} \cos \left[\frac{1}{3} \cos^{-1}(-\alpha_m) - \frac{2\pi}{3} \right]$$

and

$$\rho_H = \frac{6M}{\alpha_m} \cos \left[\frac{1}{3} \cos^{-1}(-\alpha_m) \right].$$

The rigorous bound on the greybody factor depends on the wave frequency ω , the angular momentum l , and the horizon radius ρ_H and ρ_o . The rigorous bound on the greybody factor versus the wave frequency ω is plotted for different c_2 as shown in Figure 7.

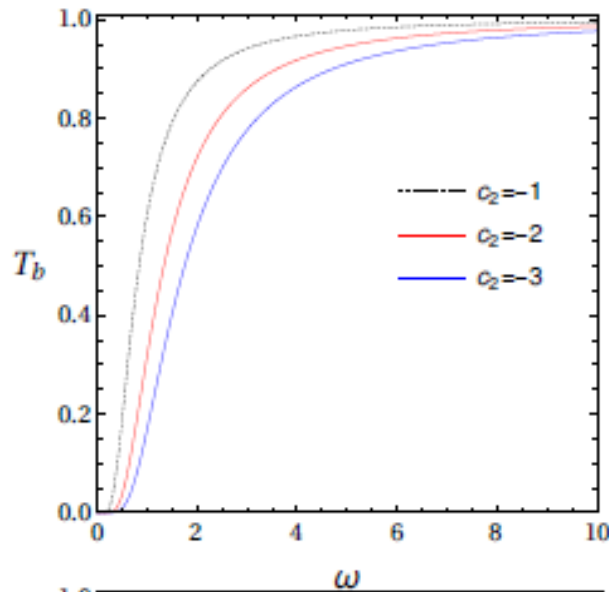


Figure 7. Dependence of the rigorous bound on the greybody factor on the wave frequency.

References

- [1] R. C. Tolman, "Relativity, Thermodynamics and Cosmology". Oxford University Press, (1934).
- [2] J. R. Oppenheimer and G. M. Volkoff, "On massive neutron cores", Physical Review, 55(4), 374-381, (1939).
- [3] R. F. Tooper, "General relativistic polytropic fluid spheres", Astrophys. J. 140(2), 434-459, (1964).
- [4] R. F. Tooper, "Adiabatic fluid spheres in general relativity", Astrophys. J. 142(4), 1541–1562, (1965).
- [5] S. S. Bayin, "Anisotropic fluid spheres in general relativity", Phys. Rev. D 26(6), 1262-1274, (1982).
- [6] S. D. Maharaj and P. M. Takisa, "Regular models with quadratic equation of state", General Relativity and Gravitation 44(6), 1419-1432, (2012).
- [7] N. Pant, N. Pradhan, and K. N. Singh, "Anisotropic charged fluid sphere in isotropic coordinates", Journal of Gravity, (2014).
- [8] A. Sulaksono, "Anisotropic pressure and hyperons in neutron stars", Int. J. Mod. Phys. E 24(1), 1550007, (2015), arXiv: 1412.7247 [nucl-th].
- [9] S. K. Maurya, Y. K. Gupta, and M. K. Jasim, "Relativistic modeling of stable anisotropic super-dense star", arXiv: 1503.04434 [gr-qc].
- [10] S. Rahman and M. Visser, "Spacetime geometry of static fluid spheres", Class. Quant. Grav. 19, 935, (2002), arXiv: gr-qc/0103065.
- [11] K. Lake, "All static spherically symmetric perfect fluid solutions of Einstein's equations", Phys. Rev. D 67, 104015, (2003), arXiv: gr-qc/0209104.
- [12] D. Martin and M. Visser, "Algorithmic construction of static perfect fluid spheres", Phys. Rev. D 69, 104028, (2004), arXiv: gr-qc/0306109.
- [13] P. Boonserm, M. Visser, and S. Weinfurter, "Generating perfect fluid spheres in general relativity", Phys. Rev. D 71, 124037, (2005), arXiv: gr-qc/0503007.
- [14] P. Boonserm and M. Visser, "Buchdahl-like transformations for perfect fluid spheres", Int. J. Mod. Phys. D 17, 135-163, (2008), arXiv 0707.0146 [gr-qc].
- [15] P. Boonserm, M. Visser, and S. Weinfurter, "Solution generating theorems for the TOV equation", Phys. Rev. D 76, 044024, (2007), arXiv: gr-qc/0607001.
- [16] P. Boonserm, T. Ngampitipan, and M. Visser, "Modelling anisotropic fluid spheres in general relativity", arXiv: 1501.07044 [gr-qc].

- [17] B. V. Ivanov, "Collapsing shear-free perfect fluid spheres with heat flow", *General Relativity and Gravitation* 44(7), 1835-1855, (2012).
- [18] J. M. Lattimer and M. Prakash, "The physics of neutron stars", *Science* 304, 536-542, (2004), arXiv: astro-ph/0405262.
- [19] J. H. Boutros, "Spherically symmetric perfect fluid solutions in isotropic coordinates", *J. Math. Phys.* 27(5), 1363-1366, (1986).
- [20] H. M. Murad and N. Pant, "A class of exact isotropic solutions of Einstein's equations and relativistic stellar models in general relativity", *Astrophysics and Space Science* 350(1), 349-359, (2014).
- [21] L. Herrera, J. Ospino, and A. D. Parisco, "All static spherically symmetric anisotropic solutions of Einstein's equations", *Phys. Rev. D* 77, 027502, (2008).
- [22] R. Lastowieckiy, D. Blaschke, T. Fischer, and T. Klahn, "Quark matter in high-mass neutron stars", arXiv: 1503.04832 [nucl-th].
- [23] N. Riazi, S. S. Hashemi, S. N. Sajadi, and S. Assyaaee, "Exact anisotropic solutions of the generalized TOV equation", arXiv: 1507.03420 [gr-qc].
- [24] P. Boonserm, N. Jongjittanon, and T. Ngampitipan, "Generating charged anisotropy and modified Tolman-Oppenheimer-Volkov equation", *Proceedings of the 6th Annual International Conference on Computational Mathematics, Computational Geometry & Statistics (CMCGS 2017) and 5th Annual International Conference on Operations Research and Statistics (ORS 2017)*.
- [25] N. Jongjittanon, P. Boonserm, and T. Ngampitipan, "Generating Theorems for Charged Anisotropy in General Relativity", *American Journal of Physics and Applications* 2016; 4(2): 50-56.
- [26] N. Jongjittanon, "Generating theorems for charged anisotropy and modified Tolman-Oppenheimer-Volkov equation", M.Sc. Thesis, Chulalongkorn University, 2015.
- [27] T. Ngampitipan, P. Boonserm, and A. Kinreewong, "The Modified Techniques for Generating Perfect Fluid Sphere in Isotropic Coordinate", *Proceedings of the 6th Annual International Conference on Computational Mathematics, Computational Geometry & Statistics (CMCGS 2017) and 5th Annual International Conference on Operations Research and Statistics (ORS 2017)*.
- [28] P. Boonserm, T. Ngampitipan, and M. Visser, "Near-Horizon Geodesics for Astrophysical and Idealised Black Holes: Coordinate Velocity and Coordinate Acceleration", *Universe* 4 (2018) 68, [arXiv: 1710.06139 [gr-qc]].

[29] P. Boonserm, T. Ngampitipan, A. Simpson, and M. Visser, “The exponential metric represents a traversable wormhole”, [arXiv:1805.03781 [gr-qc]].

[30] P. Boonserm, T. Ngampitipan, and P. Wongjun, “Greybody factor for black holes in dRGT massive gravity”, [arXiv:1705.03278 [gr-qc]].

สรุปและวิจารณ์ผลการทดลอง

In this project, we derive the generalized TOV equation and establish generating theorems for charged anisotropic fluid spheres in terms of the generalized TOV equation. Moreover, the charge density effect on fluid density is also investigated in the case of constant pressure. The results show that the fluid density at the surface is less than one at the center. Furthermore, the increase in the charge density results in a decrease in the fluid density, to keep the pressure constant.

Moreover, the solution generating theorems for anisotropy can be constructed in terms of the spacetime geometry using the Schwarzschild curvature coordinates. The theorems can generate solutions that satisfy anisotropy.

Besides generating theorems, we also present a new technique that can generate new solution for a perfect fluid sphere. We make use of the property of the Riccati equation; that is, if we have a particular solution, the general solution can be obtained. We use the Riccati equation as a focus in isotropic coordinates. These coordinates are highly interesting because the mathematical expressions are relatively simpler than in Schwarzschild curvature coordinates.

We will also show the difference between the use of inappropriate coordinates and the use of appropriate coordinates in expressing velocity and acceleration of test particles near the Schwarzschild black hole. The results show that when using the Schwarzschild curvature coordinates, which are inappropriate coordinates, a particle initially at rest from spatial infinity moves with increasing speed until it reaches a maximum speed towards the Schwarzschild black hole. After that it continues to move but with decreasing speed towards the Schwarzschild black hole and finally stops at the horizon. It appears that a particle never crosses the horizon. However, the true situation does not occur like this.

On the other hand, when using the Painlevé–Gullstrand coordinates, the particle moves with increasing speed towards the Schwarzschild black hole until it reaches the singularity. Note that it can cross the horizon.

Moreover, we will show that the exponential metric characterizes a worm hole. The results show that the unstable photon sphere is located at $r = 2m$ and there are circular orbits

for a massive particle at any radius down to $r = 2m$. This does not guarantee stability. However, there exists the innermost stable circular orbit located at $r_{\text{ISCO}} = 5.236m$.

Finally, we will show how we can obtain the rigorous bounds on the greybody factors for black holes in dRGT massive gravity. The results show that when the magnitude of c_2 increases, the rigorous bounds on the greybody factor decrease.

Output จากโครงการวิจัยที่ได้รับทุนจาก สกว.

1. ผลงานตีพิมพ์ในวารสารวิชาการนานาชาติ (ระบุชื่อผู้แต่ง ชื่อเรื่อง ชื่อวารสาร ปี เล่มที่ เลขที่ และหน้า) หรือผลงานตามที่คาดไว้ในสัญญาโครงการ

ผลงานตีพิมพ์ในวารสารวิชาการนานาชาติจำนวน 5 ฉบับ

- 1) Petarpa Boonserm, Tritos Ngampitipan, and Pitayuth Wongjun, "Greybody factor for black holes in dRGT massive gravity" European Physical Journal C, published.

EPJC 78 (2018) 492 DOI: 10.1140/epjc/s10052-018-5975-x

Impact factor: 5.331

- 2) Petarpa Boonserm, Tritos Ngampitipan, A. Simpson, and Matt Visser, "The exponential metric represents a traversable wormhole" Physical Review D, submitted.

Impact factor: 4.568

- 3) Petarpa Boonserm, Tritos Ngampitipan, and Pitayuth Wongjun, "Greybody factor for black string in dRGT massive gravity" European Physical Journal C, in progress.

Impact factor: 5.331

- 4) Petarpa Boonserm, Tritos Ngampitipan, and Matt Visser, "Non-rotating (2+1)-d perfect fluid stars" Physical Review D, in progress.

Impact factor: 4.568

- 5) Petarpa Boonserm, Tritos Ngampitipan, and Matt Visser, "Rotating perfect fluid stars in (2+1) dimensions" Physical Review D, in progress.

Impact factor: 4.568

2. การนำผลงานวิจัยไปใช้ประโยชน์

- เชิงวิชาการ (มีการพัฒนาการเรียนการสอน/สร้างนักวิจัยใหม่)
 - จัดตั้งกลุ่มวิจัย Gravity group ซึ่งทำการวิจัยหัวข้อต่าง ๆ ทางด้านทฤษฎีสัมพัทธภาพทั่วไป หลุมดำ กลศาสตร์ควอนตัม สมการเชิงอนุพันธ์ ร่วมกับนายไตรทศ งามปิติพันธ์
 - บรรยายพิเศษหัวข้อเรื่อง "Greybody Factor for Black String in dRGT massive Gravity" ที่วิทยาลัยเพื่อการค้นคว้าระดับรากฐาน มหาวิทยาลัยนเรศวร
 - สร้างนักวิจัยใหม่ ระดับปริญญาตรีคือ นางสาวกุลภัทร แสนสุข และระดับปริญญาโทคือ นางสาวภาณุรักษ์ ลิสุวรรณ

- จัดทำหนังสือเรื่อง “สมการเชิงอนุพันธ์ขั้นสูง” เพื่อให้นิสิตใช้ประกอบการเรียนการสอน

3. อื่นๆ (เช่น ผลงานตีพิมพ์ในวารสารวิชาการในประเทศ การเสนอผลงานในที่ประชุมวิชาการ หนังสือ การจดสิทธิบัตร)

**ผลงานตีพิมพ์ในวารสารวิชาการและการเสนอผลงานในที่ประชุมวิชาการในประเทศ
ไม่มี**

ผลงานตีพิมพ์ในการประชุมวิชาการในต่างประเทศจำนวน 5 ฉบับ

- 1) Petarpa Boonserm, Napasorn Jongjittanon, and Tritos Ngampitipan, “The modified Tolman-Oppenheimer-Volkov (TOV) Equation and the Effect of Charge on Pressure in Charge Anisotropy” Proceedings of the 2016 International Conference on Physics and Physics Education (ICPHY2016)
- 2) Petarpa Boonserm, Tritos Ngampitipan, and Napasorn Jongjittanon, “Generating Charged Anisotropy and Modified Tolman-Oppenheimer-Volkov Equation” Proceedings of the 6th Annual International Conference on Computational Mathematics, Computational Geometry and Statistics (CMCGS 2017)
- 3) Tritos Ngampitipan, Petarpa Boonserm, and Apisit Kinreewong, “The Modified Techniques For Generating Perfect Fluid Sphere In Isotropic Coordinate” Proceedings of the 6th Annual International Conference on Computational Mathematics, Computational Geometry and Statistics (CMCGS 2017)
- 4) Tritos Ngampitipan and Petarpa Boonserm, “The various techniques for generating perfect fluid sphere” Proceedings of the 3rd International Conference on Mathematical Sciences and Statistics (ICMSS 2018)
- 5) Petarpa Boonserm and Tritos Ngampitipan, “Variation of parameter for differential equation on Schwarzschild spacetime” Proceedings of the 12th AIMS Conference on Dynamical Systems, Differential Equations and Applications (AIMS 2018)



petarpa boonserm <petarpa.boonserm@gmail.com>

Fwd: European Physical Journal C - Decision on Manuscript ID EPJC-17-10-016.R1

1 message

Tritos Ngampitipan <tritos.ngampitipan@gmail.com>

Wed, May 30, 2018 at 11:31 AM

To: petarpa boonserm <petarpa.boonserm@gmail.com>, Pitt the pitt <pitbaa@gmail.com>

----- Forwarded message -----

From: **European Physical Journal C** <onbehalf@manuscriptcentral.com>

Date: 2018-05-29 18:24 GMT+07:00

Subject: European Physical Journal C - Decision on Manuscript ID EPJC-17-10-016.R1

To: tritos.ngampitipan@gmail.com

Cc: epjc.bologna@sif.it

29-May-2018

THE EUROPEAN PHYSICAL JOURNAL C (Particles and Fields)

Dear Dr. Ngampitipan:

Manuscript ID EPJC-17-10-016.R1 entitled "Greybody factor for black holes in dRGT massive gravity" which you submitted to the European Physical Journal C, has been reviewed. The comments of the reviewer(s) are included at the bottom of this letter.

The reviewer(s) have recommended publication, but also suggest some minor revisions to your manuscript. Therefore, I invite you to respond to the reviewer(s)' comments and revise your manuscript.

To revise your manuscript, log into <https://mc.manuscriptcentral.com/epjc> and enter your Author Center, where you will find your manuscript title listed under "Manuscripts awaiting Revision". Under "Actions," click on "Create a Revision".

You will be unable to make your revisions on the originally submitted version of the manuscript. Instead, revise your manuscript using a word processing program and save it on your computer. Please also highlight the changes to your manuscript within the document by using bold or colored text.

Once the revised manuscript is prepared, you can upload it and submit it through your Author Center.

When submitting your revised manuscript, you will be able to respond to the comments made by the reviewer(s) in the space provided. You can use this space to document any changes you make to the original manuscript. In order to expedite the processing of the revised manuscript, please be as specific as possible in your response to the reviewer(s).

IMPORTANT: Your original files are available to you when you upload your revised manuscript. Please delete any redundant files before completing the submission.

As we are trying to facilitate timely publication of manuscripts submitted to the European Physical Journal C, you have 3 months time from now to submit the revised version. In case it is not possible to upload your revision within this time period, please advise the Editorial Office to postpone the deadline.

Once again, thank you for submitting your manuscript to the European Physical Journal C and I look forward to receiving your revision.

Sincerely,

Prof. Ignatios Antoniadis

Editor in Chief, European Physical Journal C

Ignatios.Antoniadis@cph.t.polytechnique.fr-----
THE EUROPEAN PHYSICAL JOURNAL C, Editorial Office

Societa' Italiana di Fisica

[Via Saragozza 12](#)

40123 Bologna, Italy

Tel.: +39 051 581569

Fax.: +39 051 581340

E-Mail: epjc.bologna@sif.it-----
Associate Editor's Comments to Author:

Associate Editor

Comments to the Author:

EPJC-17-10-016.R1 is acceptable for publication. I have a request to the authors to modify the statement in the introduction: ".....some observations can still not be explained within the context of general relativity such as the current accelerating expansion of the universe...", which is not correct. Current Λ CDM model is a valid explanation.

Provided this is done, I do not need to see the manuscript any more.

Reviewer(s)' Comments to Author:

Greybody factor for black holes in dRGT massive gravity^{*}

Petarpa Boonserm^{a,1}, Tritos Ngampitipan^{b,2}, Pitayuth Wongjun^{c,3}

¹Department of Mathematics and Computer Science, Faculty of Science, Chulalongkorn University, Bangkok 10330, Thailand

²Faculty of Science, Chandrakasem Rajabhat University, Bangkok 10900, Thailand

³The institute for fundamental study, Naresuan University, Phitsanulok 65000, Thailand

Received: date / Accepted: date

Abstract In general relativity, greybody factor is a quantity related to the quantum nature of a black hole. A high value of greybody factor indicates a high probability that Hawking radiation can reach infinity. Although general relativity is correct and has been successful in describing many phenomena, there are some questions that general relativity cannot answer. Therefore, general relativity is often modified to attain answers. One of the modifications is the ‘massive gravity’. The viable model of the massive gravity theory belongs to de Rham, Gabadadze and Tolley (dRGT). In this paper, we calculate the gravitational potential for the de Sitter black hole and for the dRGT black hole. We also derive the rigorous bound on the greybody factor for the de Sitter black hole and the dRGT black hole. It is found that the structure of potentials determines how much the rigorous bound on the greybody factor should be. That is, the higher the potential, the lesser the bound on the greybody factor will be. Moreover, we compare the greybody factor derived from the rigorous bound with the greybody factor derived from the matching technique. The result shows that the rigorous bound is a true lower bound because it is less than the greybody factor obtained from the matching technique.

Keywords Black hole · dRGT massive gravity · Gravitational potential · Greybody factor · Rigorous bound

1 Introduction

General relativity was formulated in 1915. It offers profound insights into the concept of gravity. General relativity has succeeded in describing many gravitational phenomena such as the gravitational deflection of light, gravitational radiation, the anomalous perihelion of Mercury, and the behavior of black holes.

According to cosmological observations, today's the universe is expanding with acceleration [1, 2]. There are a number of cosmological models accounting for this current acceleration. Among these models, the simplest one is the Lambda cold dark matter (Λ CDM) model in which the cosmological constant drives the acceleration of the universe. The model assumes that general relativity is the correct theory of gravity on cosmological scales. Although the Λ CDM model is in excellent agreement with observations, the cosmological constant itself encounters a theoretical problem that the observational value of the cosmological constant is much smaller than the theoretical one. It may be possible that general relativity may not be the most suitable theory to describe the universe on a large scale, at least on a scale larger than the solar system. The dark side of the universe is evidence that some modifications of general relativity at a large scale is required [3].

Such modifications should be correct on the largest scale and then reduce to general relativity on a smaller scale. One of the candidates for such modifications is massive gravity. Massive gravity is a theory of gravity in which a graviton has a mass. The most successful theory of massive gravity is popularly known by the de Rham-Gabadadze-Tolley (dRGT) model [4, 5]. Because of the Vainshtein mechanism, adding mass to graviton keeps physics on a small scale equivalent to general relativity,

^{*}Thanks to the title

^ae-mail: petarpa.boonserm@gmail.com

^be-mail: tritos.ngampitipan@gmail.com

^ce-mail: pitbaa@gmail.com

with some small corrections [6]. However, this leads to the modification of gravity on a larger scale.

Regarding the cosmological solutions in the dRGT massive gravity theory, even though all the solutions cannot provide a viable cosmological model, for example, the solutions do not admit flat-FLRW metric [7, 8] or the model encounters instabilities [9–11], a class of solutions can provide a viable cosmological model [12–14]. The solutions for the dRGT massive gravity are not only investigated in a cosmological background, but also in a spherically symmetric background [15]. For spherically symmetric solutions, the black hole solutions have been investigated in both analytical [16–25] and non-analytical [26, 27] forms, depending on the fiducial metric form. However, they still share the same property, which is represented as an asymptotic AdS/dS behavior.

A black hole can emit thermal radiation if the quantum effects are considered. This thermal radiation is known as Hawking radiation [28]. Hawking radiation propagates on spacetime, which is curved by the black hole. The curvature of spacetime acts as a gravitational potential. Therefore, Hawking radiation is scattered from this potential. One part of the Hawking radiation is reflected back into the black hole, while the other part is transmitted to spatial infinity. The transmission probability in this context is also known as the greybody factor.

There are many methods to calculate the greybody factor. For example, one can obtain an approximate greybody factor using the matching technique [29–31]. If the gravitational potential is high enough, one can use the WKB approximation to derive the greybody factor [32–34]. Other than approximation, the greybody factor can also be obtained using the rigorous bound [35–37]. The bound can give a qualitative description of a black hole.

In this work, we investigate the greybody factor using the analytical black hole solution in dRGT massive gravity. In Section 2, the structure of the horizons of the solution is analyzed in order to generate a suitable form for the analysis of the properties of the greybody factor. In Section 3, the properties of the gravitational potential are investigated for both the de Sitter black hole and dRGT black hole. The height of their potentials are determined by the parameters of the model. In Section 4, we derive the rigorous bound on the greybody factor, and the reflection probability for the de Sitter black hole and the dRGT black hole. The value of the rigorous bound on the greybody factor corresponds to the structure of potentials. In addition, the effects of the graviton mass, cosmological constant and angular momentum quantum number on the greybody factors

will also be explored. Finally, concluding remarks are provided in Section 5.

2 dRGT black hole background

In this section, we will review the main concept of the dRGT massive gravity theory in the following manner [18]; the analytical solution of the modified Einstein equation due to the graviton mass is first presented, and then the structure of the horizons of the black hole in the dRGT massive gravity theory is investigated. The theory of the dRGT massive gravity is a covariant non-linear theory of massive gravity, which is ghost free in the decoupling limit to all orders. The action of the dRGT massive gravity model in four-dimensional spacetime can be expressed as

$$S = \int d^4x \sqrt{-g} \left[\frac{M_p^2}{2} R[g] + m_g^2 (\mathcal{L}_2[g, f] + \alpha_3 \mathcal{L}_3[g, f] + \alpha_4 \mathcal{L}_4[g, f]) \right], \quad (1)$$

where R is a Ricci scalar corresponding to a physical metric $g_{\mu\nu}$, m_g^2 to the square of the graviton mass, with \mathcal{L}_i s representing the interactions of the i th order of the massive graviton. In particular, those interactions of the massive graviton are constructed from two kinds of metrics and can be expressed as follows,

$$\mathcal{L}_2[g, f] = \frac{1}{2} ([\mathcal{K}]^2 - [\mathcal{K}^2]), \quad (2)$$

$$\mathcal{L}_3[g, f] = \frac{1}{3!} ([\mathcal{K}]^3 - 3[\mathcal{K}][\mathcal{K}^2] + 2[\mathcal{K}^3]), \quad (3)$$

$$\mathcal{L}_4[g, f] = \frac{1}{4!} ([\mathcal{K}]^4 - 6[\mathcal{K}]^2[\mathcal{K}^2] + 3[\mathcal{K}^2]^2 + 8[\mathcal{K}][\mathcal{K}^3] - 6[\mathcal{K}^4]), \quad (4)$$

where the rectangular brackets denote the traces. The tensor $\mathcal{K}_{\mu\nu}$ is constructed from the physical metric $g_{\mu\nu}$ and the fiducial metric $f_{\mu\nu}$ as

$$\mathcal{K}_{\mu}^{\nu} = \delta_{\mu}^{\nu} - \left(\sqrt{g^{-1}f} \right)_{\mu}^{\nu}, \quad (5)$$

where the square roots of those tensors are defined so that $\sqrt{g^{-1}f}^{\mu}_{\rho} \sqrt{g^{-1}f}^{\rho}_{\nu} = (g^{-1}f)^{\mu}_{\nu}$. The fiducial metric is chosen as [16, 38, 39]

$$f_{\mu\nu} = \text{diag}(0, 0, c^2, c^2 \sin^2 \theta), \quad (6)$$

where c is a constant. It can be shown in [38] that the theory of massive gravity with the choice of the singular fiducial metric such as one in equation (6) is absent of Boulware-Deser (BD) ghost. The static and spherically symmetric black hole solution satisfying this theory can be written as [18]

$$ds^2 = -f(r)dt^2 + \frac{dr^2}{f(r)} + r^2 d\Omega^2, \quad (7)$$

where

$$f(r) = 1 - \frac{2M}{r} + \frac{\Lambda}{3}r^2 + \gamma r + \zeta, \quad (8)$$

$d\Omega^2 = d\theta^2 + \sin^2\theta d\phi^2$, and M is an integration constant related to the mass of the black hole. The parameters above can be written in terms of the original parameters as

$$\Lambda = 3m_g^2(1 + \alpha + \beta), \quad (9)$$

$$\gamma = -cm_g^2(1 + 2\alpha + 3\beta), \quad (10)$$

$$\zeta = c^2m_g^2(\alpha + 3\beta), \quad (11)$$

and

$$\alpha_3 = \frac{\alpha - 1}{3}, \quad \alpha_4 = \frac{\beta}{4} + \frac{1 - \alpha}{12}. \quad (12)$$

This solution contains various kinds of black hole solutions found in literature. If $m_g = 0$, the Schwarzschild solution is recovered. In the case of $c = 0$, the solution reduces to the de Sitter solution for $1 + \alpha + \beta < 0$ and reduces to the anti-de Sitter solution for $1 + \alpha + \beta > 0$. Moreover, the global monopole solution can be obtained by setting $1 + 2\alpha + 3\beta = 0$. Note that the last term, the constant potential ζ , corresponds to the global monopole term. A global monopole usually comes from a topological defect in high energy physics of the early universe resulting from a gauge-symmetry breaking [40–42]. However, in this solution, the global monopole is contributed via the graviton mass. Note that the linear term γr is a characteristic term of this solution, distinguished from other solutions found in literature. Next, we will consider the structure of the horizons of this solution. Since the solution is an asymptotical AdS/dS solution, we first consider the structure of the AdS/dS solution and then investigate the structure of the horizons of the solution in the dRGT massive gravity theory.

2.1 Horizon structure for AdS/dS-like solutions

It is important to note that one can choose $c = 0$. This corresponds to trivial solutions since the interacting terms (or graviton mass) become constant, which is inferred from $\mathcal{K}_\nu^\mu = \delta_\nu^\mu$. Therefore, the action in Eq. (1) becomes the Einstein-Hilbert action with cosmological constant. In order to investigate the structure of the horizon, let us first consider a simple case where $c = 0$. As a result, the function in the metric solution becomes

$$f(r) = 1 - \frac{2M}{r} + \frac{\Lambda}{3}r^2. \quad (13)$$

From this function, one can see that $f(r) \rightarrow -\infty$ where $r \rightarrow 0$. In order to have two horizons, f must be increased and then decreased where r is increased. This

means that $f(r) \rightarrow -\infty$ again when $r \rightarrow \infty$. Therefore, in order to obtain two horizons, Λ must be negative. This corresponds to the de Sitter (dS) spacetime, while in the case of anti-de Sitter (AdS) spacetime, $\Lambda > 0$, there exists only one horizon. Now let us find the conditions for which there are two horizons for the de Sitter spacetime, where $\Lambda < 0$. If two horizons exist, the maximum value of f must be positive. The maximum point of f can be found by solving $f' = 0$. As a result, the maximum point is

$$r_m = \left(-\frac{3M}{\Lambda}\right)^{1/3}. \quad (14)$$

Substituting this radius into $f(r)$ in Eq. (13), the maximum value of f can be written as

$$f(r_m) = \left(-\frac{3M}{\Lambda}\right)^{1/3} - 3M. \quad (15)$$

By requiring $f(r_m) > 0$, the condition for having two horizons can be written as

$$-\frac{1}{9M^2} < \Lambda < 0. \quad (16)$$

In order to parameterize the solution properly, let us define a dimensionless parameter as

$$\alpha_m^2 = -9\Lambda M^2, \quad (17)$$

where $0 < \alpha_m^2 < 1$. By using the dimensionless variable $\bar{r} = r/M$, function f can be rewritten as

$$f(\bar{r}) = 1 - \frac{2}{\bar{r}} - \frac{\alpha_m^2}{27}\bar{r}^2. \quad (18)$$

In order to find the horizon, one has to solve the cubic equation;

$$\bar{r}^3 - \frac{27}{\alpha_m^2}\bar{r} + \frac{54}{\alpha_m^2} = 0. \quad (19)$$

This cubic equation is known as the depressed cubic equation, and the solution can be expressed as

$$\bar{r} = \frac{6}{\alpha_m} \cos \left[\frac{1}{3} \cos^{-1} \left(-\alpha_m \right) - \frac{2\pi k}{3} \right], \quad (20)$$

where $k = 0, 1, 2$ for the three distinguished solutions. Since $0 < \alpha_m < 1$, one can expand the sinusoidal function and then keep only the significant contributions. As a result, for $k = 2$, \bar{r} is negative, and for $k = 1$ and $k = 0$, the solutions can be respectively approximated as

$$\bar{r}_1 \sim 2, \quad \bar{r}_2 \sim \frac{3\sqrt{3}}{\alpha_m} - 1. \quad (21)$$

Note that these solutions are well approximated when $\alpha_m \ll 1$. Actually, this approximation can be realized to satisfy the cosmological solution in which the universe expands with acceleration, since the observed

value of Λ is very small compared to the black hole mass. The behavior of the horizon with various values of α_m is shown in the left panel of Fig. 1.

For the AdS solution, Λ is positive. Therefore, one can find the solution of the horizon by rewriting α_m as $\alpha_m = 9\Lambda M^2$. By following the same steps from the de Sitter case, the horizon in the AdS case can be written as

$$\bar{r} = \frac{6}{\alpha_m} \sinh \left[\frac{1}{3} \sinh^{-1} (\alpha_m) \right]. \quad (22)$$

As we have discussed above, there exists only one horizon for the AdS solution. This is valid for all values of α_m as show in the right panel of Fig. 1.

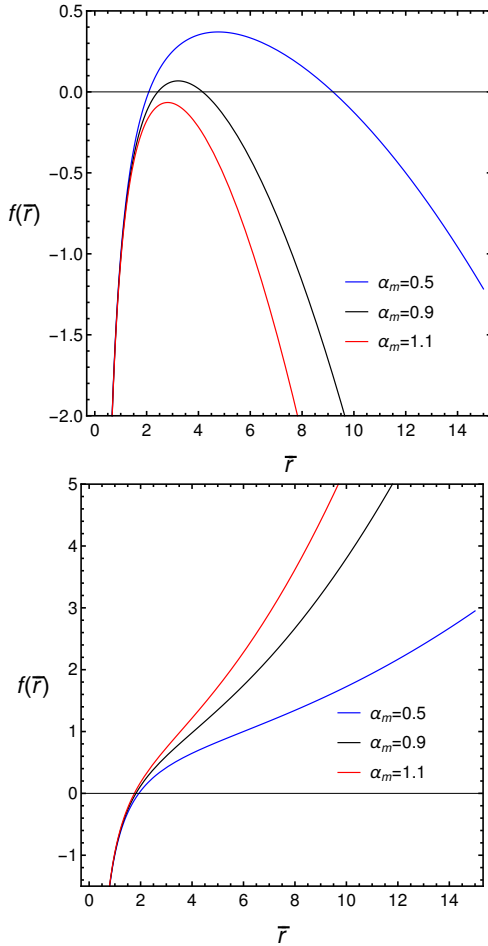


Fig. 1 The left panel shows the horizon structure of the de Sitter solution for the value of α_m as $\alpha_m = 0.5$ (Blue line), $\alpha_m = 0.9$ (Black line) and $\alpha_m = 1.1$ (Red line). The right panel shows the horizon structure of the AdS solution for the value of α_m as $\alpha_m = 0.5$ (Blue line), $\alpha_m = 0.9$ (Black line) and $\alpha_m = 1.1$ (Red line).

2.2 Horizon structure for the dRGT massive gravity solutions

For the complete massive gravity solution, it is significantly difficult and complicated to find the horizon analytically. One of the conditions for having three horizons is that $\Lambda > 0$. Therefore, we can separate our consideration into two classes; the asymptotic AdS solutions for $\Lambda > 0$ and the asymptotic de Sitter solution for $\Lambda < 0$ [43].

For the general solutions of the dRGT massive gravity, the dimension-length parameter c is not set to be zero. This means that we have to introduce a scale to the theory. It is useful to work out the solution using dimensionless variable, $\tilde{r} = r/c$, and then find out what scale c would assume. As a result, function f can be written in terms of a dimensionless variable as

$$f(\tilde{r}) = 1 - \frac{2\tilde{M}}{\tilde{r}} + \alpha_g (c_2 \tilde{r}^2 - c_1 \tilde{r} + c_0), \quad (23)$$

where

$$\tilde{M} = \frac{M}{c}, \quad \alpha_g = m_g^2 c^2, \quad c_0 = \alpha + 3\beta, \\ c_1 = 1 + 2\alpha + 3\beta, \quad c_2 = 1 + \alpha + \beta. \quad (24)$$

From this equation, it is sufficient to figure out that the scale of c takes place at $\tilde{M} \sim \alpha_g$. Therefore, one can choose the parameter c as

$$c = r_V = \left(\frac{M}{m_g^2} \right)^{1/3}. \quad (25)$$

This radius is well known as the Vainshtein radius [44, 45]. The theory in which $r < r_V$ will approach GR, while the theory in which $r > r_V$, the modification of GR will be active. The horizons can be found by solving for the solution of r through the equation

$$\alpha_g c_2 \tilde{r}^3 - \alpha_g c_1 \tilde{r}^2 + (\alpha_g c_0 + 1) \tilde{r} - 2\tilde{M} = 0. \quad (26)$$

In order to find the conditions for having three horizons for the AdS case and two horizons for the de Sitter case, let us consider the extremum points of the function f using the equation $f' = 0$ or

$$2\alpha_g c_2 \tilde{r}^3 - \alpha_g c_1 \tilde{r}^2 - 2\tilde{M} = 0. \quad (27)$$

This is the cubic equation. We can solve it by changing the variables to obtain the depressed cubic equation and then analyze the general solution to find the condition for having two real positive roots for the AdS case and one real positive root for the de Sitter case. As a result, one can constrain our consideration to case $c_1 = 3(4c_2^2)^{1/3}$. Choosing this condition will guarantee one real positive root for the de Sitter case as $\tilde{r}_{dS} = (-2c_2)^{-1/3}$ and two real positive roots for the AdS case as $\tilde{r}_{AdS1} = (2c_2)^{-1/3}$ and $\tilde{r}_{AdS2} = (1 + \sqrt{3})(2c_2)^{-1/3}$.

For the asymptotic de Sitter solutions, f at the extremum point can be written as

$$f(\tilde{r}_{dS}) = 1 + c_0\alpha_g - \frac{9}{\sqrt{3}}\alpha_g(-2c_2)^{1/3}. \quad (28)$$

In order to have two horizons, $f(\tilde{r}_{dS}) > 0$. We can parameterize the parameter c_0 such that

$$c_0 = \frac{9}{\sqrt{3}} \frac{(-2c_2)^{1/3}}{\beta_m} - \frac{1}{\alpha_g}. \quad (29)$$

Therefore, the condition for having two horizons in the case of de Sitter-like spacetime is

$$0 < \beta_m < 1. \quad (30)$$

By changing the cubic equation into the depressed cubic equation, one can find the two real positive horizons as the real roots of the depressed cubic equation as follows

$$\tilde{r}_1 = \frac{2}{(-2c_2)^{1/3}} \left[X^{1/2} \cos\left(\frac{1}{3} \sec^{-1} Y\right) - 1 \right], \quad (31)$$

$$\tilde{r}_2 = \frac{-2}{(-2c_2)^{1/3}} \left[X^{1/2} \cos\left(\frac{1}{3} \sec^{-1} Y + \frac{\pi}{3}\right) + 1 \right], \quad (32)$$

where

$$X = \frac{2\sqrt{3}}{\beta_m} + 4 \text{ and } Y = -\frac{\sqrt{\frac{\sqrt{3}}{\beta_m}} + 2(2\sqrt{2}\beta_m + \sqrt{6})}{5\beta_m + 3\sqrt{3}}. \quad (33)$$

Our analysis can be checked using the numerical method as shown in the left panel of Fig. 2. From this figure, one can see that β_m can parameterize the existence of two horizons.

Now we consider the asymptotic AdS solutions. The f at the extremum points can be written as

$$f(\tilde{r}_{AdS1}) = 1 + c_0\alpha_g - \frac{9}{2}\alpha_g(2c_2)^{1/3}, \quad (34)$$

$$f(\tilde{r}_{AdS2}) = 1 + c_0\alpha_g - \frac{9}{\sqrt{3}}\alpha_g(2c_2)^{1/3}. \quad (35)$$

In order to have three horizons, we must have $f(\tilde{r}_{AdS1}) > 0$ and $f(\tilde{r}_{AdS2}) < 0$. By using the parameter of α_0 in Eq. (29), while changing c_2 to $-c_2$, the condition for having three horizons can be written as

$$1 < \beta_m < \frac{2}{\sqrt{3}}. \quad (36)$$

By using the same step as done in the asymptotic de Sitter case, the three real positive horizons for the AdS case can be written as

$$\tilde{r}_1 = \frac{2}{(2c_2)^{1/3}} \left[1 - x^{1/2} \sin\left(\frac{1}{3} \sec^{-1} y + \frac{\pi}{6}\right) \right], \quad (37)$$

$$\tilde{r}_2 = \frac{2}{(2c_2)^{1/3}} \left[1 - x^{1/2} \cos\left(\frac{1}{3} \sec^{-1} y + \frac{\pi}{3}\right) \right], \quad (38)$$

$$\tilde{r}_3 = \frac{2}{(2c_2)^{1/3}} \left[1 + x^{1/2} \cos\left(\frac{1}{3} \sec^{-1} y\right) \right]. \quad (39)$$

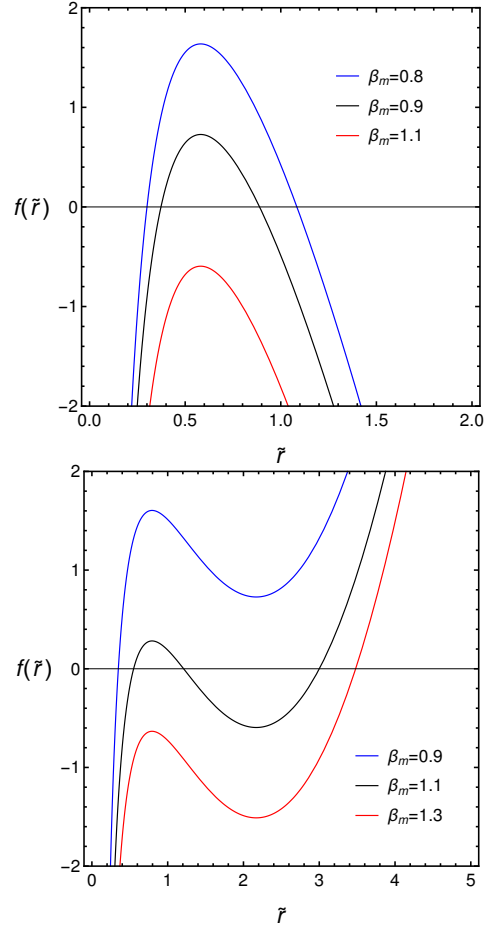


Fig. 2 The left panel shows the horizon structure of the asymptotic de Sitter solution in dRGT massive gravity for the value of β_m as $\beta_m = 0.8$ (Blue line), $\beta_m = 0.9$ (Black line) and $\beta_m = 1.1$ (Red line). The right panel shows the horizon structure of the asymptotic AdS solution in dRGT massive gravity for the value of β_m as $\beta_m = 0.9$ (Blue line), $\beta_m = 1.1$ (Black line) and $\alpha_m = 1.3$ (Red line). We set parameters as $M = 1$, $\alpha_g = 1$ and $c_2 = -1$ for the asymptotic de Sitter solution and $c_2 = 1$ for the asymptotic AdS solution.

where

$$x = \frac{4 - 2\sqrt{3}}{\beta_m} \text{ and } y = \frac{\sqrt{6} - 2\sqrt{2}\beta_m}{(3\sqrt{3} - 5\beta_m) \sqrt{-\frac{\beta_m}{\sqrt{3} - 2\beta_m}}}. \quad (40)$$

The numerical plot for these horizons is shown in the right panel of Fig. 2. From this figure, one can see that the existence of three horizons satisfy the condition $1 < \beta_m < 2/\sqrt{3}$ as we have analyzed. In the next section, we will use the expression for the horizons derived in this section to analyze the properties of the gravitational potential and the greybody factor of the black hole.

3 Equations of motion of massless scalar field

Classically, nothing can escape a black hole when approaching it. However, when a quantum effect is considered, the black hole can radiate. This radiation is known as Hawking radiation. It is a blackbody spectrum of temperature

$$kT = \frac{\hbar}{4\pi r_s}, \quad (41)$$

where r_s is the Schwarzschild radius. In this paper, we assume that Hawking radiation is a massless scalar field. The massless scalar field satisfies the Klein-Gordon equation

$$\frac{1}{\sqrt{-g}}\partial_\mu(\sqrt{-g}g^{\mu\nu}\partial_\nu\Phi) = 0. \quad (42)$$

We use the spherical coordinates. The solutions to the wave equation in spherical coordinates are of the form

$$\Phi(t, r, \Omega) = e^{i\omega t} \frac{\psi(r)}{r} Y_{\ell m}(\Omega), \quad (43)$$

where $Y_{\ell m}(\Omega)$ are spherical harmonics. The Klein-Gordon equation becomes

$$\begin{aligned} \frac{\omega^2 r^2}{f(r)} + \frac{r}{\psi(r)} \frac{d}{dr} \left[r^2 f(r) \frac{d}{dr} \left(\frac{\psi(r)}{r} \right) \right] \\ + \frac{1}{Y(\Omega)} \left[\frac{1}{\sin\theta} \frac{\partial}{\partial\theta} \left(\sin\theta \frac{\partial Y(\Omega)}{\partial\theta} \right) \right] \\ + \frac{1}{\sin^2\theta} \frac{1}{Y(\Omega)} \frac{\partial^2 Y(\Omega)}{\partial\phi^2} = 0. \end{aligned} \quad (44)$$

The angular part satisfies

$$\frac{1}{\sin\theta} \frac{\partial}{\partial\theta} \left(\sin\theta \frac{\partial Y(\Omega)}{\partial\theta} \right) + \frac{1}{\sin^2\theta} \frac{\partial^2 Y(\Omega)}{\partial\phi^2} = -\ell(\ell+1)Y(\Omega), \quad (45)$$

where ℓ is the angular momentum quantum number. Therefore, the Klein-Gordon equation (Eq. (44)) is left with the radial part

$$\frac{d^2\psi(r)}{dr_*^2} + [\omega^2 - V(r)]\psi(r) = 0, \quad (46)$$

where r_* is the tortoise coordinate defined by

$$\frac{dr_*}{dr} = \frac{1}{f(r)} \quad (47)$$

and $V(r)$ is the potential given by

$$V(r) = \frac{\ell(\ell+1)f(r)}{r^2} + \frac{f(r)f'(r)}{r}. \quad (48)$$

It can be expressed in terms of \tilde{r} as

$$V(\tilde{r}) = \frac{\ell(\ell+1)f(\tilde{r})}{c^2\tilde{r}^2} + \frac{f(\tilde{r})f'(\tilde{r})}{c^2\tilde{r}}. \quad (49)$$

Substituting the function $f(\tilde{r})$ from Eq. (23), we obtain

$$\begin{aligned} V(\tilde{r}) = & \left[1 - \frac{2\tilde{M}}{\tilde{r}} + \alpha_g (c_2\tilde{r}^2 - c_1\tilde{r} + c_0) \right] \\ & \times \left[\frac{\ell(\ell+1)}{c^2\tilde{r}^2} + \frac{1}{c^2\tilde{r}} \left[\frac{2\tilde{M}}{\tilde{r}^2} + \alpha_g (2c_2\tilde{r} - c_1) \right] \right]. \end{aligned} \quad (50)$$

From the above equation, we can see that the potential is high when the angular momentum quantum number is large. Qualitatively, the leading contribution to the transmission amplitude comes from the mode $\ell = 0$. Therefore, it is sufficient to qualitatively analyze the potential for the case of $\ell = 0$. When $\ell = 0$, the first term in Eq. 49 vanishes and the second term is proportional to $f f'$. Therefore, there are three \tilde{r} -intercepts resulting from $f = 0$ and $f' = 0$. This behavior significantly differs from the Schwarzschild case, which has only one \tilde{r} -intercept as shown in the right panel of Fig. 3.

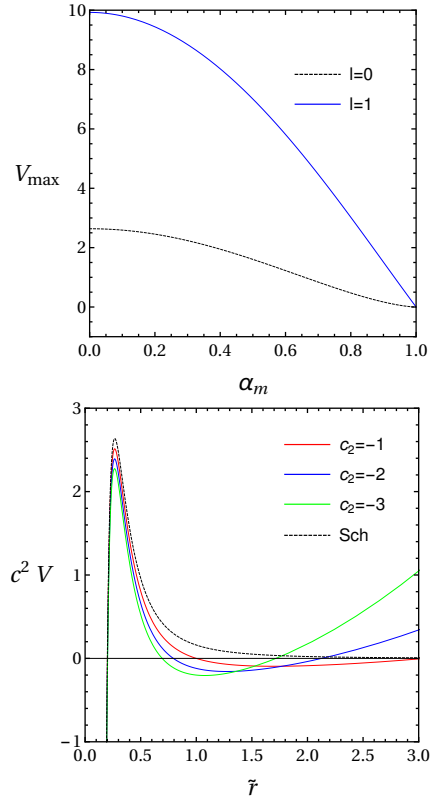


Fig. 3 The left panel shows the maximum potential for a de Sitter black hole versus the model parameter α_m with $\ell = 0, \ell = 1$, $\tilde{M} = \alpha_g = 0.1$. The right panel shows the potential for a de Sitter black hole with different values of c_2 compared to the Schwarzschild case; black-dotted line for the Schwarzschild case, red line for $c_2 = -1$, blue line for $c_2 = -2$ and green line for $c_2 = -3$.

For the de Sitter case, the potential can be obtained by setting $c_1 = c_0 = 0$. As we have analyzed in Section 2.2, it is convenient to change parameter as $\alpha_g c_2 = -\alpha_m^2/(27\tilde{M}^2)$. For this setting, the potential depends only on the parameter α_m . In the same strategy as the quantum theory, the shape of the potential controls the transmission amplitude. Therefore, it is worthwhile to consider the maximum value of the de Sitter potential compared to the Schwarzschild potential. As a result, the de Sitter potential for the $\ell = 0$ case can be written as

$$c^2 V_{dS}(\tilde{r}) = \frac{1}{\tilde{r}} \left(1 - \frac{2\tilde{M}}{\tilde{r}} - \frac{\alpha_m^2}{27\tilde{M}^2} \tilde{r}^2 \right) \times \left(\frac{2\tilde{M}}{\tilde{r}^2} - \frac{2\alpha_m^2}{27\tilde{M}^2} \tilde{r} \right). \quad (51)$$

By solving \tilde{r}_{\max} via $V'_{dS} = 0$ and then substituting the solution back into the above equation, one can find the maximum value of the potential depending on only two parameters, \tilde{M} and α_m . The expression is significantly lengthy; we do not present it in the current paper. In order to see the effect of the graviton mass or the cosmological constant, one can fix \tilde{M} and then plot this expression via α_m as shown in the left panel of Fig. 3. Note that we also show the result for the $\ell = 1$ case in this figure. From this figure, one can see that V_{\max} contributed from the de Sitter black hole is always less than one from the Schwarzschild black hole. Clearly, the cosmological constant plays a role in reducing the local maximum of the potential. The explicit form of the de Sitter potential is plotted with various values of the cosmological constant as shown in the right panel of Fig. 3. Note that we used the parameter c_2 instead of α_m^2 . This is convenient for comparing the results with one from the case of the dRGT massive gravity. Consequently, it might be expected that the transmission amplitude due to the de Sitter black hole should be greater than one in the Schwarzschild black hole. We will clarify this issue explicitly in the next section.

The dRGT potential for $\ell = 0$ can explicitly be written as

$$V_{\text{dRGT}}(\tilde{r}) = \frac{1}{c^2 \tilde{r}} \left[1 - \frac{2\tilde{M}}{\tilde{r}} + \alpha_g c_2 \tilde{r}^2 - 3\sqrt[3]{4c_2^2 \alpha_g} \tilde{r} + \frac{3\sqrt{3}\alpha_g \sqrt[3]{-2c_2}}{\beta_m} - 1 \right] \times \left(\frac{2\tilde{M}}{\tilde{r}^2} + 2\alpha_g c_2 \tilde{r} - 3\sqrt[3]{4c_2^2 \alpha_g} \tilde{r} \right). \quad (52)$$

By employing the same strategy as used in the de Sitter case, we found that the leading term of V_{\max} is proportional to $V_{\max} \propto 1/\beta_m$. By fixing $c_2 = -1$, we have

illustrated the explicit behavior of the peak of the potential in the left panel of Fig. 4. We can explicitly see that V_{\max} increases as β_m decreases. Moreover, the de Sitter potential and the dRGT potential with various values of β_m are plotted as shown in the right panel of Fig. 4. It shows that both the de Sitter potential and the dRGT potential increase with radial distance from the black hole. After that, they decrease with radial distance to reach the relative lowest point and then turn to increase again.

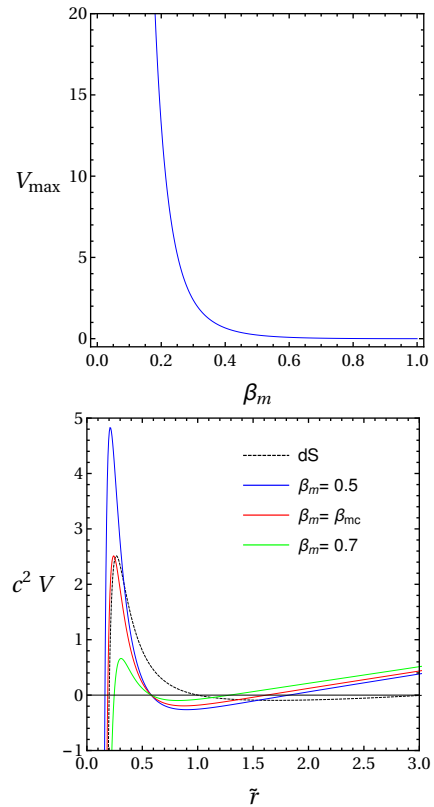


Fig. 4 The left panel shows the maximum of dRGT potential with $\ell = 0$, $\tilde{M} = 0.1$, $\alpha_g = 0.1$, $c = 1$, and $c_2 = -1$. The right panel shows the dRGT potential with $\ell = 0$, $\tilde{M} = 0.1$, $\alpha_g = 0.1$, $c = 1$, and $c_2 = -1$

In [46], the maximum points of the potentials are not chosen to be equal. We consider this point here. The equality of the maximum points allows us to draw conclusions regarding how high the rigorous bounds on the greybody factors for different types of black holes are. At the highest point, the derivative of the potential is zero. For $\ell = 0$, we obtain

$$V'(\tilde{r}) = \frac{1}{c^2} \frac{\tilde{r} f(\tilde{r}) f''(\tilde{r}) + \tilde{r} [f'(\tilde{r})]^2 - f(\tilde{r}) f'(\tilde{r})}{\tilde{r}^2}. \quad (53)$$

The solution of $V'(\tilde{r}) = 0$ is not shown here. We find that the equality of the peak of the potentials occur at

$\beta_m = 0.565375$. Moreover, the effects of parameter c_2 are shown in Fig. 5.

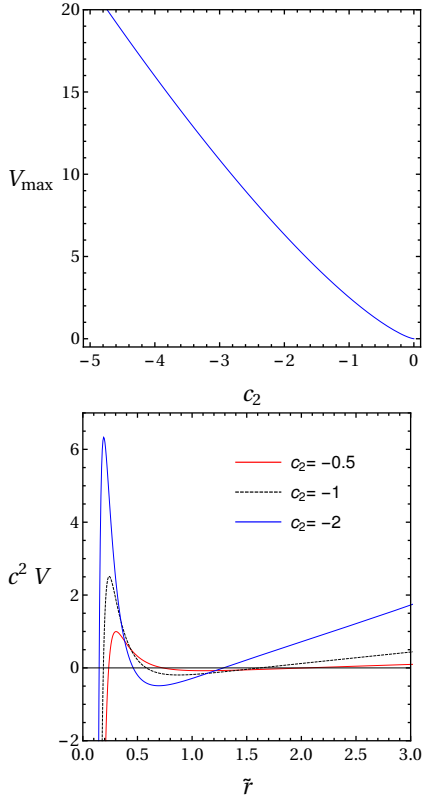


Fig. 5 The left panel shows the maximum dRGT potential with $\ell = 0$, $\tilde{M} = 0.1$, $\alpha_g = 0.1$, $c = 1$, and $\beta_m = 0.565375$. The right panel shows the dRGT potential with $\ell = 0$, $\tilde{M} = 0.1$, $\alpha_g = 0.1$, $c = 1$, and $\beta_m = 0.565375$.

To see the effect of the parameter c_2 on the potential, let us fix $\beta_m = \beta_{mc}$. The peak of the potential is plotted as shown in the left panel of Fig. 5. The potential is also plotted with various values of c_2 as shown in the right panel of Fig. 5. The parameter c_2 characterizes the strength of the graviton mass. Therefore, the graviton mass will enhance the potential in contrast to the effect of the cosmological constant in the de Sitter black hole.

In this section, we explore the behavior of the gravitational potential for both the de Sitter black hole and the dRGT black hole of a massless scalar field. By making a comparison with the potential in the Schwarzschild black hole, we found that the local maximum of the de Sitter potential is always less than one of the Schwarzschild potential. For the dRGT black hole, the local maximum of the potential depend on the model parameters; β_m characterizing the existence of two horizon ($0 < \beta_m < 1$) and c_2 characterizing the strength of the graviton mass. In contrast to the de Sitter potential,

we found that the local maximum of the dRGT potential will be larger than ones for the Schwarzschild and the de Sitter potential by setting parameter $\beta_m \ll 1$ or $c_2 \ll -1$. In the same fashion as quantum theory, the shape of the potential has an effect on the transmission amplitude or the greybody factor in this context. We will use the information of the potential to analyze the behavior of the greybody factor in the next section.

4 The rigorous bounds on the greybody factors

From a classical point of view, a black hole is believed to be black because nothing, when having entered the black hole, can escape, not even light. From a quantum point of view, however, a black hole is no longer considered ‘black’ since it has been proven to emit a type of thermal radiation known as Hawking radiation. At the event horizon of a black hole, Hawking radiation is exactly a blackbody spectrum. While Hawking radiation propagates out from the event horizon, it is, however, modified by the spacetime curvature generated by its black hole source. Thus, an observer at an infinite distance observes the modified form of Hawking radiation, which is different from the original Hawking radiation at the event horizon. This difference can be measured by the so-called greybody factor.

In this section, a greybody factor will be obtained using the rigorous bound [35–37, 47]. The bound can give a qualitative description of a black hole. It is applied to various types of black holes such as a Schwarzschild black hole [48], a non-rotating black hole [49], a dirty black hole [50], a Kerr-Newman black hole [51], a Myers-Perry black hole [52], and a dRGT black hole [46]. The rigorous bounds on the greybody factors are given by

$$T \geq \text{sech}^2 \left(\int_{-\infty}^{\infty} \vartheta dr_* \right), \quad (54)$$

where

$$\vartheta = \frac{\sqrt{[h'(r_*)]^2 + [\omega^2 - V(r_*) - h^2(r_*)]^2}}{2h(r_*)}, \quad (55)$$

where $h(r_*)$ is a positive function satisfying $h(-\infty) = h(\infty) = \omega$. See [35] for more details. We select $h = \omega$. Therefore,

$$T \geq \text{sech}^2 \left(\frac{1}{2\omega} \int_{-\infty}^{\infty} |V| dr_* \right). \quad (56)$$

4.1 de Sitter black holes

To obtain the rigorous bound, we use the potential derived in the previous section. For de Sitter black holes, the potential is given by Eq. (50), with $c_1 = c_0 = 0$.

Substituting this potential into Eq. (56), we obtain the rigorous bounds on the greybody factors

$$T \geq T_b = \text{sech}^2 \left[\frac{1}{2\omega c} \left\{ \ell(\ell+1) \left(\frac{1}{\tilde{r}_H} - \frac{1}{\tilde{R}_H} \right) + \tilde{M} \left(\frac{1}{\tilde{r}_H^2} - \frac{1}{\tilde{R}_H^2} \right) + 2\alpha_g c_2 (\tilde{R}_H - \tilde{r}_H) \right\} \right]. \quad (57)$$

The rigorous bounds on the reflection probabilities are given by

$$R \leq \tanh^2 \left[\frac{1}{2\omega c} \left\{ \ell(\ell+1) \left(\frac{1}{\tilde{r}_H} - \frac{1}{\tilde{R}_H} \right) + \tilde{M} \left(\frac{1}{\tilde{r}_H^2} - \frac{1}{\tilde{R}_H^2} \right) + 2\alpha_g c_2 (\tilde{R}_H - \tilde{r}_H) \right\} \right], \quad (58)$$

where, from Eq. (20), \tilde{r}_H and \tilde{R}_H are given by

$$\tilde{r}_H = \frac{6\tilde{M}}{\alpha_m} \cos \left[\frac{1}{3} \cos^{-1}(-\alpha_m) - \frac{2\pi}{3} \right] \quad (59)$$

$$\tilde{R}_H = \frac{6\tilde{M}}{\alpha_m} \cos \left[\frac{1}{3} \cos^{-1}(-\alpha_m) \right]. \quad (60)$$

Since \tilde{r}_H and \tilde{R}_H depend on parameters \tilde{M} and α_m , the structure of T_b depends on the strength of the cosmological constant through the parameter α_m . To see the effect of the cosmological constant qualitatively, let us consider the case $\alpha_m \ll 1$, which means that the effect of the cosmological constant is a correction to the Schwarzschild case. As a result, the horizons can be approximated as

$$\tilde{r}_H \sim 2\tilde{M}, \quad \tilde{R}_H \sim \left(\frac{3\sqrt{3}}{\alpha_m} - 1 \right) \tilde{M}. \quad (61)$$

By substituting these results into Eq. 57, the rigorous bound on the greybody factor for a de Sitter black hole can be approximated as

$$T_b = \text{sech}^2 \left[\frac{1}{2\omega c} \left\{ \frac{\ell(\ell+1)}{\tilde{r}_H} \left(1 - \frac{2|\alpha_m|}{3\sqrt{3}} \right) + \frac{\tilde{M}}{r_H^2} \left(1 - \frac{4\alpha_m^2}{27} \right) - \frac{2\sqrt{3}|\alpha_m|}{9\tilde{M}} \right\} \right]. \quad (62)$$

From this equation, one can see that if $\alpha_m = 0$, the bound for Schwarzschild is recovered. Moreover, for $\alpha_m \neq 0$, the cosmological constant provides a negative correction to the Schwarzschild bound. Therefore, the greybody factor for the de Sitter black hole is greater than one for the Schwarzschild black hole. This is also consistent with the behavior of the potential, since the local maximum of the potential in the de Sitter black hole is always less than one in the Schwarzschild black hole. To confirm this result, we also used a numerical method to

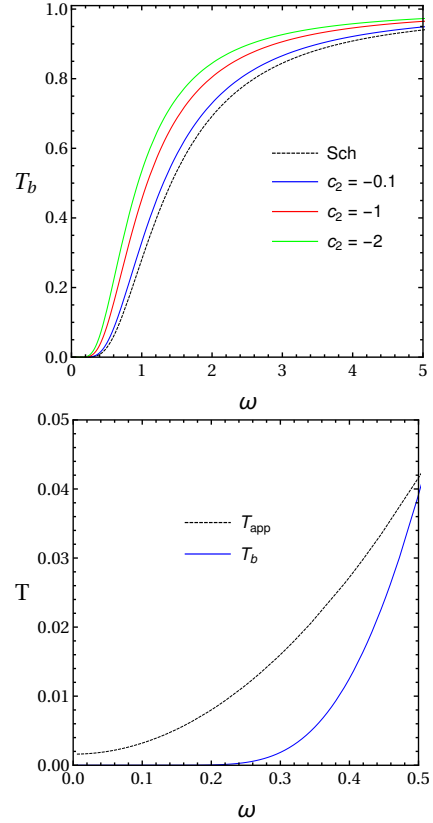


Fig. 6 The left panel shows a comparison between the rigorous bound on the greybody factor for a de Sitter black hole and a Schwarzschild black hole with $\ell = 0$, $c = 1$, and $\tilde{M} = \alpha_g = 0.1$. The right panel shows a comparison between the rigorous bound on the greybody factor and the approximation with $\ell = 0$, $c = 1$, $c_2 = -1$ and $\tilde{M} = \alpha_g = 0.1$.

show that $T_{b(\text{dS})} \geq T_{b(\text{Sch})}$ by plotting T_b with various values of c_2 as illustrated in the left panel of Fig. 6.

The rigorous bound on the greybody factor is useful in any problem, especially in qualitative work. Moreover, the rigorous bound is accurate and its method of derivation is simpler than any other method such as the approximation derived from the matching technique. To see this, let us compare the rigorous bound with the matching technique. The analytical approximation from the matching technique in the low frequency limit for $\ell = 0$ is given by [53, 54]

$$T_{\text{app}} = 4(\kappa r_H)^2 \left(1 + \frac{\omega^2}{\kappa^2} \right) = 4(\kappa \tilde{r}_H)^2 \left(1 + \frac{\omega^2}{\kappa^2} \right), \quad (63)$$

where $\kappa^2 = -\alpha_g c_2 / c^2$. The rigorous bound on the greybody factor and the approximation are plotted as shown in the right panel of Fig. 6. The graph shows that the rigorous bound is less than the approximation, which satisfies the inequality (57).

4.2 dRGT black holes

For dRGT black holes, the potential is given by Eq. (50). Substituting this potential into Eq. (56), we obtain the rigorous bounds on the greybody factors

$$T \geq \text{sech}^2 \left[\frac{1}{2\omega c} \left\{ \ell(\ell+1) \left(\frac{1}{\tilde{r}_H} - \frac{1}{\tilde{R}_H} \right) + \tilde{M} \left(\frac{1}{\tilde{r}_H^2} - \frac{1}{\tilde{R}_H^2} \right) + 2\alpha_g c_2 (\tilde{R}_H - \tilde{r}_H) - \alpha_g c_1 \ln \left| \frac{\tilde{R}_H}{\tilde{r}_H} \right| \right\} \right]. \quad (64)$$

The rigorous bounds on the reflection probabilities are given by

$$R \leq \tanh^2 \left[\frac{1}{2\omega c} \left\{ \ell(\ell+1) \left(\frac{1}{\tilde{r}_H} - \frac{1}{\tilde{R}_H} \right) + \tilde{M} \left(\frac{1}{\tilde{r}_H^2} - \frac{1}{\tilde{R}_H^2} \right) + 2\alpha_g c_2 (\tilde{R}_H - \tilde{r}_H) - \alpha_g c_1 \ln \left| \frac{\tilde{R}_H}{\tilde{r}_H} \right| \right\} \right], \quad (65)$$

where, from Eqs. (31) and (32), $\tilde{r}_H = \tilde{r}_{dS1}$ and $\tilde{R}_H = \tilde{r}_{dS2}$ are given by

$$\tilde{r}_{dS1} = \frac{-2}{(-2c_2)^{1/3}} \left[X^{1/2} \cos \left(\frac{1}{3} \sec^{-1} Y + \frac{\pi}{3} \right) + 1 \right], \quad (66)$$

$$\tilde{r}_{dS2} = \frac{2}{(-2c_2)^{1/3}} \left[X^{1/2} \cos \left(\frac{1}{3} \sec^{-1} Y \right) - 1 \right]. \quad (67)$$

From Eq. (64), we find that the rigorous bound on the greybody factor in massive gravity crucially depends on two parameters, c_1 and c_2 , which determines how the structure of the graviton mass affects the bound. As we have discussed in Section 3, the parameter c_1 must be positive in order to have two horizons. Therefore, the last term in Eq. (64) always provides the negative correction to the bound, so that, for the potentials with the same height, the bound from the dRGT black hole is always larger than the bound from the de Sitter black hole. Moreover, this behavior can be qualitatively expressed by analyzing the potential for both cases. From Fig. 4, for the potentials with the same height, the potential from the dRGT case is always thinner than one from the de Sitter case. Therefore, the transmission amplitude for the dRGT case is always greater than one for the de Sitter case as seen in the left panel of Fig. 7. As we have analyzed earlier, the height of the potential can be controlled by two parameters, β_m and c_2 . Now let us figure out how the parameters affect the dRGT bound compared to the de Sitter bound.

By fixing c_2 , one can see that the bound crucially depends on $|\tilde{R}_H - \tilde{r}_H|$, which is proportional to $1/\beta_m$. Therefore, one finds that the larger the value of β_m , the higher is the value of the bound. This can be seen explicitly by numerically plotting T_b with various values of β_m as illustrated in the right panel of Fig. 7. Moreover, this behavior can also be seen by analyzing the potential. From Fig. 4, we found that the larger the value of β_m , the lower is the peak of the potential. Therefore, one finds that the larger the value of β_m , the higher is the value of the bound.

In terms of fixing β_m , one can see that the maximum value of the potential decreases when $|c_2|$ decreases as such that the bound will increase when $|c_2|$ decreases as shown in the left panel of Fig. 8. Moreover, to compare the bound from the dRGT black hole to one from the de Sitter and the Schwarzschild black hole, we also plot the bound by fixing ω as seen in the right panel of Fig. 8. From this figure, we found that the bound from the dRGT black hole can be larger or smaller than ones from both the de Sitter and the Schwarzschild black holes, depending on c_2 . On the other hand, the bound from the de Sitter black hole is always larger than the bound from the Schwarzschild black hole. Therefore, it is found that there is more room for the dRGT black hole to increase or decrease the greybody factor.

5 Conclusion

In this paper, we obtain the gravitational potential from Schwarzschild black holes, de Sitter black holes, and dRGT black holes. We also derive the rigorous bound on the greybody factor for the de Sitter black hole and the dRGT black hole. It is found that the structure of potentials determines how much the rigorous bound on the greybody factor should be. Since V_{max} contributed from a de Sitter black hole is always less than one in a Schwarzschild black hole, the bound for a de Sitter black hole is greater than one for a Schwarzschild black hole. In case of potentials with the same height, the result shows that the bound from a dRGT black hole is always larger than the bound from a de Sitter black hole. Otherwise, the bound from a dRGT black hole can be larger or smaller than ones from both de Sitter and Schwarzschild black holes due to different effects of the parameter c_2 on de Sitter and dRGT spacetimes. Furthermore, we compare the greybody factor derived from the rigorous bound with the greybody factor derived from the matching technique. The results show that the greybody factor obtained from the rigorous bound is less than the one from the matching technique, which means that the rigorous bound is a true lower bound.

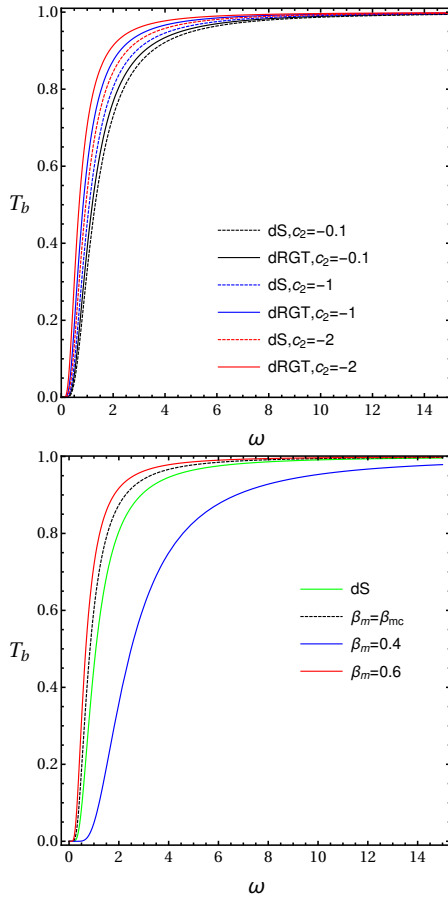


Fig. 7 The left panel shows a comparison of the rigorous bound of greybody factor for the dRGT and the de Sitter black holes with $\ell = 0$, $\tilde{M} = \alpha_g = 0.1$, while the parameter β_m is chosen to have the same height of potential. The right panel shows the rigorous bound for $c_2 = -1$.

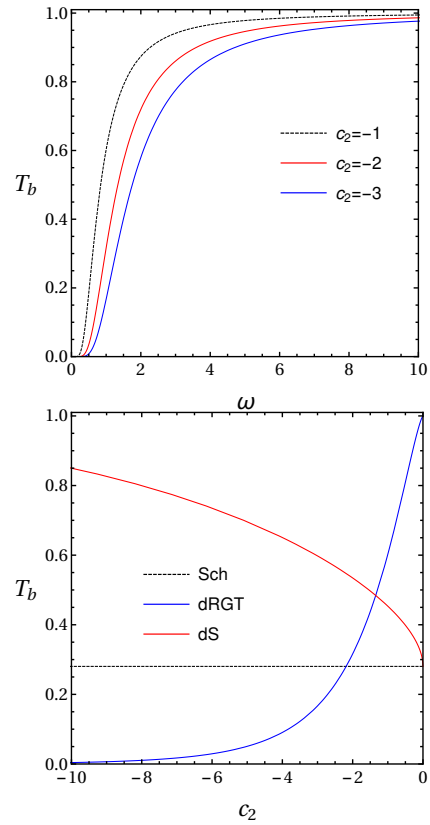


Fig. 8 The left panel shows the effect of parameter c_2 on the rigorous bound on the greybody factor for a dRGT black hole with $\ell = 0$, $\tilde{M} = \alpha_g = 0.1$, and $\beta_m = 0.565375$. The right panel shows a comparison of the rigorous bound on the greybody factor for a dRGT black hole with $\tilde{M} = \alpha_g = 0.1$, $\omega = 1$, and $\beta_m = 0.565375$.

Acknowledgements This project was funded by the Ratchadapisek Sompoch Endowment Fund, Chulalongkorn University (Sci-Super 2014-032), by a grant for the professional development of new academic staff from the Ratchadapisek Somphot Fund at Chulalongkorn University, by the Thailand Research Fund (TRF), and by the Office of the Higher Education Commission (OHEC), Faculty of Science, Chulalongkorn University (RSA5980038). PB was additionally supported by a scholarship from the Royal Government of Thailand. TN was also additionally supported by a scholarship from the Development and Promotion of Science and Technology Talents Project (DPST). PW was also additional supported by the Naresuan University Research Fund through grant No. R2559C235 and the ICTP through grant No. OEA-NET-01.

References

1. Supernova Search Team Collaboration, A. G. Riess et al., *Astron. J.* **116**, 1009-1038 (1998), [arXiv:astro-ph/9805201].
2. Supernova Cosmology Project Collaboration, S. Perlmutter et al., *Astrophys. J.* **517**, 565-586 (1999), [arXiv:astro-ph/9812133].
3. T. Clifton, P. G. Ferreira, A. Padilla, and C. Skordis, *Physics Reports* **513**, 1-189 (2012), [arXiv:1106.2476 [astro-ph.CO]].
4. C. de Rham, G. Gabadadze, *Phys. Rev. D* **82**, 044020 (2010), [arXiv: 1007.0443 [hep-th]].
5. C. de Rham, G. Gabadadze, and A. J. Tolley, *Phys. Rev. Lett.* **106**, 231101 (2011), [arXiv: 1011.1232 [hep-th]].
6. C. de Rham, *Living Rev. Relativity* **17**, 7 (2014), [arXiv:1401.4173 [hep-th]].
7. G. D'Amico, C. de Rham, S. Dubovsky, G. Gabadadze, D. Pirtskhalava and A. J. Tolley, *Phys. Rev. D* **84**, 124046 (2011) [arXiv:1108.5231 [hep-th]].
8. A. E. Gumrukcuoglu, C. Lin and S. Mukohyama, *JCAP* **1111**, 030 (2011) [arXiv:1109.3845 [hep-th]].
9. A. E. Gumrukcuoglu, K. Hinterbichler, C. Lin, S. Mukohyama and M. Trodden, *Phys. Rev. D* **88**, 024023 (2013) [arXiv:1304.0449 [hep-th]].
10. G. D'Amico, G. Gabadadze, L. Hui and D. Pirtskhalava, *Class. Quant. Grav.* **30**, 184005 (2013) [arXiv:1304.0723 [hep-th]].
11. T. Chullaphan, L. Tannukij and P. Wongjun, *JHEP* **06**, 038 (2015) [arXiv:1502.08018 [gr-qc]].
12. A. De Felice and S. Mukohyama, *Phys. Lett. B* **728**, 622 (2014) doi:10.1016/j.physletb.2013.12.041 [arXiv:1306.5502 [hep-th]].
13. A. De Felice, A. Emir Gumrukcuoglu and S. Mukohyama, *Phys. Rev. D* **88**, no. 12, 124006 (2013)

- doi:10.1103/PhysRevD.88.124006 [arXiv:1309.3162 [hep-th]].
14. L. Tannukij and P. Wongjun, *Eur. Phys. J. C* **76**, no. 1, 17 (2016) doi:10.1140/epjc/s10052-015-3872-0 [arXiv:1511.02164 [gr-qc]].
 15. E. Babichev and R. Brito, *Class. Quant. Grav.* **32**, 154001 (2015) doi:10.1088/0264-9381/32/15/154001 [arXiv:1503.07529 [gr-qc]].
 16. M. S. Volkov, *Class. Quant. Grav.* **30**, 184009 (2013), [arXiv: 1304.0238 [hep-th]].
 17. G. Tasinato, K. Koyama, and G. Niz, *Class. Quant. Grav.* **30**, 184002 (2013), [arXiv: 1304.0601 [hep-th]].
 18. S. G. Ghosh, L. Tannukij and P. Wongjun, *Eur. Phys. J. C* **76**, no. 3, 119 (2016) doi:10.1140/epjc/s10052-016-3943-x [arXiv:1506.07119 [gr-qc]].
 19. A. Salam and J. A. Strathdee, *Phys. Rev. D* **16**, 2668 (1977)
 20. D. Zou, R. Yue, and M. Zhang, *Eur. Phys. J. C* **77**, 256 (2017), [arXiv:1612.08056 [gr-qc]].
 21. D. Zou, Y. Liu, and R. Yue, [arXiv:1702.08118 [gr-qc]].
 22. S. H. Hendi, R. B. Mann, S. Panahiyan, and B. E. Panah, *Phys. Rev. D* **95**, 021501(R) (2017), [arXiv:1702.00432 [gr-qc]].
 23. S. H. Hendi, G. Q. Li, J. X. Mo, S. Panahiyan, and B. E. Panah, *Eur. Phys. J. C* **76**, 571 (2016), [arXiv:1608.03148 [gr-qc]].
 24. S. H. Hendi, B. E. Panah, S. Panahiyan, *JHEP* **05**, 029 (2016), [arXiv:1604.00370 [hep-th]].
 25. P. Kanti, T. Pappas, and N. Pappas, *Phys. Rev. D* **90**, 124077 (2014), [arXiv: 1409.8664[hep-th]].
 26. K. Koyama, G. Niz, and G. Tasinato, *Phys. Rev. Lett.* **107**, 131101 (2011), [arXiv: 1103.4708 [hep-th]].
 27. K. Koyama, G. Niz, and G. Tasinato, *Phys. Rev. D* **84**, 064033 (2011) [arXiv: 1104.2143 [hep-th]].
 28. S. W. Hawking, *Commun. Math. Phys.* **43**, 199 (1975)
 29. S. Fernando, *Gen. Relativ. Gravit.* **37**, 461 (2005)
 30. W. Kim and J. J. Oh, *JKPS* **52**, 986 (2008)
 31. J. Escobedo, “Greybody Factors Hawking Radiation in Disguise”, Masters Thesis, University of Amsterdam (2008).
 32. M. K. Parikh and F. Wilczek, *Phys. Rev. Lett.* **85**, 5042 (2000), [arXiv: hep-th/9907001].
 33. C. H. Fleming, (2005) <http://www.physics.umd.edu/grt/taj/776b/fleming.pdf>.
 34. P. Lange, “Calculation of Hawking Radiation as Quantum Mechanical Tunneling”, Thesis, Uppsala Universitet (2007).
 35. M. Visser, *Phys. Rev. A* **59**, 427438 (1999), [arXiv: quant-ph/9901030].
 36. P. Boonserm and M. Visser, *Annals Phys.* **323**, 2779 (2008), [arXiv: 0801.0610 [quant-ph]].
 37. P. Boonserm, “Rigorous Bounds on Transmission, Reflection, and Bogoliubov Coefficients”, Ph. D. Thesis, Victoria University of Wellington (2009), [arXiv: 0907.0045 [mathph]].
 38. H. Zhang and X. Z. Li, *Phys. Rev. D* **93**, 124039 (2016)
 39. S. H. Hendi, R. B. Mann, S. Panahiyan, and B. E. Panah, *Phys. Rev. D* **95**, 021501(R) (2017)
 40. M. Barriola and A. Vilenkin, *Phys. Rev. Lett.* **63**, 341 (1989)
 41. Q. Huang, J. Chen and Y. Wang, *Int. J. Theor. Phys.* **54**, no. 2, 459 (2015) [arXiv:1408.6901 [gr-qc]].
 42. T. Tamaki and N. Sakai, *Phys. Rev. D* **69**, 044018 (2004) [gr-qc/0309068].
 43. H. Kodama and I. Arraut, *Prog. Theor. Exp. Phys.*, 023E02 (2014), [arXiv:1312.0370 [hep-th]].
 44. A. I. Vainshtein, *Phys. Lett. B* **39**, 393 (1972)
 45. I. Arraut, *Int. J. Mod. Phys. D* **24**, 1550022 (2015), [arXiv:1311.0732 [gr-qc]].
 46. T. Ngampitipan, P. Boonserm, and P. Wongjun, *AJPA* **4**, 64 (2016)
 47. T. Ngampitipan, “Rigorous bounds on greybody factors for various types of black holes”, Ph. D. Thesis, Chulalongkorn University (2014).
 48. P. Boonserm and M. Visser, *Phys. Rev. D* **78**, 101502 (2008), [arXiv: 0806.2209 [gr-qc]].
 49. T. Ngampitipan and P. Boonserm, *Int. J. Mod. Phys. D* **22**, 1350058 (2013), [arXiv: 1211.4070 [math-ph]].
 50. P. Boonserm, T. Ngampitipan and M. Visser, *Phys. Rev. D* **88**, 041502 (2013), [arXiv: 1305.1416 [gr-qc]].
 51. P. Boonserm, T. Ngampitipan, and M. Visser, *JHEP* **113**, (2014), [arXiv: 1401.0568 [gr-qc]].
 52. P. Boonserm, A. Chatrabhuti, T. Ngampitipan and M. Visser, *J. Math. Phys.* **55**, 112502 (2014) doi:10.1063/1.4901127 [arXiv:1405.5678 [gr-qc]].
 53. T. Harmark, J. Natario, and R. Schiappa, *Adv. Theor. Math. Phys.* **14**, 727 (2010), [arXiv: 0708.0017[hep-th]].
 54. R. Dong and D. Stojkovic, *Phys. Rev. D* **92**, 084045 (2015), [arXiv: 1505.03145[gr-qc]].

icmss2018

Gmail

Move to Inbox

More

COMPOSE

Fwd: ICMSS2018: Decision on Manuscript #DE-9121

Inbox x

Inbox

Starred

Important

Sent Mail

Drafts

Categories

[Gmail]Trash

Notes

Personal

Travel

More

Tritos Ngampitipan <tritos.ngampitipan@gmail.com>

to me

----- Forwarded message -----

From: **ICMSS2018 / UPM** <icmss2018@upm.edu.my>

Date: 2018-03-01 9:34 GMT+07:00

Subject: ICMSS2018: Decision on Manuscript #DE-9121

To: tritos.ngampitipan@gmail.com

Dear Dr. Tritos Ngampitipan,

Greetings from ICMSS2018!

We are pleased to inform you that your manuscript **#DE-9121**, entitled

has been accepted by our reviewers and scientific committee, provided **minor revision** of the manuscript are made to your manuscript.

We look forward to receiving the revised manuscript, together with a letter of response to each modification made,

Regards,
SECRETARIAT OF ICMSS2018
Department of Mathematics
Faculty of Science
Universiti Putra Malaysia

icmss2018@upm.edu.my
<http://einspem.upm.edu.my/icmss2018>

2 Attachments

INTERNATIONAL CONFERENCE
ON MATHEMATICAL SCIENCES
AND STATISTICS 2018

UPM ICMSS2018
AN INTERNATIONAL CONFERENCE
ON MATHEMATICAL SCIENCES
AND STATISTICS 2018
PUTRAJAYA, MALAYSIA

Manuscript ID : 08-0021
Manuscript Title : The various techniques for generating perfect fluid sphere
Reviewer ID :
Date Sent : 29 January 2018
Date Due : 12 February 2018

Dear Reviewer:
Please review the attached manuscript that has been submitted to the 8th International Conference on Mathematical Sciences and Statistics (ICMSS2018). This is a double blind review, neither your identity nor the author's is revealed. Please return only the completed evaluation form to the scientific committee via email.

Section 1: General Observation (Please use " " in the relevant box)

PDF MEF_DE-9121_R..

INTERNATIONAL CONFERENCE
ON MATHEMATICAL SCIENCES
AND STATISTICS 2018

UPM ICMSS2018
AN INTERNATIONAL CONFERENCE
ON MATHEMATICAL SCIENCES
AND STATISTICS 2018
PUTRAJAYA, MALAYSIA

Manuscript ID : 08-0021
Manuscript Title : The various techniques for generating perfect fluid sphere
Reviewer ID :
Date Sent : 29 January 2018
Date Due : 12 February 2018

Dear Reviewer:
Please review the attached manuscript that has been submitted to the 8th International Conference on Mathematical Sciences and Statistics (ICMSS2018). This is a double blind review, neither your identity nor the author's is revealed. Please return only the completed evaluation form to the scientific committee via email.


Section 1: General Observation (Please use " " in the relevant box)

PDF MEF_DE-9121_R..

https://mail.google.com/mail/u/0/#search/icmss2018/161e4c3ecac98066

1/1

The exponential metric represents a traversable wormhole

Petarpa Boonserm^{1,2}, **Tritos Ngampitipan**³,
Alex Simpson⁴, and **Matt Visser**⁴ 

¹ *Department of Mathematics and Computer Science, Faculty of Science,
Chulalongkorn University, Bangkok 10330, Thailand.*

² *Thailand Center of Excellence in Physics, Ministry of Education,
Bangkok 10400, Thailand.*

³ *Faculty of Science, Chandrakasem Rajabhat University, Bangkok 10900, Thailand.*

⁴ *School of Mathematics and Statistics, Victoria University of Wellington,
PO Box 600, Wellington 6140, New Zealand*

E-mail: petarpa.boonserm@gmail.com; tritos.ngampitipan@gmail.com;
alex.simpson@sms.vuw.ac.nz; matt.visser@sms.vuw.ac.nz

ABSTRACT:

For various reasons a number of authors have mooted an “exponential form” for the spacetime metric:

$$ds^2 = -e^{-2m/r} dt^2 + e^{+2m/r} \{dr^2 + r^2(d\theta^2 + \sin^2 \theta d\phi^2)\}.$$

While the weak-field behaviour matches nicely with weak-field general relativity, and so also automatically matches nicely with the Newtonian gravity limit, the strong-field behaviour is markedly different. Proponents of these exponential metrics have very much focussed on the absence of horizons — it is certainly clear that this geometry does not represent a black hole. However, the proponents of these exponential metrics have failed to note that instead one is dealing with a traversable wormhole — with all of the interesting and potentially problematic features that such an observation raises. If one wishes to replace all the black hole candidates astronomers have identified with traversable wormholes, then certainly a careful phenomenological analysis of this quite radical proposal should be carried out.

DATE: 10 May 2018; 17 May 2018; 21 May 2018; L^AT_EX-ed May 22, 2018

KEYWORDS: exponential metric; traversable wormholes; black holes.

PACS: 04.20.-q; 04.20.-q; 04.20.Jb; 04.70.Bw

Contents

1	Introduction	2
2	Traversable wormhole throat	3
3	Comparison: Exponential versus Schwarzschild	3
3.1	Isotropic coordinates	3
3.2	Curvature coordinates	4
4	Curvature tensor	6
5	Ricci convergence conditions	7
6	Effective refractive index — lensing properties	8
7	ISCO (innermost stable circular orbit) and photon sphere	10
8	Regge–Wheeler equation	13
8.1	Spin zero	15
8.2	Spin one	16
8.3	Spin two	17
9	GR interpretation for the exponential metric	18
10	Discussion	19

1 Introduction

The so-called “exponential metric”

$$ds^2 = -e^{-2m/r} dt^2 + e^{+2m/r} \{dr^2 + r^2(d\theta^2 + \sin^2 \theta d\phi^2)\}, \quad (1.1)$$

has now been in circulation for some 60 years [1–19]; at least since 1958. Motivations for considering this metric vary quite markedly, (even between different papers written by the same author), and the theoretical “justifications” advanced for considering this particular space-time metric are often rather dubious. Nevertheless a small segment of the community has consistently advocated for this particular spacetime metric for over 60 years, with significant activity continuing up to the present day. Regardless of one’s views regarding the purported theoretical “justifications” for this metric, one can simply take this metric as given, and then try to understand its phenomenological properties; some of which are significantly problematic.

A particularly attractive feature of this exponential metric is that in weak fields, ($2m/r \ll 1$), one has

$$ds^2 = \{-dt^2 + dr^2 + r^2(d\theta^2 + \sin^2 \theta d\phi^2)\} + \frac{2m}{r} \{dt^2 + dr^2 + r^2(d\theta^2 + \sin^2 \theta d\phi^2)\}. \quad (1.2)$$

That is

$$g_{ab} = \eta_{ab} + \frac{2m}{r} \delta_{ab}. \quad (1.3)$$

This exactly matches the lowest-order weak-field expansion of general relativity, and so this exponential metric will automatically pass all of the standard lowest-order weak-field tests of general relativity. However strong-field behaviour, ($2m/r \gg 1$), and even medium-field behaviour, ($2m/r \sim 1$), is markedly different.

The exponential metric has no horizons, $g_{tt} \neq 0$, and so is not a black hole. On the other hand, it does not seem to have been previously remarked that the exponential metric describes a traversable wormhole in the sense of Morris and Thorne [20–45]. We shall demonstrate that the exponential metric has a wormhole throat at $r = m$, with the region $r < m$ corresponding to an infinite-volume “other universe” that exhibits the “underhill effect”; time runs slower on the other side of the wormhole throat.

2 Traversable wormhole throat

Consider the area of the spherical surfaces of constant r coordinate:

$$A(r) = 4\pi r^2 e^{2m/r}. \quad (2.1)$$

Then

$$\frac{dA(r)}{dr} = 8\pi(r - m)e^{2m/r}; \quad (2.2)$$

and

$$\frac{d^2 A(r)}{dr^2} = 8\pi e^{2m/r} \left(1 - \frac{2m}{r} + \frac{2m^2}{r^2}\right) = 8\pi e^{2m/r} \left\{ \left(1 - \frac{m}{r}\right)^2 + \frac{m^2}{r^2} \right\} > 0. \quad (2.3)$$

That is: The area is a concave function of the r coordinate, and has a minimum at $r = m$, where it satisfies the “flare out” condition $A''|_{r=m} = +8\pi e^2 > 0$. Furthermore, all metric components are finite at $r = m$, and the diagonal components are non-zero. This is sufficient to guarantee that the surface $r = m$ is a traversable wormhole throat, in the sense of Morris and Thorne [20–45]. There is a rich phenomenology of traversable wormhole physics that has been developed over the last 30 years, (since the Morris-Thorne paper [20]), much of which can be readily adapted (*mutatis mutandi*) to the exponential metric.

3 Comparison: Exponential versus Schwarzschild

Let us briefly compare the exponential and Schwarzschild metrics.

3.1 Isotropic coordinates

In isotropic coordinates the Schwarzschild spacetime is

$$ds_{\text{Sch}}^2 = - \left(\frac{1 - \frac{m}{2r}}{1 + \frac{m}{2r}} \right)^2 dt^2 + \left(1 + \frac{m}{2r} \right)^4 \{ dr^2 + r^2(d\theta^2 + \sin^2 \theta d\phi^2) \}, \quad (3.1)$$

which we should compare with the exponential metric in isotropic coordinates

$$ds^2 = -e^{-2m/r} dt^2 + e^{+2m/r} \{ dr^2 + r^2(d\theta^2 + \sin^2 \theta d\phi^2) \}. \quad (3.2)$$

It is clear that in the Schwarzschild spacetime there is a horizon present at $r = \frac{m}{2}$. Recalling that the domain for the r -coordinate in the isotropic coordinate system for Schwarzschild is $r \in (0, +\infty)$, we see that the horizon also corresponds to where the area of spherical constant- r surfaces is minimised:

$$A(r) = 4\pi r^2 \left(1 + \frac{m}{2r}\right)^4; \quad (3.3)$$

$$(3.4)$$

$$\frac{dA(r)}{dr} = 8\pi r \left(1 - \frac{m}{2r}\right) \left(1 + \frac{m}{2r}\right)^3; \quad (3.5)$$

$$(3.6)$$

$$\frac{d^2 A(r)}{dr^2} = 8\pi \left(1 + \frac{m}{2r}\right)^2 \left(\frac{3}{4} \left(\frac{m}{r}\right)^2 - \frac{m}{r} + 1\right). \quad (3.7)$$

So for the Schwarzschild geometry in isotropic coordinates the area has a minimum at $r = \frac{m}{2}$, where $A'|_{r=\frac{m}{2}} = 0$, and $A''|_{r=\frac{m}{2}} = 64\pi > 0$. While this satisfies the “flare-out” condition the corresponding wormhole (the Einstein–Rosen bridge) is *non-traversable* due to the presence of the horizon.

In contrast the geometry described by the exponential metric clearly has no horizons, since $\forall r \in (0, +\infty)$ we have $\exp\left(\frac{-2m}{r}\right) \neq 0$. As already demonstrated, there is a traversable wormhole throat located at $r = m$, where the area of the spherical surfaces is minimised, and the “flare out” condition is satisfied, in the *absence* of a horizon. Thus the Schwarzschild horizon at $r = \frac{m}{2}$ in isotropic coordinates is replaced by a wormhole throat at $r = m$ in the exponential metric.

Furthermore, for the exponential metric, since $\exp\left(\frac{-2m}{r}\right) > 0$ is monotone decreasing as $r \rightarrow 0$, it follows that proper time evolves increasingly slowly as a function of coordinate time as one moves closer to the centre $r \rightarrow 0$.

3.2 Curvature coordinates

To go to so-called “curvature coordinates”, (often called “Schwarzschild curvature coordinates”), for the exponential metric we make the coordinate transformation

$$r_s = r e^{m/r}; \quad dr_s = e^{m/r} (1 - m/r) dr. \quad (3.8)$$

So for the exponential metric in curvature coordinates

$$ds^2 = -e^{-2m/r} dt^2 + \frac{dr_s^2}{(1 - m/r)^2} + r_s^2(d\theta^2 + \sin^2 \theta d\phi^2). \quad (3.9)$$

Here r is regarded as an implicit function of r_s . Note that as the isotropic coordinate r ranges over the interval $(0, \infty)$, the curvature coordinate r_s has a minimum at $r_s = m e$. In fact for the exponential metric the curvature coordinate r_s double-covers the interval $r_s \in [m e, \infty)$, first descending from ∞ to $m e$ and then increasing again to ∞ . Indeed, looking for the minimum of the coordinate r_s :

$$\frac{dr_s}{dr} = e^{\frac{m}{r}} \left(1 - \frac{m}{r}\right) \implies \left. \frac{dr_s}{dr} \right|_{r=m} = 0. \quad (3.10)$$

So we have a stationary point at $r = m$, which corresponds to $r_s = m e$, and furthermore

$$\frac{d^2 r_s}{dr^2} = \frac{m^2}{r^3} e^{\frac{m}{r}} \implies \left. \frac{d^2 r_s}{dr^2} \right|_{r=m} > 0. \quad (3.11)$$

The curvature coordinate r_s therefore has a minimum at $r_s = m e$, and in these curvature coordinates the exponential metric exhibits a wormhole throat at $r_s = m e$.

Compare this with the Schwarzschild metric in curvature coordinates:

$$ds_{\text{Sch}}^2 = -(1 - 2m/r_s) dt^2 + \frac{dr_s^2}{1 - 2m/r_s} + r_s^2(d\theta^2 + \sin^2 \theta d\phi^2). \quad (3.12)$$

By inspection it is clear that there is a horizon at $r_s = 2m$, since at that location $g_{tt}|_{r_s=2m} = 0$. For the Schwarzschild metric the isotropic and curvature coordinates are related by $r_s = r \left(1 + \frac{m}{2r}\right)^2$.

If for the exponential metric one really wants the fully explicit inversion of r as a function of r_s , then observe

$$r = r_s \exp(W(-m/r_s)) = -\frac{m}{W(-m/r_s)}. \quad (3.13)$$

Here $W(x)$ is “appropriate branch” of the Lambert W function — implicitly defined by the relation $W(x) e^{W(x)} = x$. This function has a convoluted 250-year history; only recently has it become common to view it as one of the standard “special functions” [46]. Applications vary [46, 47], including combinatorics (enumeration of rooted trees) [46], delay differential equations [46], falling objects subject to linear drag [48], evaluating the numerical constant in Wien’s displacement law [49, 50], quantum statistics [51], the distribution of prime numbers [52], constructing the “tortoise” coordinate for Schwarzschild black holes [53], *etcetera*.

In terms of the W function and the curvature coordinate r_s the explicit version of the exponential metric becomes

$$ds^2 = -e^{2W(-m/r_s)} dt^2 + \frac{dr_s^2}{(1 + W(-m/r_s))^2} + r_s^2(d\theta^2 + \sin^2 \theta d\phi^2). \quad (3.14)$$

The $W_0(x)$ branch corresponds to the region $r > m$ outside the wormhole throat; whereas the $W_{-1}(x)$ branch corresponds to the region $r < m$ inside the wormhole. The Taylor series for $W_0(x)$ for $|x| < e^{-1}$ is [46]

$$W_0(x) = \sum_{n=1}^{\infty} \frac{(-n)^{n-1} x^n}{n!}. \quad (3.15)$$

A key asymptotic formula for $W_{-1}(x)$ is [46].

$$W_{-1}(x) = \ln(-x) - \ln(-\ln(-x)) + o(1); \quad (x \rightarrow 0^-). \quad (3.16)$$

The two real branches meet at $W_0(-1/e) = W_{-1}(-1/e) = -1$, and in the vicinity of that meeting point

$$W(x) = -1 + \sqrt{2(1+ex)} - \frac{2}{3}(1+ex) + O[(1+ex)^{3/2}]. \quad (3.17)$$

More details regarding the Lambert W function can be found in Corless *et al*, see [46].

4 Curvature tensor

The curvature components for the exponential metric (in isotropic coordinates) are easily computed. For the Riemann tensor the non-vanishing components are:

$$R^{tr}_{tr} = -2R^{t\theta}_{t\theta} = -2R^{t\phi}_{t\phi} = \frac{2m(r-m)e^{-2m/r}}{r^4}; \quad (4.1)$$

$$R^{r\theta}_{r\theta} = R^{r\phi}_{r\phi} = -\frac{me^{-2m/r}}{r^3}; \quad (4.2)$$

$$R^{\theta\phi}_{\theta\phi} = \frac{m(2r-m)e^{-2m/r}}{r^4}. \quad (4.3)$$

$$(4.4)$$

For the Weyl tensor the non-vanishing components are even simpler:

$$C^{tr}_{tr} = -2C^{t\theta}_{t\theta} = -2C^{t\phi}_{t\phi} = -2C^{r\theta}_{r\theta} = -2C^{r\phi}_{r\phi} = C^{\theta\phi}_{\theta\phi} = \frac{2}{3} \frac{m(3r - 2m)e^{-2m/r}}{r^4}. \quad (4.5)$$

For the Ricci and Einstein tensors:

$$R^a_b = -\frac{2m^2 e^{-2m/r}}{r^4} \text{diag}\{0, 1, 0, 0\}^a_b; \quad (4.6)$$

$$R = -\frac{2m^2 e^{-2m/r}}{r^4}; \quad (4.7)$$

$$G^a_b = \frac{m^2 e^{-2m/r}}{r^4} \text{diag}\{1, -1, 1, 1\}^a_b. \quad (4.8)$$

For the Kretschmann and other related scalars we have

$$R_{abcd} R^{abcd} = \frac{4m^2(12r^2 - 16mr + 7m^2)e^{-4m/r}}{r^8}; \quad (4.9)$$

$$C_{abcd} C^{abcd} = \frac{16}{3} \frac{m^2(3r - 2m)^2 e^{-4m/r}}{r^8}; \quad (4.10)$$

$$R_{ab} R^{ab} = R^2 = \frac{4m^4 e^{-4m/r}}{r^8}. \quad (4.11)$$

All of the curvature components and scalar invariants exhibited above are finite everywhere in the exponential spacetime — in particular they are finite at the throat ($r = m$) and decay to zero both as $r \rightarrow \infty$ and as $r \rightarrow 0$. They take on maximal values near the throat, at $r = (\text{dimensionless number}) \times m$.

5 Ricci convergence conditions

Since most of the advocates of the exponential metric are typically not working within the framework of general relativity, and typically do not want to enforce the Einstein equations, the standard energy conditions are to some extent moot. In the usual framework of general relativity the standard energy conditions are useful because they feed back into the Raychaudhuri equations and its generalizations, and so give information about the focussing and defocussing of geodesic congruences. In the absence of the Einstein equations one can instead impose conditions directly on the Ricci tensor.

Specifically, a Lorentzian spacetime is said to satisfy the timelike, null, or spacelike Ricci convergence condition if for all timelike, null, or spacelike vectors t^a one has:

$$R_{ab} t^a t^b \geq 0 . \quad (5.1)$$

For the exponential metric one has

$$R_{ab} = -\frac{2m^2}{r^4} \text{diag}\{0, 1, 0, 0\}_{ab}. \quad (5.2)$$

So the Ricci convergence condition amounts to

$$R_{ab} t^a t^b = -\frac{2m^2}{r^4} (t^r)^2 \leq 0. \quad (5.3)$$

This clearly will not be satisfied for all timelike, null, or spacelike vectors t^a . Specifically, the violation of the null Ricci convergence condition is crucial for understanding the flare out at the throat of the traversable wormhole [24].

6 Effective refractive index — lensing properties

The exponential metric can be written in the form

$$ds^2 = e^{2m/r} \{ -e^{-4m/r} dt^2 + \{ dr^2 + r^2(d\theta^2 + \sin^2 \theta d\phi^2) \} \}. \quad (6.1)$$

If we are only interested in photon propagation, then the overall conformal factor is irrelevant, and we might as well work with

$$d\hat{s}^2 = -e^{-4m/r} dt^2 + \{ dr^2 + r^2(d\theta^2 + \sin^2 \theta d\phi^2) \}. \quad (6.2)$$

That is

$$d\hat{s}^2 = -e^{-4m/r} dt^2 + \{ dx^2 + dy^2 + dz^2 \}. \quad (6.3)$$

But this metric has a very simple physical interpretation: It corresponds to a coordinate speed of light $c(r) = e^{-2m/r}$, or equivalently an effective refractive index

$$n(r) = e^{2m/r}. \quad (6.4)$$

This effective refractive index is well defined all the way down to $r = 0$, and (via Fermat's principle of least time) completely characterizes the focussing/defocussing of null geodesics. This notion of “effective refractive index” for the gravitational field has in the weak field limit been considered in [55], and in the strong-field limit falls naturally into the “analogue spacetime” programme [56, 57].

Compare the above with Schwarzschild spacetime in isotropic coordinates where the effective refractive index is

$$n(r) = \frac{(1 + \frac{m}{2r})^3}{|1 - \frac{m}{2r}|}. \quad (6.5)$$

The two effective refractive indices have the same large- r limit, $n(r) \approx 1 + \frac{2m}{r}$, but differ markedly once $r \lesssim m/2$.

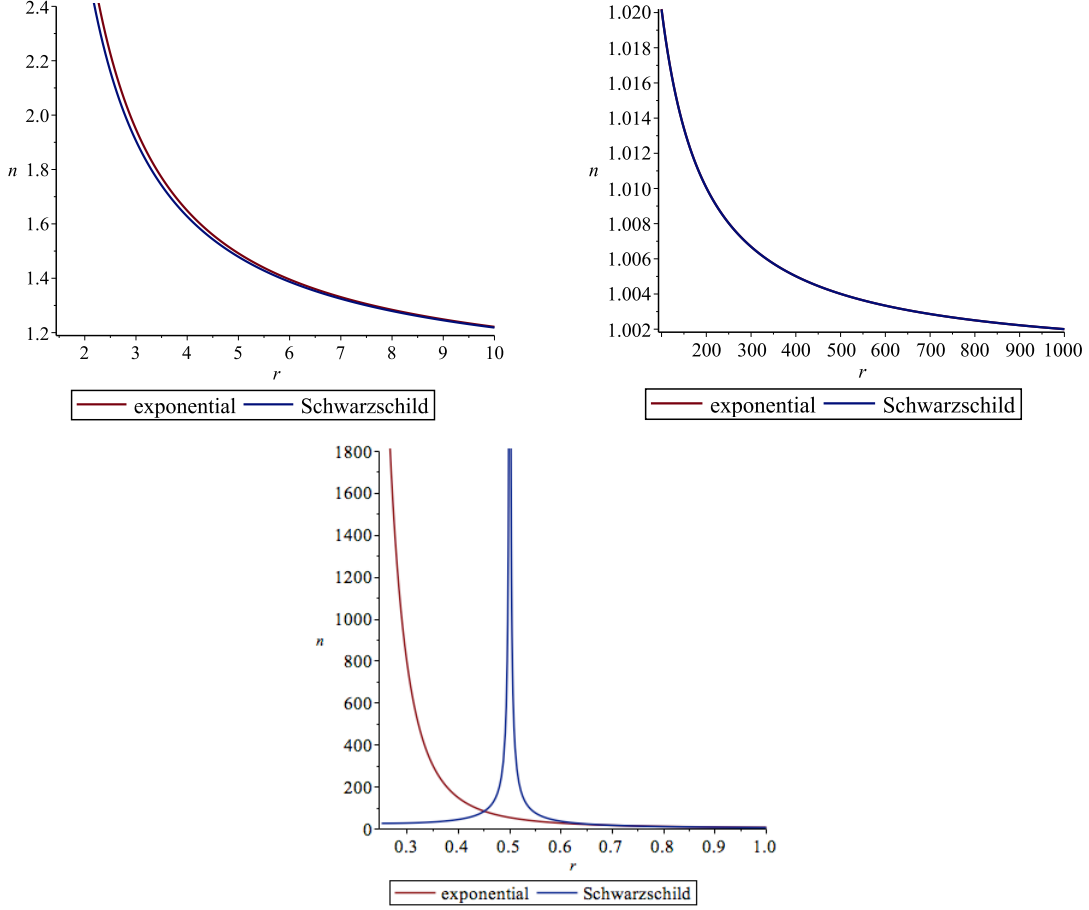


Figure 1. The graph shows the refractive index for the exponential metric compared to the Schwarzschild metric in the isotropic coordinate. The parameter $m = 1$. The left panel is for relatively small $r \gtrsim 2m$ and the right panel is for large r . The bottom panel is for the strong field region $r \sim m/2$.

From the graphs presented in Figure 1, we can see that the refractive index for the exponential metric is greater than that of the Schwarzschild metric in the isotropic coordinate at tolerably small $r \gtrsim 2m$. For large r , they converge to each other and

hence are asymptotically equal. In the strong field region they differ radically. Observationally, once you get close enough to where you would have expected to see the Schwarzschild horizon, the lensing properties differ markedly.

7 ISCO (innermost stable circular orbit) and photon sphere

For massive particles, it is relatively easy to find the innermost stable circular orbit (ISCO) for the exponential metric; while for massless particles such as photons there is a unique unstable circular orbit. These can then be compared with Schwarzschild spacetime. We emphasize that the notion of ISCO depends only on the geodesic equations, not on the assumed field equations chosen for setting up the spacetime. Since Schwarzschild ISCOs for massive particles at $r_s = 6m$ have already been seen by astronomers; this might place interesting bounds somewhat restraining the exponential-metric enthusiasts. Additionally, the Schwarzschild unstable circular photon orbit for massless particles is at $r_s = 3m$ (the photon sphere); the equivalent for the exponential metric is relatively easy to find.

To determine the circular orbits, consider the affinely parameterized tangent vector to the worldline of a massive or massless particle

$$g_{ab} \frac{dx^a}{d\lambda} \frac{dx^b}{d\lambda} = -e^{-2m/r} \left(\frac{dt}{d\lambda} \right)^2 + e^{2m/r} \left\{ \left(\frac{dr}{d\lambda} \right)^2 + r^2 \left[\left(\frac{d\theta}{d\lambda} \right)^2 + \sin^2 \theta \left(\frac{d\phi}{d\lambda} \right)^2 \right] \right\} = \epsilon. \quad (7.1)$$

Here $\epsilon \in \{-1, 0\}$; with -1 corresponding to a timelike trajectory and 0 corresponding to a null trajectory. In view of the spherical symmetry we might as well just set $\theta = \pi/2$ and work with the reduced equatorial problem

$$g_{ab} \frac{dx^a}{d\lambda} \frac{dx^b}{d\lambda} = -e^{-2m/r} \left(\frac{dt}{d\lambda} \right)^2 + e^{2m/r} \left\{ \left(\frac{dr}{d\lambda} \right)^2 + r^2 \left(\frac{d\phi}{d\lambda} \right)^2 \right\} = \epsilon \in \{-1, 0\}. \quad (7.2)$$

The Killing symmetries imply two conserved quantities (energy and angular momentum)

$$e^{-2m/r} \left(\frac{dt}{d\lambda} \right) = E; \quad e^{2m/r} r^2 \left(\frac{d\phi}{d\lambda} \right) = L. \quad (7.3)$$

Thence

$$e^{2m/r} \left\{ -E^2 + \left(\frac{dr}{d\lambda} \right)^2 \right\} + e^{-2m/r} \frac{L^2}{r^2} = \epsilon. \quad (7.4)$$

That is

$$\left(\frac{dr}{d\lambda}\right)^2 = E^2 + e^{-2m/r} \left\{ \epsilon - e^{-2m/r} \frac{L^2}{r^2} \right\}. \quad (7.5)$$

This defines the “effective potential” for geodesic orbits

$$V_\epsilon(r) = e^{-2m/r} \left\{ -\epsilon + e^{-2m/r} \frac{L^2}{r^2} \right\}. \quad (7.6)$$

- For $\epsilon = 0$ (massless particles such as photons), the effective potential simplifies to

$$V_0(r) = \frac{e^{-4m/r} L^2}{r^2}. \quad (7.7)$$

This has a single peak at $r = 2m$ corresponding to $V_{0,max} = \frac{L^2}{(2me)^2}$. This is the only place where $V'_0(r) = 0$, and at this point $V''(r) < 0$. Thus there is an unstable photon sphere at $r = 2m$, corresponding to the curvature coordinate $r_s = 2m e^{1/2} \approx 3.297442542 m$. (This is not too far from what we would expect for Schwarzschild, where the photon sphere is at $r_s = 3m$.)

For extensive discussion on the importance of the photon sphere for astrophysical imaging see for instance references [58–63].

- For $\epsilon = -1$ (massive particles such as atoms, electrons, protons, or planets), the effective potential is

$$V_1(r) = e^{-2m/r} \left\{ 1 + e^{-2m/r} \frac{L^2}{r^2} \right\} = e^{2W(m/r_s)} \left\{ 1 + \frac{L^2}{r_s^2} \right\}. \quad (7.8)$$

It is easy to verify that

$$V'_1(r) = \frac{2e^{-2m/r} (L^2 e^{-2m/r} [2m - r] + mr^2)}{r^4}. \quad (7.9)$$

and that

$$V''_1(r) = \frac{2e^{-2m/r} (L^2 e^{-2m/r} [8m^2 - 12mr + 3r^2] + 2m^2 r^2 - 2mr^3)}{r^6}. \quad (7.10)$$

Circular orbits, denoted r_c , occur at $V'_1(r) = 0$, but there is no simple analytic way of determining $r_c(m, L)$ as a function of m and L . Working more indirectly, by assuming a circular orbit at $r = r_c$, one can solve for the required angular

momentum $L_c(r_c, m)$ as a function of r_c and m . Explicitly:

$$L_c(r_c, m) = \frac{r_c e^{m/r_c} \sqrt{m}}{\sqrt{r_c - 2m}}. \quad (7.11)$$

(Note that at large r_c we have $L_c(r_c, m) \sim \sqrt{mr_c}$ as one would expect from considering circular orbits in Newtonian gravity.) This is enough to tell you that circular orbits for massive particles do exist all the way down to $r_c = 2m$, the location of the unstable photon orbit; but this does not yet guarantee stability. Noting that

$$\frac{\partial L_c(r_c, m)}{\partial r_c} = \frac{e^{m/r_c} (r_c^2 - 6mr_c + 4m^2) \sqrt{m}}{2r_c (r_c - 2m)^{3/2}}, \quad (7.12)$$

we observe that the curve $L_c(r_c, m)$ has a minimum at $r_c = (3 + \sqrt{5})m$ where $L_{\min} \approx 3.523216438m$. (See Figure 2.)

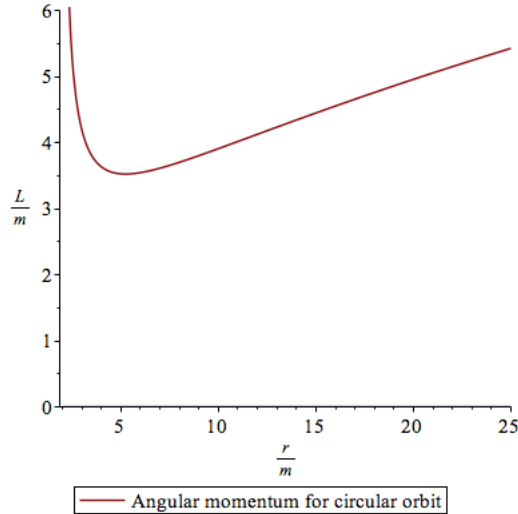


Figure 2. The graph shows the angular momentum L/m required to establish a circular orbit at radius r/m . Note the minimum at $r = (3 + \sqrt{5})m$ where $L_{\min} \approx 3.523216438m$. Circular orbits for $r \geq (3 + \sqrt{5})m$ are stable; whereas circular orbits for $r < (3 + \sqrt{5})m$ are unstable. (Circular orbits for $r < 2m$ do not exist.)

To check stability substitute $L_c(r_c, m)$ into $V''(r)$ to obtain

$$V_1''(r_c) = \frac{2me^{-2m/r_c} (r_c^2 - 6mr_c + 4m^2)}{r_c^4 (r_c - 2m)}. \quad (7.13)$$

This changes sign when $r_c^2 - 6mr_c + 4m^2 = 0$, that is $r_c = (3 \pm \sqrt{5})m$. Only the positive root is relevant (the negative root lies below $r_c = 2m$ where there are no circular orbits, stable or unstable). Consequently we identify the location for the massive particle ISCO (for the exponential metric in isotropic coordinates) as

$$r_{\text{ISCO}} = (3 + \sqrt{5})m \approx 5.236067977m. \quad (7.14)$$

In curvature coordinates

$$r_{s,\text{ISCO}} = (3 + \sqrt{5}) \exp\left\{\frac{1}{4}(3 - \sqrt{5})\right\}m \approx 6.337940263m. \quad (7.15)$$

This is not too far from what would have been expected in Schwarzschild spacetime, where the Schwarzschild geometry ISCO is at $r_{s,\text{ISCO}} = 6m$.

8 Regge–Wheeler equation

Consider now the Regge–Wheeler equation for scalar and vector perturbations around the exponential metric spacetime. We will invoke the inverse Cowling approximation (wherein we keep the geometry fixed while letting the scalar and vector fields oscillate; we do this since we do not *a priori* know the spacetime dynamics). The analysis closely parallels the general formalism developed in [54].

Start from the exponential metric:

$$ds^2 = -e^{-2m/r}dt^2 + e^{+2m/r}\{dr^2 + r^2(d\theta^2 + \sin^2\theta d\phi^2)\}. \quad (8.1)$$

Define a tortoise coordinate by $dr_* = e^{2m/r}dr$ then

$$ds^2 = e^{-2m/r}(-dt^2 + dr_*^2) + e^{+2m/r}r^2(d\theta^2 + \sin^2\theta d\phi^2). \quad (8.2)$$

Here r is now implicitly a function of r_* . We can also write this as

$$ds^2 = e^{-2m/r}(-dt^2 + dr_*^2) + r_s^2(d\theta^2 + \sin^2\theta d\phi^2). \quad (8.3)$$

Using the formalism developed in [54], the Regge–Wheeler equation can be written, (using ∂_* as shorthand for ∂_{r_*}), in the form

$$\partial_*^2 \hat{\phi} + \{\omega^2 - \mathcal{V}\} \hat{\phi} = 0. \quad (8.4)$$

For a general spherically symmetric metric, (specifying the metric components in curvature coordinates), the Regge–Wheeler potential for spins $S \in \{0, 1, 2\}$ and angular momentum $\ell \geq S$ is [54]

$$\mathcal{V}_S = (-g_{tt}) \left[\frac{\ell(\ell+1)}{r_s^2} + \frac{S(S-1)(g^{rr} - 1)}{r_s^2} \right] + (1-S) \frac{\partial_*^2 r_s}{r_s}. \quad (8.5)$$

For the exponential metric in curvature coordinates we have already seen that both $g_{tt} = -e^{-2m/r}$ and $g^{rr} = (1 - m/r)^2$. Therefore

$$\mathcal{V}_S = e^{-2m/r} \left[\frac{\ell(\ell+1)}{r_s^2} + \frac{S(S-1)[(1 - m/r)^2 - 1]}{r_s^2} \right] + (1-S) \frac{\partial_*^2 r_s}{r_s}. \quad (8.6)$$

It is important to realize that both r_s and r occur in the equation above. By noting that $\partial_* = e^{-2m/r} \partial_r$ it is possible to evaluate

$$\frac{\partial_*^2 r_s}{r_s} = \frac{e^{-4m/r} m(2r - m)}{r^4} = -\frac{e^{-4m/r} [(1 - m/r)^2 - 1]}{r^2}, \quad (8.7)$$

and so rephrase the Regge–Wheeler potential as

$$\mathcal{V}_S = e^{-4m/r} \left[\frac{\ell(\ell+1)}{r^2} + \frac{(S^2 - 1)[(1 - m/r)^2 - 1]}{r^2} \right]. \quad (8.8)$$

This is always zero at $r = 0$ and $r = \infty$, with some extrema at non-trivial values of r .

The corresponding result for the Schwarzschild spacetime is

$$\mathcal{V}_{S,\text{Sch}} = \left(1 - \frac{2m}{r_s} \right) \left[\frac{\ell(\ell+1)}{r_s^2} - \frac{S(S-1)2m}{r_s^3} \right] + (1-S) \frac{\partial_*^2 r_s}{r_s}. \quad (8.9)$$

For the Schwarzschild metric $\partial_* = (1 - 2m/r_s) \partial_{r_s}$ and so it is possible to evaluate

$$\frac{\partial_*^2 r_s}{r_s} = \left(1 - \frac{2m}{r_s} \right) \frac{2m}{r_s^3}. \quad (8.10)$$

Then

$$\mathcal{V}_{S,\text{Sch}} = \left(1 - \frac{2m}{r_s} \right) \left[\frac{\ell(\ell+1)}{r_s^2} - \frac{(S^2 - 1)2m}{r_s^3} \right]. \quad (8.11)$$

Converting to isotropic coordinates, which for the Schwarzschild geometry means one

is applying $r_s = r \left(1 + \frac{m}{2r}\right)^2$, we have

$$\mathcal{V}_{S,\text{Sch}} = \left(\frac{1 - \frac{m}{2r}}{1 + \frac{m}{2r}}\right)^2 \left[\frac{\ell(\ell+1)}{r^2 \left(1 + \frac{m}{2r}\right)^4} - \frac{(S^2 - 1)2m}{r^3 \left(1 + \frac{m}{2r}\right)^6} \right]. \quad (8.12)$$

This is always zero at the horizon $r = m/2$ and at $r = \infty$, with some extrema at non-trivial values of r .

8.1 Spin zero

In particular for spin zero one has

$$\begin{aligned} \mathcal{V}_0 &= e^{-2m/r} \frac{\ell(\ell+1)}{r_s^2} + \frac{\partial_*^2 r_s}{r_s} \\ &= e^{-4m/r} \frac{\ell(\ell+1)}{r^2} + \frac{\partial_*^2 r_s}{r_s} \\ &= e^{-4m/r} \left[\frac{\ell(\ell+1) - [(1 - m/r)^2 - 1]}{r^2} \right]. \end{aligned} \quad (8.13)$$

This result can also be readily checked by brute force computation. The corresponding result for Schwarzschild spacetime is

$$\mathcal{V}_{0,\text{Sch}} = \left(\frac{1 - \frac{m}{2r}}{1 + \frac{m}{2r}}\right)^2 \left[\frac{\ell(\ell+1)}{r^2 \left(1 + \frac{m}{2r}\right)^4} + \frac{2m}{r^3 \left(1 + \frac{m}{2r}\right)^6} \right]. \quad (8.14)$$

For scalars the s -wave ($\ell = 0$) is particularly important

$$\mathcal{V}_{0,\ell=0} = e^{-4m/r} \left[\frac{1 - (1 - m/r)^2}{r^2} \right] = e^{-4m/r} \left[\frac{2m}{r^3} \left(1 - \frac{m}{2r}\right) \right]; \quad (8.15)$$

versus

$$\mathcal{V}_{0,\ell=0,\text{Sch}} = \left(\frac{1 - \frac{m}{2r}}{1 + \frac{m}{2r}}\right)^2 \left[\frac{2m}{r^3 \left(1 + \frac{m}{2r}\right)^6} \right]. \quad (8.16)$$

Note that these potentials both have zeros at $r = m/2$ and that for $r < m/2$ only the exponential Regge–Wheeler potential is of physical interest, (thanks to the horizon at $r = m/2$ in the Schwarzschild metric). See Figure 3. The potential peaks are at $r = \left(1 + \frac{1}{\sqrt{3}}\right)m$ and $r = \frac{3m}{2}$ respectively. For the exponential metric there is also a trough (a local minimum) at $r = \left(1 - \frac{1}{\sqrt{3}}\right)m$.

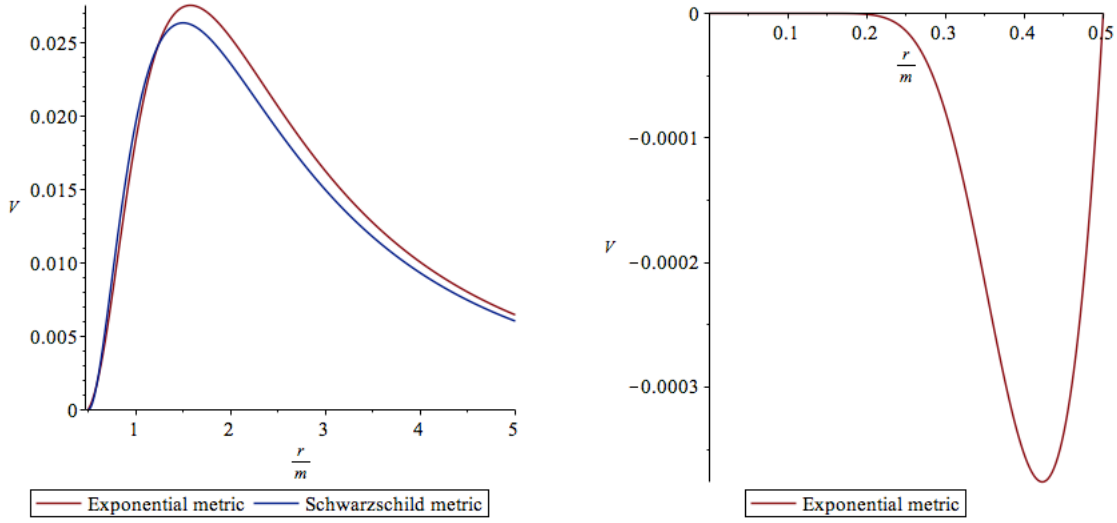


Figure 3. The graph shows the spin zero Regge–Wheeler potential for $\ell = 0$. While the Regge–Wheeler potentials are not dissimilar for $r > m/2$, they are radically different once one goes to small $r < m/2$, (where the Regge–Wheeler potential for Schwarzschild is only formal since one is behind a horizon and cannot interact with the domain of outer communication).

8.2 Spin one

For the spin one vector field the $\{r_s^{-1}\partial_*^2 r_s\}$ term drops out; this can ultimately be traced back to the conformal invariance of massless spin 1 particles in (3+1) dimensions. We are left with the particularly simple result ($\ell \geq 1$)

$$\mathcal{V}_1 = \frac{e^{-4m/r}\ell(\ell+1)}{r^2}. \quad (8.17)$$

See related brief comments regarding conformal invariance in [54]. Note that this rises from zero ($r \rightarrow 0$) to some maximum at $r = 2m$, where $\mathcal{V}_1 \rightarrow \frac{\ell(\ell+1)}{(2me)^2}$ and then decays back to zero ($r \rightarrow \infty$). The corresponding result for Schwarzschild spacetime is

$$\mathcal{V}_{1,\text{Sch}} = \frac{\left(1 - \frac{m}{2r}\right)^2}{\left(1 + \frac{m}{2r}\right)^6} \frac{\ell(\ell+1)}{r^2}. \quad (8.18)$$

Note that this rises from zero (at $r = m/2$) to some maximum at $r = \left(1 + \frac{\sqrt{3}}{2}\right)m$, where $\mathcal{V}_1 \rightarrow \frac{2\ell(\ell+1)}{27m^2}$, and then decays back to zero ($r \rightarrow \infty$). See Figure 4 for qualitative features of the potential.

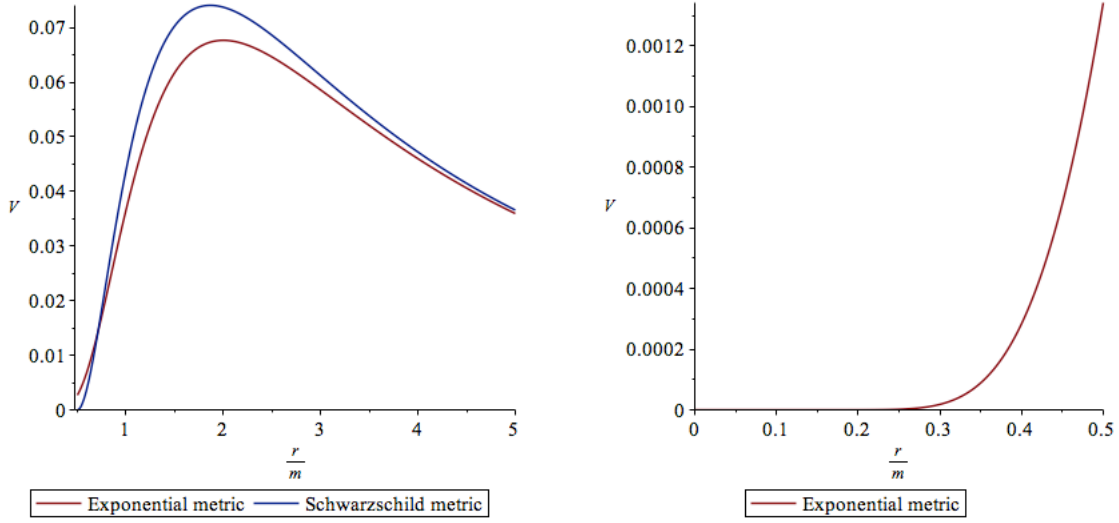


Figure 4. The graph shows the spin one Regge–Wheeler potential for $\ell = 1$. While the Regge–Wheeler potentials are not dissimilar for $r > m/2$, they are radically different once one goes to small $r < m/2$, (where the Regge–Wheeler potential for Schwarzschild is only formal since one is behind a horizon and cannot interact with the domain of outer communication).

8.3 Spin two

For spin two, more precisely for spin 2 axial perturbations, (see [54]) one has ($\ell \geq 2$)

$$\begin{aligned}
 \mathcal{V}_2 &= e^{-2m/r} \frac{\ell(\ell+1)}{r_s^2} - 3 \frac{\partial_*^2 r_s}{r_s} \\
 &= e^{-4m/r} \frac{\ell(\ell+1)}{r^2} - 3 \frac{\partial_*^2 r_s}{r_s} \\
 &= e^{-4m/r} \left[\frac{\ell(\ell+1) + 3[(1 - m/r)^2 - 1]}{r^2} \right].
 \end{aligned} \tag{8.19}$$

The corresponding result for Schwarzschild spacetime is

$$\mathcal{V}_{2,\text{Sch}} = \left(\frac{1 - \frac{m}{2r}}{1 + \frac{m}{2r}} \right)^2 \left[\frac{\ell(\ell+1)}{r^2 \left(1 + \frac{m}{2r}\right)^4} - \frac{6m}{r^3 \left(1 + \frac{m}{2r}\right)^6} \right]. \tag{8.20}$$

See Figure 5 for qualitative features of the potential.

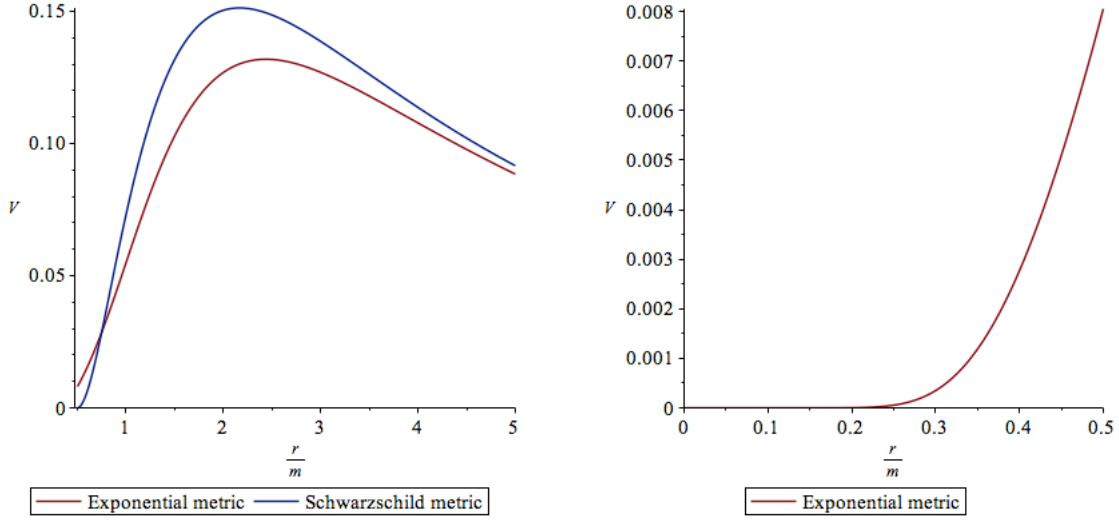


Figure 5. The graph shows the spin two (axial) Regge–Wheeler potential for $\ell = 2$. The Regge–Wheeler potentials are somewhat dissimilar for $r > m/2$, and are radically different once one goes to small $r < m/2$, (where the Regge–Wheeler potential for Schwarzschild is only formal since one is behind a horizon and cannot interact with the domain of outer communication).

9 GR interpretation for the exponential metric

While many of the proponents of the exponential metric have for one reason or another been trying to build “alternatives” to standard general relativity, there is nevertheless a relatively simple interpretation of the exponential metric within the framework of standard general relativity and the standard Einstein equations, albeit with an “exotic” matter source. The key starting point is to note:

$$R_{ab} = -\frac{2m^2}{r^4} \text{diag}\{0, 1, 0, 0\}_{ab} = -\frac{1}{2} \nabla_a \left(\frac{2m}{r} \right) \nabla_b \left(\frac{2m}{r} \right) = -\frac{1}{2} \nabla_a \Phi \nabla_b \Phi. \quad (9.1)$$

Equivalently

$$G_{ab} = -\frac{1}{2} \left\{ \nabla_a \Phi \nabla_b \Phi - \frac{1}{2} g_{ab} (g^{cd} \nabla_c \Phi \nabla_d \Phi) \right\}. \quad (9.2)$$

This is just the usual Einstein equation for a *negative kinetic energy massless scalar field*, a “ghost” or “phantom” field. The contracted Bianchi identity $G^{ab}_{;b}$ then automatically yields the scalar field EOM $(g^{ab} \nabla_a \nabla_b) \Phi = 0$. That the scalar field has negative kinetic energy is intimately related to the fact that the exponential metric describes a traversable wormhole [20, 24].

So, perhaps ironically, despite the fact that many of the proponents of the exponential metric for one reason or another reject general relativity, the exponential metric they advocate has a straightforward if somewhat exotic general relativistic interpretation.¹

10 Discussion

Regardless of one’s views regarding the merits of some of the “justifications” used for advocating the exponential metric, the exponential metric can simply be viewed as a phenomenological model that can be studied in its own right. Viewed in this way the exponential metric has a number of interesting features:

- It is a traversable wormhole, with time slowed down on the other side of the wormhole throat.
- Strong field lensing phenomena are markedly different from Schwarzschild.
- ISCOs and unstable photon orbits still exist, and are moderately shifted from where they would be located in Schwarzschild spacetime.
- Regge–Wheeler potentials can still be extracted, and are moderately different from what they would be in Schwarzschild spacetime.

Many of the proponents of the exponential metric are arguing for using it as a replacement for the Schwarzschild geometry of general relativity — however typically without any detailed assessment of the phenomenology. We strongly feel that if one wishes to replace all the black hole candidates astronomers have identified with traversable wormholes, then certainly a careful phenomenological analysis of this quite radical proposal (somewhat along the lines above) should be carried out. Perhaps most ironically, despite the fact that many of the proponents of the exponential metric reject general relativity, the exponential metric has a natural interpretation in terms of general relativity coupled to a phantom scalar field.

¹It is also possible to interpret the exponential metric as a special sub-case of the Brans class IV solution of Brans–Dicke theory, which in turn is a special case of the general spherical, asymptotically flat, vacuum solution [64, 65]; in this context it is indeed known that some solutions admit a wormhole throat, but that message seems not to have reached the wider community.

Acknowledgements

This project was funded by the Ratchadapisek Sompoch Endowment Fund, Chulalongkorn University (Sci-Super 2014-032), by a grant for the professional development of new academic staff from the Ratchadapisek Somphot Fund at Chulalongkorn University, by the Thailand Research Fund (TRF), and by the Office of the Higher Education Commission (OHEC), Faculty of Science, Chulalongkorn University (RSA5980038). PB was additionally supported by a scholarship from the Royal Government of Thailand. TN was also additionally supported by a scholarship from the Development and Promotion of Science and Technology talent project (DPST). MV was supported by the Marsden Fund, via a grant administered by the Royal Society of New Zealand.

The authors wish to thank Kumar Virbhadra and Valerio Faraoni for their interest and comments.

References

- [1] Huseyin Yilmaz, “New approach to general relativity”,
Physical Review, **111** #5 (1958) 1417–1426; doi: 10.1103/PhysRev.111.1417
- [2] Hüseyin Yilmaz, “New yheory of gravitation”,
Physical Review Letters, **27** #20 (1971) 1399–1402. doi: 10.1103/PhysRevLett.27.1399
- [3] Hüseyin Yilmaz, “New approach to relativity and gravitation”,
Ann. Phys. (USA), **81** (1973) 179–200 doi: 10.1016/0003-4916(73)90485-5
- [4] Roger E. Clapp,
“Preliminary quasar model based on the Yilmaz exponential metric”,
Physical Review D, **7** #2 (1973) 345–355 doi: 10.1103/PhysRevD.7.345
- [5] Peter Rastall, “Gravity without geometry”,
American Journal of Physics **43** (1975) 591–595; <https://doi.org/10.1119/1.9773>
(Note the exponential metric is here *implicit*, rather than *explicit*, hiding in the rescaling of space and time in the author’s preferred coordinate system.)
- [6] A. J. Fennelly and R. Pavelle, “Nonviability of Yilmaz’ gravitation theories and his criticisms of Rosen’s gravitation theory”, Print-76-0905.
- [7] C. W. Misner, “Yilmaz cancels Newton”, Nuovo Cim. B **114** (1999) 1079
[gr-qc/9504050].
- [8] C. O. Alley, P. K. Aschan and H. Yilmaz, “Refutation of C.W. Misner’s claims in his article ‘Yilmaz cancels Newton’”, gr-qc/9506082.
- [9] Stanley L. Robertson, “X-Ray novae, event horizons, and the exponential metric”,
The Astrophysical Journal **515** # 1 (1999) 365-380. doi: 10.1086/306995

- [10] S. L. Robertson, “Bigger bursts from merging neutron stars”,
Astrophys. J. **517** (1999) L117 doi:10.1086/312043 [astro-ph/9902232].
- [11] M. Ibison, “The Yilmaz cosmology”, AIP Conf. Proc. **822** (2006) 181.
doi:10.1063/1.2189135
- [12] M. Ibison, “Cosmological test of the Yilmaz theory of gravity”,
Class. Quant. Grav. **23** (2006) 577 doi:10.1088/0264-9381/23/3/001
[arXiv:0705.0080 [gr-qc]].
- [13] N. Ben-Amots,
“Relativistic exponential gravitation and exponential potential of electric charge”,
Found. Phys. **37** (2007) 773. doi:10.1007/s10701-007-9112-1
- [14] A. A. Svidzinsky,
“Vector theory of gravity in Minkowski space-time: Flat universe without black holes”,
arXiv:0904.3155 [gr-qc].
- [15] M. Martinis and N. Perkovic,
“Is exponential metric a natural space-time metric of Newtonian gravity?”,
arXiv:1009.6017 [gr-qc].
- [16] N. Ben-Amots, “Some features and implications of exponential gravitation”,
J. Phys. Conf. Ser. **330** (2011) 012017. doi:10.1088/1742-6596/330/1/012017
- [17] A. A. Svidzinsky,
“Vector theory of gravity: Universe without black holes and solution of dark energy problem”,
Phys. Scripta **92** (2017) no.12, 125001 doi:10.1088/1402-4896/aa93a8 [arXiv:1511.07058 [gr-qc]].
- [18] M. E. Aldama, “The gravity apple tree”, J. Phys. Conf. Ser. **600** (2015) no.1, 012050.
doi:10.1088/1742-6596/600/1/012050
- [19] Stanley L. Robertson, “MECO in an exponential metric”, arXiv:1606.01417 [gen-ph].
- [20] M. S. Morris and K. S. Thorne,
“Wormholes in space-time and their use for interstellar travel:
A tool for teaching general relativity”,
Am. J. Phys. **56** (1988) 395. doi:10.1119/1.15620
- [21] M. S. Morris, K. S. Thorne and U. Yurtsever,
“Wormholes, Time Machines, and the Weak Energy Condition”,
Phys. Rev. Lett. **61** (1988) 1446. doi:10.1103/PhysRevLett.61.1446
- [22] M. Visser, “Traversable wormholes: Some simple examples”,
Phys. Rev. D **39** (1989) 3182 doi:10.1103/PhysRevD.39.3182 [arXiv:0809.0907 [gr-qc]].
- [23] M. Visser, “Traversable wormholes from surgically modified Schwarzschild
space-times”, Nucl. Phys. B **328** (1989) 203 doi:10.1016/0550-3213(89)90100-4
[arXiv:0809.0927 [gr-qc]].

- [24] M. Visser, *Lorentzian wormholes: From Einstein to Hawking*, (AIP Press, now Springer, New York, 1995).
- [25] J. G. Cramer, R. L. Forward, M. S. Morris, M. Visser, G. Benford and G. A. Landis, “Natural wormholes as gravitational lenses”, *Phys. Rev. D* **51** (1995) 3117 doi:10.1103/PhysRevD.51.3117 [astro-ph/9409051].
- [26] E. Poisson and M. Visser, “Thin shell wormholes: Linearization stability”, *Phys. Rev. D* **52** (1995) 7318 doi:10.1103/PhysRevD.52.7318 [gr-qc/9506083].
- [27] D. Hochberg and M. Visser, “Geometric structure of the generic static traversable wormhole throat”, *Phys. Rev. D* **56** (1997) 4745 doi:10.1103/PhysRevD.56.4745 [gr-qc/9704082].
- [28] M. Visser and D. Hochberg, “Generic wormhole throats”, *Annals of the Israeli Physics Society* **13** (1997) 249 [gr-qc/9710001].
- [29] D. Hochberg and M. Visser, “Dynamic wormholes, anti-trapped surfaces, and energy conditions”, *Phys. Rev. D* **58** (1998) 044021 doi:10.1103/PhysRevD.58.044021 [gr-qc/9802046].
- [30] D. Hochberg and M. Visser, “The Null energy condition in dynamic wormholes”, *Phys. Rev. Lett.* **81** (1998) 746 doi:10.1103/PhysRevLett.81.746 [gr-qc/9802048].
- [31] C. Barceló and M. Visser, “Traversable wormholes from massless conformally coupled scalar fields”, *Phys. Lett. B* **466** (1999) 127 doi:10.1016/S0370-2693(99)01117-X [gr-qc/9908029].
- [32] C. Barceló and M. Visser, “Scalar fields, energy conditions, and traversable wormholes”, *Class. Quant. Grav.* **17** (2000) 3843 doi:10.1088/0264-9381/17/18/318 [gr-qc/0003025].
- [33] N. Dadhich, S. Kar, S. Mukherji and M. Visser, “ $R = 0$ space-times and self-dual Lorentzian wormholes”, *Phys. Rev. D* **65** (2002) 064004 doi:10.1103/PhysRevD.65.064004 [gr-qc/0109069].
- [34] M. Visser, S. Kar and N. Dadhich, “Traversable wormholes with arbitrarily small energy condition violations”, *Phys. Rev. Lett.* **90** (2003) 201102 doi:10.1103/PhysRevLett.90.201102 [gr-qc/0301003].
- [35] J. P. S. Lemos, F. S. N. Lobo and S. Quinet de Oliveira, “Morris-Thorne wormholes with a cosmological constant”, *Phys. Rev. D* **68** (2003) 064004 doi:10.1103/PhysRevD.68.064004 [gr-qc/0302049].
- [36] S. Kar, N. Dadhich and M. Visser, “Quantifying energy condition violations in traversable wormholes”, *Pramana* **63** (2004) 859 doi:10.1007/BF02705207 [gr-qc/0405103].
- [37] F. S. N. Lobo, “Phantom energy traversable wormholes”, *Phys. Rev. D* **71** (2005) 084011 doi:10.1103/PhysRevD.71.084011 [gr-qc/0502099].

- [38] S. V. Sushkov, “Wormholes supported by a phantom energy”,
Phys. Rev. D **71** (2005) 043520 doi:10.1103/PhysRevD.71.043520 [gr-qc/0502084].
- [39] N. M. Garcia, F. S. N. Lobo and M. Visser, “Generic spherically symmetric dynamic thin-shell traversable wormholes in standard general relativity”, Phys. Rev. D **86** (2012) 044026 doi:10.1103/PhysRevD.86.044026 [arXiv:1112.2057 [gr-qc]].
- [40] Biplab Bhawal and Sayan Kar, “Lorentzian wormholes in Einstein-Gauss-Bonnet theory”, Phys. Rev. D **46** (1992) 2464-2468
- [41] Raul E. Arias, Marcelo Botta Cantcheff, and Guillermo A. Silva, “Lorentzian AdS, wormholes and holography”, Phys. Rev. D **83** (2011) 066015
- [42] Ping Gao, Daniel Louis Jafferis, Aron C. Wall, “Traversable wormholes via a double trace deformation”, JHEP **12** (2017) 151 doi:10.1007/JHEP12(2017)151 arXiv:1608.05687 [hep-th].
- [43] Juan Maldacena, Douglas Stanford, Zhenbin Yang, “Diving into traversable wormholes”, doi:10.1002/prop.201700034 arXiv:1704.05333 [hep-th].
- [44] Felix Willenborg, Saskia Grunau, Burkhard Kleihaus, Jutta Kunz, “Geodesic motion around traversable wormholes supported by a massless conformally-coupled scalar field”, arXiv:1801.09769 [gr-qc].
- [45] P.K. Sahoo, P.H.R.S. Moraes, Parbati Sahoo, G. Ribeiro, “Phantom fluid supporting traversable wormholes in alternative gravity with extra material terms”, arXiv:1802.02465 [gr-qc].
- [46] Corless, R. M.; Gonnet, G. H.; Hare, D. E. G.; Jeffrey, D. J.; and Knuth, D. E., “On the Lambert W function”,
Advances in Computational Mathematics **5** (1996) 329–359. doi:10.1007/BF02124750.
- [47] S. R. Valluri, D. J. Jeffrey, R. M. Corless,
“Some Applications of the Lambert W Function to Physics”,
Canadian Journal of Physics **78** (2000) 823–831, doi:10.1139/p00-065
- [48] Alexandre Vial, “Fall with linear drag and Wien’s displacement law: approximate solution and Lambert function”,
European Journal of Physics, **33** (2012) 751, doi:10.1088/0143-0807/33/4/751
- [49] Seán M Stewart, “Wien peaks and the Lambert W function”,
Revista Brasileira de Ensino de Física **33** (2011) 3308, www.sbfisica.org.br
- [50] Seán M. Stewart, “Spectral peaks and Wien’s displacement law”,
Journal of Thermophysics and Heat Transfer, **26** (2012) 689–692. doi: 10.2514/1.T3789
- [51] S. R. Valluri, M. Gil, D. J. Jeffrey, and Shantanu Basu,
“The Lambert W function and quantum statistics”,
Journal of Mathematical Physics **50** (2009) 102103, doi:10.1063/1.3230482

- [52] Matt Visser, “Primes and the Lambert W function”, *Mathematics* **6**(4) (2018) 56; doi:10.3390/math6040056 [arXiv:1311.2324 [math.NT]].
- [53] Petarpa Boonserm and Matt Visser,
“Bounding the greybody factors for Schwarzschild black holes”,
Phys. Rev. D **78** (2008) 101502 [arXiv:0806.2209 [gr-qc]].
- [54] P. Boonserm, T. Ngampitipan and M. Visser,
“Regge–Wheeler equation, linear stability, and greybody factors for dirty black holes”,
Phys. Rev. D **88** (2013) 041502 doi:10.1103/PhysRevD.88.041502
[arXiv:1305.1416 [gr-qc]].
- [55] P. Boonserm, C. Cattöen, T. Faber, M. Visser and S. Weinfurtner,
“Effective refractive index tensor for weak field gravity”,
Class. Quant. Grav. **22** (2005) 1905 doi:10.1088/0264-9381/22/11/001 [gr-qc/0411034].
- [56] C. Barceló, S. Liberati and M. Visser, “Analogue gravity”,
Living Rev. Rel. **8** (2005) 12 [Living Rev. Rel. **14** (2011) 3] doi:10.12942/lrr-2005-12
[gr-qc/0505065].
- [57] M. Visser, “Survey of analogue spacetimes”, *Lect. Notes Phys.* **870** (2013) 31
doi:10.1007/978-3-319-00266-8_2 [arXiv:1206.2397 [gr-qc]].
- [58] K. S. Virbhadra and G. F. R. Ellis, “Schwarzschild black hole lensing”, *Phys. Rev. D*
62 (2000) 084003 doi:10.1103/PhysRevD.62.084003 [astro-ph/9904193].
- [59] K. S. Virbhadra and G. F. R. Ellis, “Gravitational lensing by naked singularities”,
Phys. Rev. D **65** (2002) 103004. doi:10.1103/PhysRevD.65.103004
- [60] K. S. Virbhadra, D. Narasimha and S. M. Chitre, “Role of the scalar field in
gravitational lensing”, *Astron. Astrophys.* **337** (1998) 1 [astro-ph/9801174].
- [61] K. S. Virbhadra and C. R. Keeton, “Time delay and magnification centroid due to
gravitational lensing by black holes and naked singularities”, *Phys. Rev. D* **77** (2008)
124014 doi:10.1103/PhysRevD.77.124014 [arXiv:0710.2333 [gr-qc]].
- [62] C. M. Claudel, K. S. Virbhadra and G. F. R. Ellis, “The Geometry of photon
surfaces”, *J. Math. Phys.* **42** (2001) 818 doi:10.1063/1.1308507 [gr-qc/0005050].
- [63] K. S. Virbhadra, “Relativistic images of Schwarzschild black hole lensing”, *Phys. Rev.*
D **79** (2009) 083004 doi:10.1103/PhysRevD.79.083004 [arXiv:0810.2109 [gr-qc]].
- [64] V. Faraoni, F. Hammad and S. D. Belknap-Keet, “Revisiting the Brans solutions of
scalar-tensor gravity”, *Phys. Rev. D* **94** (2016) no.10, 104019
doi:10.1103/PhysRevD.94.104019 [arXiv:1609.02783 [gr-qc]].
- [65] V. Faraoni, F. Hammad, A. M. Cardini and T. Gobeil, “Revisiting the analogue of the
Jebsen-Birkhoff theorem in Brans-Dicke gravity”, *Phys. Rev. D* **97** (2018) no.8, 084033
doi:10.1103/PhysRevD.97.084033 [arXiv:1801.00804 [gr-qc]].

Greybody factor for black holes in dRGT massive gravity

Petarpa Boonserm^{1,a}, Tritos Ngampitipan^{2,b}, Pitayuth Wongjun^{3,c}

¹ Department of Mathematics and Computer Science, Faculty of Science, Chulalongkorn University, Bangkok 10330, Thailand

² Faculty of Science, Chandrakasem Rajabhat University, Bangkok 10900, Thailand

³ The Institute for Fundamental Study, Naresuan University, Phitsanulok 65000, Thailand

Received: 4 October 2017 / Accepted: 4 June 2018

© The Author(s) 2018

Abstract In general relativity, greybody factor is a quantity related to the quantum nature of a black hole. A high value of greybody factor indicates a high probability that Hawking radiation can reach infinity. Although general relativity is correct and has been successful in describing many phenomena, there are some questions that general relativity cannot answer. Therefore, general relativity is often modified to attain answers. One of the modifications is the ‘massive gravity’. The viable model of the massive gravity theory belongs to de Rham, Gabadadze and Tolley (dRGT). In this paper, we calculate the gravitational potential for the de Sitter black hole and for the dRGT black hole. We also derive the rigorous bound on the greybody factor for the de Sitter black hole and the dRGT black hole. It is found that the structure of potentials determines how much the rigorous bound on the greybody factor should be. That is, the higher the potential, the lesser the bound on the greybody factor will be. Moreover, we compare the greybody factor derived from the rigorous bound with the greybody factor derived from the matching technique. The result shows that the rigorous bound is a true lower bound because it is less than the greybody factor obtained from the matching technique.

1 Introduction

General relativity was formulated in 1915. It offers profound insights into the concept of gravity. General relativity has succeeded in describing many gravitational phenomena such as the gravitational deflection of light, gravitational radiation, the anomalous perihelion of Mercury, and the behavior of black holes.

According to cosmological observations, today's the universe is expanding with acceleration [1, 2]. There are a num-

ber of cosmological models accounting for this current acceleration. Among these models, the simplest one is the Lambda cold dark matter (Λ CDM) model in which the cosmological constant drives the acceleration of the universe. The model assumes that general relativity is the correct theory of gravity on cosmological scales. Although the Λ CDM model is in excellent agreement with observations, the cosmological constant itself encounters a theoretical problem that the observational value of the cosmological constant is much smaller than the theoretical one. It may be possible that general relativity may not be the most suitable theory to describe the universe on a large scale, at least on a scale larger than the solar system. The dark side of the universe is evidence that some modifications of general relativity at a large scale is required [3].

Such modifications should be correct on the largest scale and then reduce to general relativity on a smaller scale. One of the candidates for such modifications is massive gravity. Massive gravity is a theory of gravity in which a graviton has a mass. The most successful theory of massive gravity is popularly known by the de Rham–Gabadadze–Tolley (dRGT) model [4, 5]. Because of the Vainshtein mechanism, adding mass to graviton keeps physics on a small scale equivalent to general relativity, with some small corrections [6]. However, this leads to the modification of gravity on a larger scale.

Regarding the cosmological solutions in the dRGT massive gravity theory, even though all the solutions cannot provide a viable cosmological model, for example, the solutions do not admit flat-FLRW metric [7, 8] or the model encounters instabilities [9–11], a class of solutions can provide a viable cosmological model [12–14]. The solutions for the dRGT massive gravity are not only investigated in a cosmological background, but also in a spherically symmetric background [15]. For spherically symmetric solutions, the black hole solutions have been investigated in both analytical [16–25] and non-analytical [26, 27] forms, depending

^a e-mail: petarpa.boonserm@gmail.com

^b e-mail: tritos.ngampitipan@gmail.com

^c e-mail: pitbaa@gmail.com

on the fiducial metric form. However, they still share the same property, which is represented as an asymptotic AdS/dS behavior.

A black hole can emit thermal radiation if the quantum effects are considered. This thermal radiation is known as Hawking radiation [28]. Hawking radiation propagates on spacetime, which is curved by the black hole. The curvature of spacetime acts as a gravitational potential. Therefore, Hawking radiation is scattered from this potential. One part of the Hawking radiation is reflected back into the black hole, while the other part is transmitted to spatial infinity. The transmission probability in this context is also known as the greybody factor.

There are many methods to calculate the greybody factor. For example, one can obtain an approximate greybody factor using the matching technique [29–31]. If the gravitational potential is high enough, one can use the WKB approximation to derive the greybody factor [32–34]. Other than approximation, the greybody factor can also be obtained using the rigorous bound [35–37]. The bound can give a qualitative description of a black hole.

In this work, we investigate the greybody factor using the analytical black hole solution in dRGT massive gravity. In Sect. 2, the structure of the horizons of the solution is analyzed in order to generate a suitable form for the analysis of the properties of the greybody factor. In Sect. 3, the properties of the gravitational potential are investigated for both the de Sitter black hole and dRGT black hole. The height of their potentials are determined by the parameters of the model. In Sect. 4, we derive the rigorous bound on the greybody factor, and the reflection probability for the de Sitter black hole and the dRGT black hole. The value of the rigorous bound on the greybody factor corresponds to the structure of potentials. In addition, the effects of the graviton mass, cosmological constant and angular momentum quantum number on the greybody factors will also be explored. Finally, concluding remarks are provided in Sect. 5.

2 dRGT black hole background

In this section, we will review the main concept of the dRGT massive gravity theory in the following manner [18]; the analytical solution of the modified Einstein equation due to the graviton mass is first presented, and then the structure of the horizons of the black hole in the dRGT massive gravity theory is investigated. The theory of the dRGT massive gravity is a covariant non-linear theory of massive gravity, which is ghost free in the decoupling limit to all orders. The action of the dRGT massive gravity model in four-dimensional spacetime can be expressed as

$$S = \int d^4x \sqrt{-g} \left[\frac{M_p^2}{2} R[g] + m_g^2 (\mathcal{L}_2[g, f] + \alpha_3 \mathcal{L}_3[g, f] + \alpha_4 \mathcal{L}_4[g, f]) \right], \quad (1)$$

where R is a Ricci scalar corresponding to a physical metric $g_{\mu\nu}$, m_g^2 to the square of the graviton mass, with \mathcal{L}_i s representing the interactions of the i th order of the massive graviton. In particular, those interactions of the massive graviton are constructed from two kinds of metrics and can be expressed as follows,

$$\mathcal{L}_2[g, f] = \frac{1}{2} ([\mathcal{K}]^2 - [\mathcal{K}^2]), \quad (2)$$

$$\mathcal{L}_3[g, f] = \frac{1}{3!} ([\mathcal{K}]^3 - 3[\mathcal{K}][\mathcal{K}^2] + 2[\mathcal{K}^3]), \quad (3)$$

$$\mathcal{L}_4[g, f] = \frac{1}{4!} ([\mathcal{K}]^4 - 6[\mathcal{K}]^2[\mathcal{K}^2] + 3[\mathcal{K}^2]^2 + 8[\mathcal{K}][\mathcal{K}^3] - 6[\mathcal{K}^4]), \quad (4)$$

where the rectangular brackets denote the traces. The tensor $\mathcal{K}_{\mu\nu}$ is constructed from the physical metric $g_{\mu\nu}$ and the fiducial metric $f_{\mu\nu}$ as

$$\mathcal{K}^\mu_\nu = \delta^\mu_\nu - \left(\sqrt{g^{-1}f} \right)^\mu_\nu, \quad (5)$$

where the square roots of those tensors are defined so that $\sqrt{g^{-1}f}^\mu_\rho \sqrt{g^{-1}f}^\rho_\nu = (g^{-1}f)^\mu_\nu$. The fiducial metric is chosen as [16, 38, 39]

$$f_{\mu\nu} = \text{diag}(0, 0, c^2, c^2 \sin^2 \theta), \quad (6)$$

where c is a constant. It can be shown in [38] that the theory of massive gravity with the choice of the singular fiducial metric such as one in equation (6) is absent of Boulware–Deser (BD) ghost. The static and spherically symmetric black hole solution satisfying this theory can be written as [18]

$$ds^2 = -f(r)dt^2 + \frac{dr^2}{f(r)} + r^2 d\Omega^2, \quad (7)$$

where

$$f(r) = 1 - \frac{2M}{r} + \frac{\Lambda}{3}r^2 + \gamma r + \zeta, \quad (8)$$

$d\Omega^2 = d\theta^2 + \sin^2 \theta d\phi^2$, and M is an integration constant related to the mass of the black hole. The parameters above can be written in terms of the original parameters as

$$\Lambda = 3m_g^2 (1 + \alpha + \beta), \quad (9)$$

$$\gamma = -cm_g^2 (1 + 2\alpha + 3\beta), \quad (10)$$

$$\zeta = c^2 m_g^2 (\alpha + 3\beta), \quad (11)$$

and

$$\alpha_3 = \frac{\alpha - 1}{3}, \quad \alpha_4 = \frac{\beta}{4} + \frac{1 - \alpha}{12}. \quad (12)$$

This solution contains various kinds of black hole solutions found in literature. If $m_g = 0$, the Schwarzschild solution is recovered. In the case of $c = 0$, the solution reduces to the de Sitter solution for $1 + \alpha + \beta < 0$ and reduces to the anti-de Sitter solution for $1 + \alpha + \beta > 0$. Moreover, the global monopole solution can be obtained by setting $1 + 2\alpha + 3\beta = 0$. Note that the last term, the constant potential ζ , corresponds to the global monopole term. A global monopole usually comes from a topological defect in high energy physics of the early universe resulting from a gauge-symmetry breaking [40–42]. However, in this solution, the global monopole is contributed via the graviton mass. Note that the linear term γr is a characteristic term of this solution, distinguished from other solutions found in literature. Next, we will consider the structure of the horizons of this solution. Since the solution is an asymptotical AdS/dS solution, we first consider the structure of the AdS/dS solution and then investigate the structure of the horizons of the solution in the dRGT massive gravity theory.

2.1 Horizon structure for AdS/dS-like solutions

It is important to note that one can choose $c = 0$. This corresponds to trivial solutions since the interacting terms (or graviton mass) become constant, which is inferred from $\mathcal{K}_\nu^\mu = \delta_\nu^\mu$. Therefore, the action in Eq. (1) becomes the Einstein–Hilbert action with cosmological constant. In order to investigate the structure of the horizon, let us first consider a simple case where $c = 0$. As a result, the function in the metric solution becomes

$$f(r) = 1 - \frac{2M}{r} + \frac{\Lambda}{3}r^2. \quad (13)$$

From this function, one can see that $f(r) \rightarrow -\infty$ where $r \rightarrow 0$. In order to have two horizons, f must be increased and then decreased where r is increased. This means that $f(r) \rightarrow -\infty$ again when $r \rightarrow \infty$. Therefore, in order to obtain two horizons, Λ must be negative. This corresponds to the de Sitter (dS) spacetime, while in the case of anti-de Sitter (AdS) spacetime, $\Lambda > 0$, there exists only one horizon. Now let us find the conditions for which there are two horizons for the de Sitter spacetime, where $\Lambda < 0$. If two horizons exist, the maximum value of f must be positive. The maximum point of f can be found by solving $f' = 0$. As a result, the maximum point is

$$r_m = \left(-\frac{3M}{\Lambda}\right)^{1/3}. \quad (14)$$

Substituting this radius into $f(r)$ in Eq. (13), the maximum value of f can be written as

$$f(r_m) = \left(-\frac{3M}{\Lambda}\right)^{1/3} - 3M. \quad (15)$$

By requiring $f(r_m) > 0$, the condition for having two horizons can be written as

$$-\frac{1}{9M^2} < \Lambda < 0. \quad (16)$$

In order to parameterize the solution properly, let us define a dimensionless parameter as

$$\alpha_m^2 = -9\Lambda M^2, \quad (17)$$

where $0 < \alpha_m^2 < 1$. By using the dimensionless variable $\bar{r} = r/M$, function f can be rewritten as

$$f(\bar{r}) = 1 - \frac{2}{\bar{r}} - \frac{\alpha_m^2}{27}\bar{r}^2. \quad (18)$$

In order to find the horizon, one has to solve the cubic equation;

$$\bar{r}^3 - \frac{27}{\alpha_m^2}\bar{r} + \frac{54}{\alpha_m^2} = 0. \quad (19)$$

This cubic equation is known as the depressed cubic equation, and the solution can be expressed as

$$\bar{r} = \frac{6}{\alpha_m} \cos \left[\frac{1}{3} \cos^{-1} \left(-\alpha_m \right) - \frac{2\pi k}{3} \right], \quad (20)$$

where $k = 0, 1, 2$ for the three distinguished solutions. Since $0 < \alpha_m < 1$, one can expand the sinusoidal function and then keep only the significant contributions. As a result, for $k = 2$, \bar{r} is negative, and for $k = 1$ and $k = 0$, the solutions can be respectively approximated as

$$\bar{r}_1 \sim 2, \quad \bar{r}_2 \sim \frac{3\sqrt{3}}{\alpha_m} - 1. \quad (21)$$

Note that these solutions are well approximated when $\alpha_m \ll 1$. Actually, this approximation can be realized to satisfy the cosmological solution in which the universe expands with acceleration, since the observed value of Λ is very small compared to the black hole mass. The behavior of the horizon with various values of α_m is shown in the left panel of Fig. 1.

For the AdS solution, Λ is positive. Therefore, one can find the solution of the horizon by rewriting α_m as $\alpha_m =$

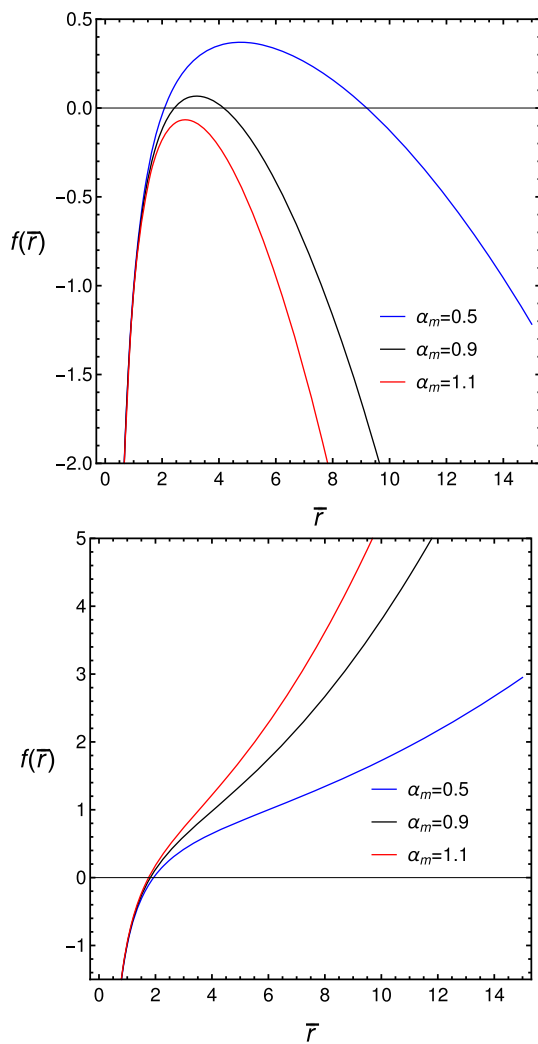


Fig. 1 The left panel shows the horizon structure of the de Sitter solution for the value of α_m as $\alpha_m = 0.5$ (blue line), $\alpha_m = 0.9$ (black line) and $\alpha_m = 1.1$ (red line). The right panel shows the horizon structure of the AdS solution for the value of α_m as $\alpha_m = 0.5$ (blue line), $\alpha_m = 0.9$ (black line) and $\alpha_m = 1.1$ (red line)

$9\Lambda M^2$. By following the same steps from the de Sitter case, the horizon in the AdS case can be written as

$$\tilde{r} = \frac{6}{\alpha_m} \sinh \left[\frac{1}{3} \sinh^{-1} (\alpha_m) \right]. \quad (22)$$

As we have discussed above, there exists only one horizon for the AdS solution. This is valid for all values of α_m as show in the right panel of Fig. 1.

2.2 Horizon structure for the dRGT massive gravity solutions

For the complete massive gravity solution, it is significantly difficult and complicated to find the horizon analytically. One of the conditions for having three horizons is that

$\Lambda > 0$. Therefore, we can separate our consideration into two classes; the asymptotic AdS solutions for $\Lambda > 0$ and the asymptotic de Sitter solution for $\Lambda < 0$ [43].

For the general solutions of the dRGT massive gravity, the dimension-length parameter c is not set to be zero. This means that we have to introduce a scale to the theory. It is useful to work out the solution using dimensionless variable, $\tilde{r} = r/c$, and then find out what scale c would assume. As a result, function f can be written in terms of a dimensionless variable as

$$f(\tilde{r}) = 1 - \frac{2\tilde{M}}{\tilde{r}} + \alpha_g (c_2 \tilde{r}^2 - c_1 \tilde{r} + c_0), \quad (23)$$

where

$$\begin{aligned} \tilde{M} &= \frac{M}{c}, \quad \alpha_g = m_g^2 c^2, \quad c_0 = \alpha + 3\beta, \\ c_1 &= 1 + 2\alpha + 3\beta, \quad c_2 = 1 + \alpha + \beta. \end{aligned} \quad (24)$$

From this equation, it is sufficient to figure out that the scale of c takes place at $\tilde{M} \sim \alpha_g$. Therefore, one can choose the parameter c as

$$c = r_V = \left(\frac{M}{m_g^2} \right)^{1/3}. \quad (25)$$

This radius is well known as the Vainshtein radius [44,45]. The theory in which $r < r_V$ will approach GR, while the theory in which $r > r_V$, the modification of GR will be active. The horizons can be found by solving for the solution of r through the equation

$$\alpha_g c_2 \tilde{r}^3 - \alpha_g c_1 \tilde{r}^2 + (\alpha_g c_0 + 1) \tilde{r} - 2\tilde{M} = 0. \quad (26)$$

In order to find the conditions for having three horizons for the AdS case and two horizons for the de Sitter case, let us consider the extremum points of the function f using the equation $f' = 0$ or

$$2\alpha_g c_2 \tilde{r}^3 - \alpha_g c_1 \tilde{r}^2 - 2\tilde{M} = 0. \quad (27)$$

This is the cubic equation. We can solve it by changing the variables to obtain the depressed cubic equation and then analyze the general solution to find the condition for having two real positive roots for the AdS case and one real positive root for the de Sitter case. As a result, one can constrain our consideration to case $c_1 = 3(4c_2^2)^{1/3}$. Choosing this condition will guarantee one real positive root for the de Sitter case as $\tilde{r}_{dS} = (-2c_2)^{-1/3}$ and two real positive roots for the AdS case as $\tilde{r}_{AdS1} = (2c_2)^{-1/3}$ and $\tilde{r}_{AdS2} = (1 + \sqrt{3})(2c_2)^{-1/3}$.

For the asymptotic de Sitter solutions, f at the extremum point can be written as

$$f(\tilde{r}_{dS}) = 1 + c_0 \alpha_g - \frac{9}{\sqrt{3}} \alpha_g (-2c_2)^{1/3}. \quad (28)$$

In order to have two horizons, $f(\tilde{r}_{dS}) > 0$. We can parameterize the parameter c_0 such that

$$c_0 = \frac{9}{\sqrt{3}} \frac{(-2c_2)^{1/3}}{\beta_m} - \frac{1}{\alpha_g}. \quad (29)$$

Therefore, the condition for having two horizons in the case of de Sitter-like spacetime is

$$0 < \beta_m < 1. \quad (30)$$

By changing the cubic equation into the depressed cubic equation, one can find the two real positive horizons as the real roots of the depressed cubic equation as follows

$$\tilde{r}_1 = \frac{2}{(-2c_2)^{1/3}} \left[X^{1/2} \cos \left(\frac{1}{3} \sec^{-1} Y \right) - 1 \right], \quad (31)$$

$$\tilde{r}_2 = \frac{-2}{(-2c_2)^{1/3}} \left[X^{1/2} \cos \left(\frac{1}{3} \sec^{-1} Y + \frac{\pi}{3} \right) + 1 \right], \quad (32)$$

where

$$X = \frac{2\sqrt{3}}{\beta_m} + 4 \text{ and } Y = -\frac{\sqrt{\frac{\sqrt{3}}{\beta_m}} + 2(2\sqrt{2}\beta_m + \sqrt{6})}{5\beta_m + 3\sqrt{3}}. \quad (33)$$

Our analysis can be checked using the numerical method as shown in the left panel of Fig. 2. From this figure, one can see that β_m can parameterize the existence of two horizons.

Now we consider the asymptotic AdS solutions. The f at the extremum points can be written as

$$f(\tilde{r}_{AdS1}) = 1 + c_0\alpha_g - \frac{9}{2}\alpha_g(2c_2)^{1/3}, \quad (34)$$

$$f(\tilde{r}_{AdS2}) = 1 + c_0\alpha_g - \frac{9}{\sqrt{3}}\alpha_g(2c_2)^{1/3}. \quad (35)$$

In order to have three horizons, we must have $f(\tilde{r}_{AdS1}) > 0$ and $f(\tilde{r}_{AdS2}) < 0$. By using the parameter of α_0 in Eq. (29), while changing c_2 to $-c_2$, the condition for having three horizons can be written as

$$1 < \beta_m < \frac{2}{\sqrt{3}}. \quad (36)$$

By using the same step as done in the asymptotic de Sitter case, the three real positive horizons for the AdS case can be written as

$$\tilde{r}_1 = \frac{2}{(2c_2)^{1/3}} \left[1 - x^{1/2} \sin \left(\frac{1}{3} \sec^{-1} y + \frac{\pi}{6} \right) \right], \quad (37)$$

$$\tilde{r}_2 = \frac{2}{(2c_2)^{1/3}} \left[1 - x^{1/2} \cos \left(\frac{1}{3} \sec^{-1} y + \frac{\pi}{3} \right) \right], \quad (38)$$

$$\tilde{r}_3 = \frac{2}{(2c_2)^{1/3}} \left[1 + x^{1/2} \cos \left(\frac{1}{3} \sec^{-1} y \right) \right]. \quad (39)$$

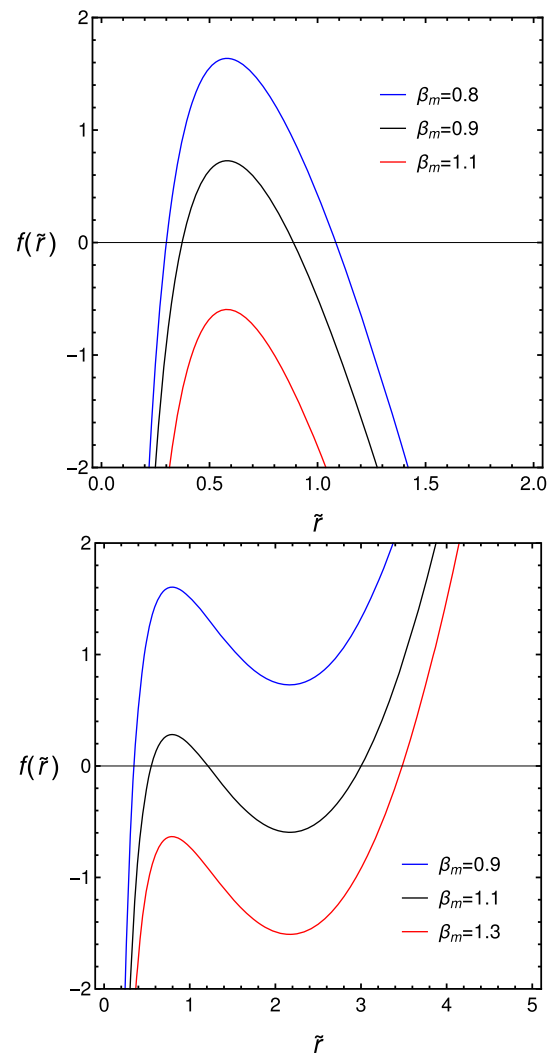


Fig. 2 The left panel shows the horizon structure of the asymptotic de Sitter solution in dRGT massive gravity for the value of β_m as $\beta_m = 0.8$ (blue line), $\beta_m = 0.9$ (black line) and $\beta_m = 1.1$ (red line). The right panel shows the horizon structure of the asymptotic AdS solution in dRGT massive gravity for the value of β_m as $\beta_m = 0.9$ (blue line), $\beta_m = 1.1$ (black line) and $\alpha_m = 1.3$ (red line). We set parameters as $M = 1$, $\alpha_g = 1$ and $c_2 = -1$ for the asymptotic de Sitter solution and $c_2 = 1$ for the asymptotic AdS solution

where

$$x = \frac{4 - 2\sqrt{3}}{\beta_m} \text{ and } y = \frac{\sqrt{6} - 2\sqrt{2}\beta_m}{(3\sqrt{3} - 5\beta_m)\sqrt{-\frac{\beta_m}{\sqrt{3}-2\beta_m}}}. \quad (40)$$

The numerical plot for these horizons is shown in the right panel of Fig. 2. From this figure, one can see that the existence of three horizons satisfy the condition $1 < \beta_m < 2/\sqrt{3}$ as we have analyzed. In the next section, we will use the expression for the horizons derived in this section to analyze the properties of the gravitational potential and the greybody factor of the black hole.

3 Equations of motion of massless scalar field

Classically, nothing can escape a black hole when approaching it. However, when a quantum effect is considered, the black hole can radiate. This radiation is known as Hawking radiation. It is a blackbody spectrum of temperature

$$kT = \frac{\hbar}{4\pi r_s}, \quad (41)$$

where r_s is the Schwarzschild radius. In this paper, we assume that Hawking radiation is a massless scalar field. The massless scalar field satisfies the Klein–Gordon equation

$$\frac{1}{\sqrt{-g}} \partial_\mu (\sqrt{-g} g^{\mu\nu} \partial_\nu \Phi) = 0. \quad (42)$$

We use the spherical coordinates. The solutions to the wave equation in spherical coordinates are of the form

$$\Phi(t, r, \Omega) = e^{i\omega t} \frac{\psi(r)}{r} Y_{\ell m}(\Omega), \quad (43)$$

where $Y_{\ell m}(\Omega)$ are spherical harmonics. The Klein–Gordon equation becomes

$$\begin{aligned} \frac{\omega^2 r^2}{f(r)} + \frac{r}{\psi(r)} \frac{d}{dr} \left[r^2 f(r) \frac{d}{dr} \left(\frac{\psi(r)}{r} \right) \right] \\ + \frac{1}{Y(\Omega)} \left[\frac{1}{\sin \theta} \frac{\partial}{\partial \theta} \left(\sin \theta \frac{\partial Y(\Omega)}{\partial \theta} \right) \right] \\ + \frac{1}{\sin^2 \theta} \frac{1}{Y(\Omega)} \frac{\partial^2 Y(\Omega)}{\partial \phi^2} = 0. \end{aligned} \quad (44)$$

The angular part satisfies

$$\begin{aligned} \frac{1}{\sin \theta} \frac{\partial}{\partial \theta} \left(\sin \theta \frac{\partial Y(\Omega)}{\partial \theta} \right) + \frac{1}{\sin^2 \theta} \frac{\partial^2 Y(\Omega)}{\partial \phi^2} \\ = -\ell(\ell+1)Y(\Omega), \end{aligned} \quad (45)$$

where ℓ is the angular momentum quantum number. Therefore, the Klein–Gordon equation (Eq. 44) is left with the radial part

$$\frac{d^2 \psi(r)}{dr_*^2} + [\omega^2 - V(r)] \psi(r) = 0, \quad (46)$$

where r_* is the tortoise coordinate defined by

$$\frac{dr_*}{dr} = \frac{1}{f(r)} \quad (47)$$

and $V(r)$ is the potential given by

$$V(r) = \frac{\ell(\ell+1)f(r)}{r^2} + \frac{f(r)f'(r)}{r}. \quad (48)$$

It can be expressed in terms of \tilde{r} as

$$V(\tilde{r}) = \frac{\ell(\ell+1)f(\tilde{r})}{c^2 \tilde{r}^2} + \frac{f(\tilde{r})f'(\tilde{r})}{c^2 \tilde{r}}. \quad (49)$$

Substituting the function $f(\tilde{r})$ from Eq. (23), we obtain

$$\begin{aligned} V(\tilde{r}) = \left[1 - \frac{2\tilde{M}}{\tilde{r}} + \alpha_g (c_2 \tilde{r}^2 - c_1 \tilde{r} + c_0) \right] \\ \times \left[\frac{\ell(\ell+1)}{c^2 \tilde{r}^2} + \frac{1}{c^2 \tilde{r}} \left[\frac{2\tilde{M}}{\tilde{r}^2} + \alpha_g (2c_2 \tilde{r} - c_1) \right] \right]. \end{aligned} \quad (50)$$

From the above equation, we can see that the potential is high when the angular momentum quantum number is large. Qualitatively, the leading contribution to the transmission amplitude comes from the mode $\ell = 0$. Therefore, it is sufficient to qualitatively analyze the potential for the case of $\ell = 0$. When $\ell = 0$, the first term in Eq. (49) vanishes and the second term is proportional to ff' . Therefore, there are three \tilde{r} -intercepts resulting from $f = 0$ and $f' = 0$. This behavior significantly differs from the Schwarzschild case, which has only one \tilde{r} -intercept as shown in the right panel of Fig. 3.

For the de Sitter case, the potential can be obtained by setting $c_1 = c_0 = 0$. As we have analyzed in Sect. 2.2, it is convenient to change parameter as $\alpha_g c_2 = -\alpha_m^2/(27\tilde{M}^2)$. For this setting, the potential depends only on the parameter α_m . In the same strategy as the quantum theory, the shape of the potential controls the transmission amplitude. Therefore, it is worthwhile to consider the maximum value of the de Sitter potential compared to the Schwarzschild potential. As a result, the de Sitter potential for the $\ell = 0$ case can be written as

$$\begin{aligned} c^2 V_{dS}(\tilde{r}) = \frac{1}{\tilde{r}} \left(1 - \frac{2\tilde{M}}{\tilde{r}} - \frac{\alpha_m^2}{27\tilde{M}^2} \tilde{r}^2 \right) \\ \times \left(\frac{2\tilde{M}}{\tilde{r}^2} - \frac{2\alpha_m^2}{27\tilde{M}^2} \tilde{r} \right). \end{aligned} \quad (51)$$

By solving \tilde{r}_{\max} via $V'_{dS} = 0$ and then substituting the solution back into the above equation, one can find the maximum value of the potential depending on only two parameters, \tilde{M} and α_m . The expression is significantly lengthy; we do not present it in the current paper. In order to see the effect of the graviton mass or the cosmological constant, one can fix \tilde{M} and then plot this expression via α_m as shown in the left panel of Fig. 3. Note that we also show the result for the $\ell = 1$ case in this figure. From this figure, one can see that V_{\max} contributed from the de Sitter black hole is always less than one from the Schwarzschild black hole. Clearly, the cosmological constant plays a role in reducing the local maximum of the potential. The explicit form of the de Sitter potential is plotted with various values of the cosmological constant as shown in the right panel of Fig. 3. Note that we used the

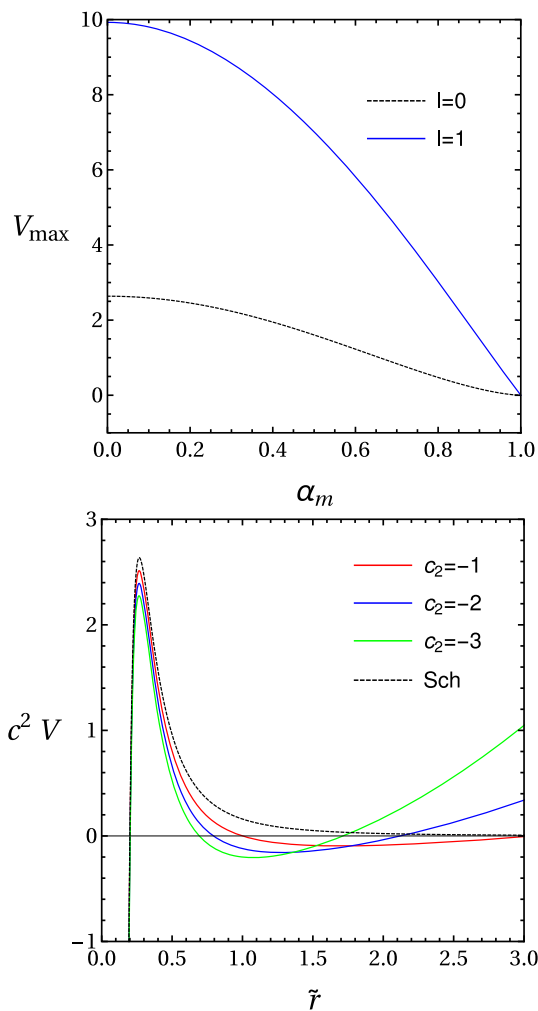


Fig. 3 The left panel shows the maximum potential for a de Sitter black hole versus the model parameter α_m with $\ell = 0$, $\ell = 1$, $\tilde{M} = \alpha_g = 0.1$. The right panel shows the potential for a de Sitter black hole with different values of c_2 compared to the Schwarzschild case; black-dotted line for the Schwarzschild case, red line for $c_2 = -1$, blue line for $c_2 = -2$ and green line for $c_2 = -3$

parameter c_2 instead of α_m^2 . This is convenient for comparing the results with one from the case of the dRGT massive gravity. Consequently, it might be expected that the transmission amplitude due to the de Sitter black hole should be greater than one in the Schwarzschild black hole. We will clarify this issue explicitly in the next section.

The dRGT potential for $\ell = 0$ can explicitly be written as

$$V_{\text{dRGT}}(\tilde{r}) = \frac{1}{c^2 \tilde{r}} \left[1 - \frac{2\tilde{M}}{\tilde{r}} + \alpha_g c_2 \tilde{r}^2 - 3\sqrt[3]{4c_2^2 \alpha_g} \tilde{r} + \frac{3\sqrt[3]{3\alpha_g} \sqrt[3]{-2c_2}}{\beta_m} - 1 \right] \times \left(\frac{2\tilde{M}}{\tilde{r}^2} + 2\alpha_g c_2 \tilde{r} - 3\sqrt[3]{4c_2^2 \alpha_g} \tilde{r} \right). \quad (52)$$

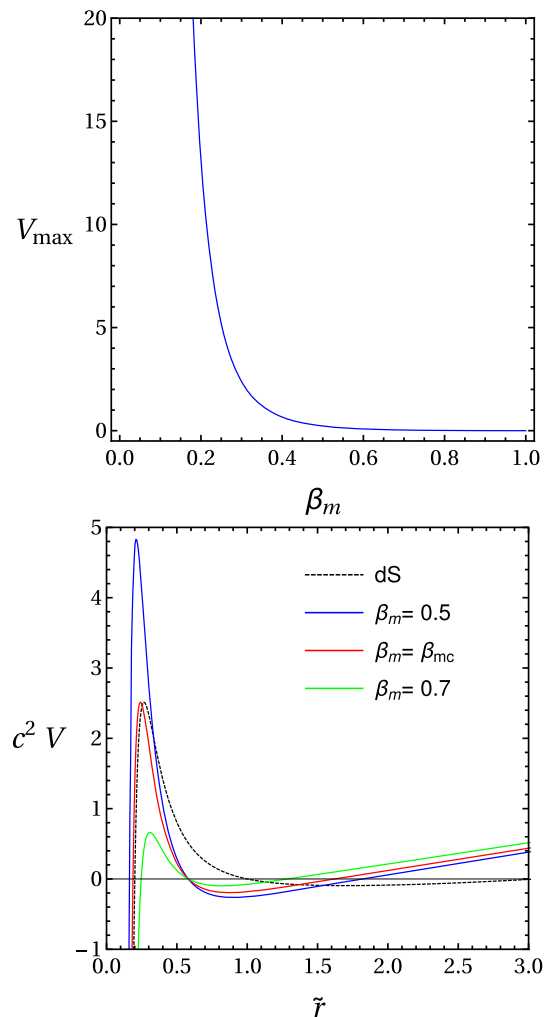


Fig. 4 The left panel shows the maximum of dRGT potential with $\ell = 0$, $\tilde{M} = 0.1$, $\alpha_g = 0.1$, $c = 1$, and $c_2 = -1$. The right panel shows the dRGT potential with $\ell = 0$, $\tilde{M} = 0.1$, $\alpha_g = 0.1$, $c = 1$, and $c_2 = -1$

By employing the same strategy as used in the de Sitter case, we found that the leading term of V_{max} is proportional to $V_{\text{max}} \propto 1/\beta_m$. By fixing $c_2 = -1$, we have illustrated the explicit behavior of the peak of the potential in the left panel of Fig. 4. We can explicitly see that V_{max} increases as β_m decreases. Moreover, the de Sitter potential and the dRGT potential with various values of β_m are plotted as shown in the right panel of Fig. 4. It shows that both the de Sitter potential and the dRGT potential increase with radial distance from the black hole. After that, they decrease with radial distance to reach the relative lowest point and then turn to increase again.

In [46], the maximum points of the potentials are not chosen to be equal. We consider this point here. The equality of the maximum points allows us to draw conclusions regarding how high the rigorous bounds on the greybody factors for different types of black holes are. At the highest point,

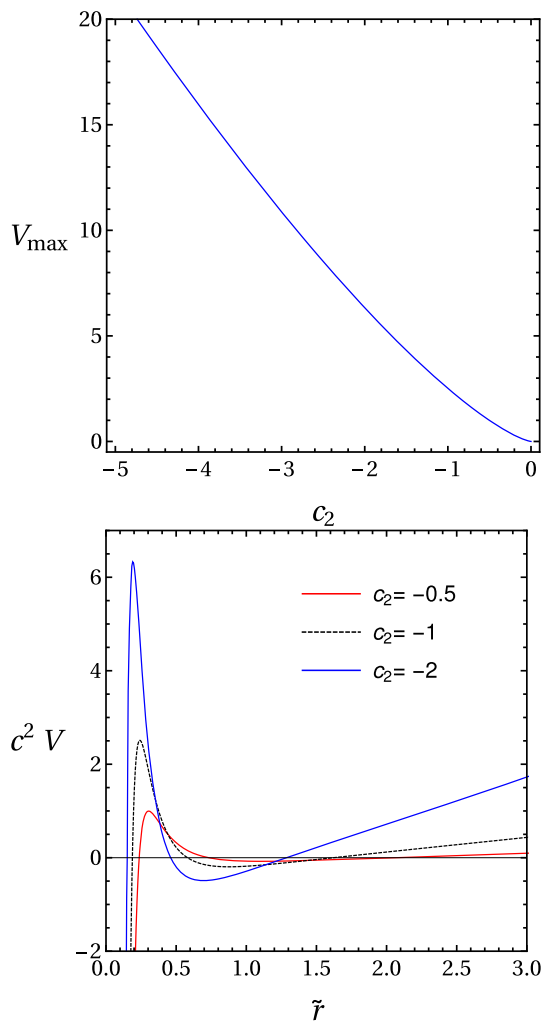


Fig. 5 The left panel shows the maximum dRGT potential with $\ell = 0$, $\tilde{M} = 0.1$, $\alpha_g = 0.1$, $c = 1$, and $\beta_m = 0.565375$. The right panel shows the dRGT potential with $\ell = 0$, $\tilde{M} = 0.1$, $\alpha_g = 0.1$, $c = 1$, and $\beta_m = 0.565375$

the derivative of the potential is zero. For $\ell = 0$, we obtain

$$V'(\tilde{r}) = \frac{1}{c^2} \frac{\tilde{r} f(\tilde{r}) f''(\tilde{r}) + \tilde{r} [f'(\tilde{r})]^2 - f(\tilde{r}) f'(\tilde{r})}{\tilde{r}^2}. \quad (53)$$

The solution of $V'(\tilde{r}) = 0$ is not shown here. We find that the equality of the peak of the potentials occur at $\beta_m = 0.565375$. Moreover, the effects of parameter c_2 are shown in Fig. 5.

To see the effect of the parameter c_2 on the potential, let us fix $\beta_m = \beta_{mc}$. The peak of the potential is plotted as shown in the left panel of Fig. 5. The potential is also plotted with various values of c_2 as shown in the right panel of Fig. 5. The parameter c_2 characterizes the strength of the graviton mass. Therefore, the graviton mass will enhance the potential in contrast to the effect of the cosmological constant in the de Sitter black hole.

In this section, we explore the behavior of the gravitational potential for both the de Sitter black hole and the dRGT black hole of a massless scalar field. By making a comparison with the potential in the Schwarzschild black hole, we found that the local maximum of the de Sitter potential is always less than one of the Schwarzschild potential. For the dRGT black hole, the local maximum of the potential depend on the model parameters; β_m characterizing the existence of two horizon ($0 < \beta_m < 1$) and c_2 characterizing the strength of the graviton mass. In contrast to the de Sitter potential, we found that the local maximum of the dRGT potential will be larger than ones for the Schwarzschild and the de Sitter potential by setting parameter $\beta_m \ll 1$ or $c_2 \ll -1$. In the same fashion as quantum theory, the shape of the potential has an effect on the transmission amplitude or the greybody factor in this context. We will use the information of the potential to analyze the behavior of the greybody factor in the next section.

4 The rigorous bounds on the greybody factors

From a classical point of view, a black hole is believed to be black because nothing, when having entered the black hole, can escape, not even light. From a quantum point of view, however, a black hole is no longer considered 'black' since it has been proven to emit a type of thermal radiation known as Hawking radiation. At the event horizon of a black hole, Hawking radiation is exactly a blackbody spectrum. While Hawking radiation propagates out from the event horizon, it is, however, modified by the spacetime curvature generated by its black hole source. Thus, an observer at an infinite distance observes the modified form of Hawking radiation, which is different from the original Hawking radiation at the event horizon. This difference can be measured by the so-called greybody factor.

In this section, a greybody factor will be obtained using the rigorous bound [35–37, 47]. The bound can give a qualitative description of a black hole. It is applied to various types of black holes such as a Schwarzschild black hole [48], a non-rotating black hole [49], a dirty black hole [50], a Kerr–Newman black hole [51], a Myers–Perry black hole [52], and a dRGT black hole [46]. The rigorous bounds on the greybody factors are given by

$$T \geq \text{sech}^2 \left(\int_{-\infty}^{\infty} \vartheta dr_* \right), \quad (54)$$

where

$$\vartheta = \frac{\sqrt{[h'(r_*)]^2 + [\omega^2 - V(r_*) - h^2(r_*)]^2}}{2h(r_*)}, \quad (55)$$

where $h(r_*)$ is a positive function satisfying $h(-\infty) = h(\infty) = \omega$. See [35] for more details. We select $h = \omega$. Therefore,

$$T \geq \text{sech}^2 \left(\frac{1}{2\omega} \int_{-\infty}^{\infty} |V| dr_* \right). \quad (56)$$

4.1 de Sitter black holes

To obtain the rigorous bound, we use the potential derived in the previous section. For de Sitter black holes, the potential is given by Eq. (50), with $c_1 = c_0 = 0$. Substituting this potential into Eq. (56), we obtain the rigorous bounds on the greybody factors

$$T \geq T_b = \text{sech}^2 \left[\frac{1}{2\omega c} \left\{ \ell(\ell+1) \left(\frac{1}{\tilde{r}_H} - \frac{1}{\tilde{R}_H} \right) + \tilde{M} \left(\frac{1}{\tilde{r}_H^2} - \frac{1}{\tilde{R}_H^2} \right) + 2\alpha_g c_2 (\tilde{R}_H - \tilde{r}_H) \right\} \right]. \quad (57)$$

The rigorous bounds on the reflection probabilities are given by

$$R \leq \tanh^2 \left[\frac{1}{2\omega c} \left\{ \ell(\ell+1) \left(\frac{1}{\tilde{r}_H} - \frac{1}{\tilde{R}_H} \right) + \tilde{M} \left(\frac{1}{\tilde{r}_H^2} - \frac{1}{\tilde{R}_H^2} \right) + 2\alpha_g c_2 (\tilde{R}_H - \tilde{r}_H) \right\} \right], \quad (58)$$

where, from Eq. (20), \tilde{r}_H and \tilde{R}_H are given by

$$\tilde{r}_H = \frac{6\tilde{M}}{\alpha_m} \cos \left[\frac{1}{3} \cos^{-1} \left(-\alpha_m \right) - \frac{2\pi}{3} \right] \quad (59)$$

$$\tilde{R}_H = \frac{6\tilde{M}}{\alpha_m} \cos \left[\frac{1}{3} \cos^{-1} \left(-\alpha_m \right) \right]. \quad (60)$$

Since \tilde{r}_H and \tilde{R}_H depend on parameters \tilde{M} and α_m , the structure of T_b depends on the strength of the cosmological constant through the parameter α_m . To see the effect of the cosmological constant qualitatively, let us consider the case $\alpha_m \ll 1$, which means that the effect of the cosmological constant is a correction to the Schwarzschild case. As a result, the horizons can be approximated as

$$\tilde{r}_H \sim 2\tilde{M}, \quad \tilde{R}_H \sim \left(\frac{3\sqrt{3}}{\alpha_m} - 1 \right) \tilde{M}. \quad (61)$$

By substituting these results into Eq. (57), the rigorous bound on the greybody factor for a de Sitter black hole can be

approximated as

$$T_b = \text{sech}^2 \left[\frac{1}{2\omega c} \left\{ \frac{\ell(\ell+1)}{\tilde{r}_H} \left(1 - \frac{2|\alpha_m|}{3\sqrt{3}} \right) + \frac{\tilde{M}}{r_H^2} \left(1 - \frac{4\alpha_m^2}{27} \right) - \frac{2\sqrt{3}|\alpha_m|}{9\tilde{M}} \right\} \right]. \quad (62)$$

From this equation, one can see that if $\alpha_m = 0$, the bound for Schwarzschild is recovered. Moreover, for $\alpha_m \neq 0$, the cosmological constant provides a negative correction to the Schwarzschild bound. Therefore, the greybody factor for the de Sitter black hole is greater than one for the Schwarzschild black hole. This is also consistent with the behavior of the potential, since the local maximum of the potential in the de Sitter black hole is always less than one in the Schwarzschild black hole. To confirm this result, we also used a numerical method to show that $T_{b(\text{dS})} \geq T_{b(\text{Sch})}$ by plotting T_b with various values of c_2 as illustrated in the left panel of Fig. 6.

The rigorous bound on the greybody factor is useful in any problem, especially in qualitative work. Moreover, the rigorous bound is accurate and its method of derivation is simpler than any other method such as the approximation derived from the matching technique. To see this, let us compare the rigorous bound with the matching technique. The analytical approximation from the matching technique in the low frequency limit for $\ell = 0$ is given by [53, 54]

$$T_{\text{app}} = 4(\kappa r_H)^2 \left(1 + \frac{\omega^2}{\kappa^2} \right) = 4(\kappa \tilde{r}_H)^2 \left(1 + \frac{\omega^2}{\kappa^2} \right), \quad (63)$$

where $\kappa^2 = -\alpha_g c_2 / c^2$. The rigorous bound on the greybody factor and the approximation are plotted as shown in the right panel of Fig. 6. The graph shows that the rigorous bound is less than the approximation, which satisfies the inequality (57).

4.2 dRGT black holes

For dRGT black holes, the potential is given by Eq. (50). Substituting this potential into Eq. (56), we obtain the rigorous bounds on the greybody factors

$$T \geq \text{sech}^2 \left[\frac{1}{2\omega c} \left\{ \ell(\ell+1) \left(\frac{1}{\tilde{r}_H} - \frac{1}{\tilde{R}_H} \right) + \tilde{M} \left(\frac{1}{\tilde{r}_H^2} - \frac{1}{\tilde{R}_H^2} \right) + 2\alpha_g c_2 (\tilde{R}_H - \tilde{r}_H) - \alpha_g c_1 \ln \left| \frac{\tilde{R}_H}{\tilde{r}_H} \right| \right\} \right]. \quad (64)$$

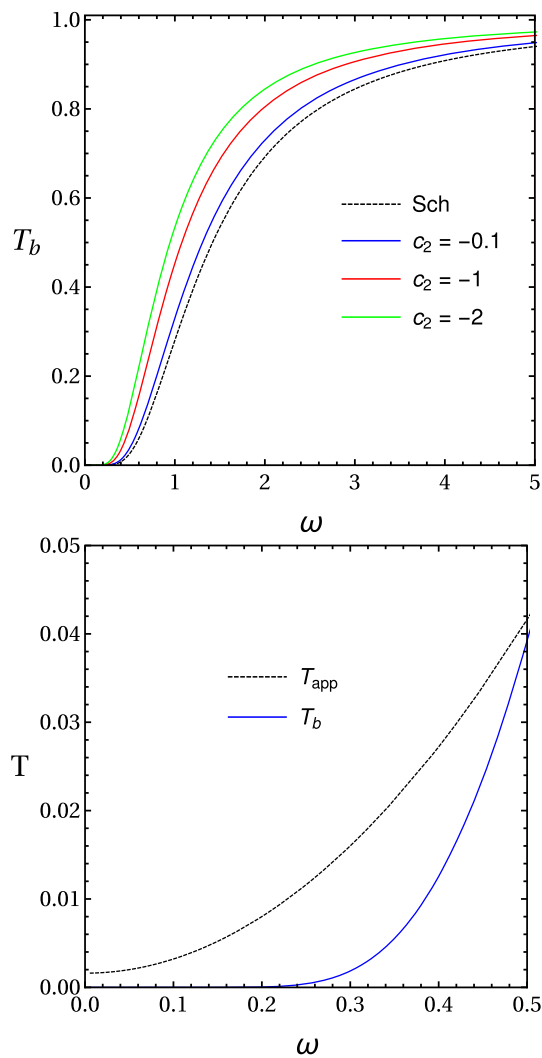


Fig. 6 The left panel shows a comparison between the rigorous bound on the greybody factor for a de Sitter black hole and a Schwarzschild black hole with $\ell = 0$, $c = 1$, and $\tilde{M} = \alpha_g = 0.1$. The right panel shows a comparison between the rigorous bound on the greybody factor and the approximation with $\ell = 0$, $c = 1$, $c_2 = -1$ and $\tilde{M} = \alpha_g = 0.1$

The rigorous bounds on the reflection probabilities are given by

$$R \leq \tanh^2 \left[\frac{1}{2\omega c} \left\{ \ell(\ell+1) \left(\frac{1}{\tilde{r}_H} - \frac{1}{\tilde{R}_H} \right) + \tilde{M} \left(\frac{1}{\tilde{r}_H^2} - \frac{1}{\tilde{R}_H^2} \right) + 2\alpha_g c_2 (\tilde{R}_H - \tilde{r}_H) - \alpha_g c_1 \ln \left| \frac{\tilde{R}_H}{\tilde{r}_H} \right| \right\} \right], \quad (65)$$

where, from Eqs. (31) and (32), $\tilde{r}_H = \tilde{r}_{dS1}$ and $\tilde{R}_H = \tilde{r}_{dS2}$ are given by

$$\tilde{r}_{dS1} = \frac{-2}{(-2c_2)^{1/3}} \left[X^{1/2} \cos \left(\frac{1}{3} \sec^{-1} Y + \frac{\pi}{3} \right) + 1 \right], \quad (66)$$

$$\tilde{r}_{dS2} = \frac{2}{(-2c_2)^{1/3}} \left[X^{1/2} \cos \left(\frac{1}{3} \sec^{-1} Y \right) - 1 \right]. \quad (67)$$

From Eq. (64), we find that the rigorous bound on the greybody factor in massive gravity crucially depends on two parameters, c_1 and c_2 , which determines how the structure of the graviton mass affects the bound. As we have discussed in Sect. 3, the parameter c_1 must be positive in order to have two horizons. Therefore, the last term in Eq. (64) always provides the negative correction to the bound, so that, for the potentials with the same height, the bound from the dRGT black hole is always larger than the bound from the de Sitter black hole. Moreover, this behavior can be qualitatively expressed by analyzing the potential for both cases. From Fig. 4, for the potentials with the same height, the potential from the dRGT case is always thinner than one from the de Sitter case. Therefore, the transmission amplitude for the dRGT case is always greater than one for the de Sitter case as seen in the left panel of Fig. 7. As we have analyzed earlier, the height of the potential can be controlled by two parameters, β_m and c_2 . Now let us figure out how the parameters affect the dRGT bound compared to the de Sitter bound.

By fixing c_2 , one can see that the bound crucially depends on $|\tilde{R}_H - \tilde{r}_H|$, which is proportional to $1/\beta_m$. Therefore, one finds that the larger the value of β_m , the higher is the value of the bound. This can be seen explicitly by numerically plotting T_b with various values of β_m as illustrated in the right panel of Fig. 7. Moreover, this behavior can also be seen by analyzing the potential. From Fig. 4, we found that the larger the value of β_m , the lower is the peak of the potential. Therefore, one finds that the larger the value of β_m , the higher is the value of the bound.

In terms of fixing β_m , one can see that the maximum value of the potential decreases when $|c_2|$ decreases as such that the bound will increase when $|c_2|$ decreases as shown in the left panel of Fig. 8. Moreover, to compare the bound from the dRGT black hole to one from the de Sitter and the Schwarzschild black hole, we also plot the bound by fixing ω as seen in the right panel of Fig. 8. From this figure, we found that the bound from the dRGT black hole can be larger or smaller than ones from both the de Sitter and the Schwarzschild black holes, depending on c_2 . On the other hand, the bound from the de Sitter black hole is always larger than the bound from the Schwarzschild black hole. Therefore, it is found that there is more room for the dRGT black hole to increase or decrease the greybody factor.

5 Conclusion

In this paper, we obtain the gravitational potential from Schwarzschild black holes, de Sitter black holes, and dRGT black holes. We also derive the rigorous bound on the grey-

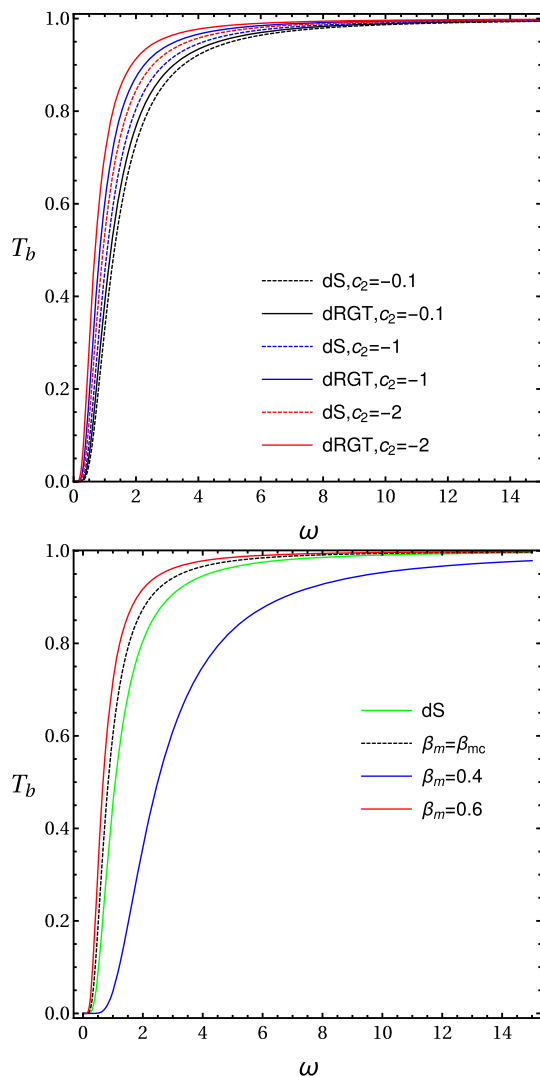


Fig. 7 The left panel shows a comparison of the rigorous bound of greybody factor for the dRGT and the de Sitter black holes with $\ell = 0$, $M = \alpha_g = 0.1$, while the parameter β_m is chosen to have the same height of potential. The right panel shows the rigorous bound on the greybody factor for a dRGT black hole with $c_2 = -1$

body factor for the de Sitter black hole and the dRGT black hole. It is found that the structure of potentials determines how much the rigorous bound on the greybody factor should be. Since V_{\max} contributed from a de Sitter black hole is always less than one in a Schwarzschild black hole, the bound for a de Sitter black hole is greater than one for a Schwarzschild black hole. In case of potentials with the same height, the result shows that the bound from a dRGT black hole is always larger than the bound from a de Sitter black hole. Otherwise, the bound from a dRGT black hole can be larger or smaller than ones from both de Sitter and Schwarzschild black holes due to different effects of the parameter c_2 on de Sitter and dRGT spacetimes. Furthermore, we compare the greybody factor derived from the

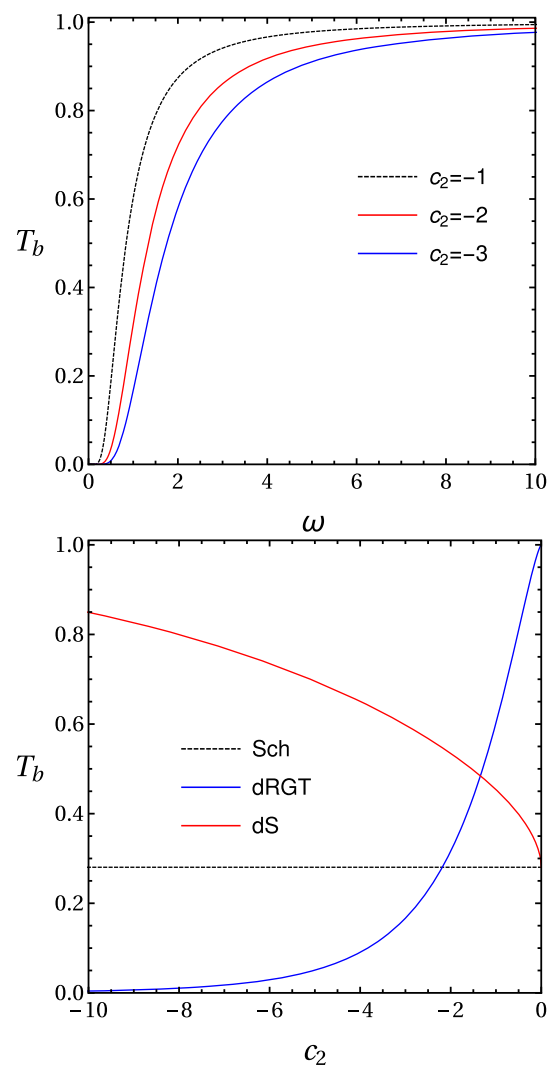


Fig. 8 The left panel shows the effect of parameter c_2 on the rigorous bound on the greybody factor for a dRGT black hole with $\ell = 0$, $M = \alpha_g = 0.1$, and $\beta_m = 0.565375$. The right panel shows a comparison of the rigorous bound on the greybody factor for a dRGT black hole with $M = \alpha_g = 0.1$, $\omega = 1$, and $\beta_m = 0.565375$

rigorous bound with the greybody factor derived from the matching technique. The results show that the greybody factor obtained from the rigorous bound is less than the one from the matching technique, which means that the rigorous bound is a true lower bound.

Acknowledgements This project was funded by the Ratchadapisek Sompoch Endowment Fund, Chulalongkorn University (Sci-Super 2014-032), by a Grant for the professional development of new academic staff from the Ratchadapisek Somphot Fund at Chulalongkorn University, by the Thailand Research Fund (TRF), and by the Office of the Higher Education Commission (OHEC), Faculty of Science, Chulalongkorn University (RSA5980038). PB was additionally supported by a scholarship from the Royal Government of Thailand. TN was also additionally supported by a scholarship from the Development and Promotion of Science and Technology Talents Project (DPST). PW was also

additional supported by the Naresuan University Research Fund through Grant no. R2559C235 and the ICTP through Grant no. OEA-NET-01

Open Access This article is distributed under the terms of the Creative Commons Attribution 4.0 International License (<http://creativecommons.org/licenses/by/4.0/>), which permits unrestricted use, distribution, and reproduction in any medium, provided you give appropriate credit to the original author(s) and the source, provide a link to the Creative Commons license, and indicate if changes were made. Funded by SCOAP³.

References

- Supernova Search Team Collaboration, A.G. Riess et al., *Astron. J.* **116**, 1009–1038 (1998). [[arXiv:astro-ph/9805201](#)]
- Supernova Cosmology Project Collaboration, S. Perlmutter et al., *Astrophys. J.* **517**, 565–586 (1999). [[arXiv:astro-ph/9812133](#)]
- T. Clifton, P.G. Ferreira, A. Padilla, C. Skordis, *Phys. Rep.* **513**, 1–189 (2012). [[arXiv:1106.2476](#) [astro-ph.CO]]
- C. de Rham, G. Gabadadze, *Phys. Rev. D* **82**, 044020 (2010). [[arXiv:1007.0443](#) [hep-th]]
- C. de Rham, G. Gabadadze, A.J. Tolley, *Phys. Rev. Lett.* **106**, 231101 (2011). [[arXiv:1011.1232](#) [hep-th]]
- C. de Rham, *Living Rev. Relat.* **17**, 7 (2014). [[arXiv:1401.4173](#) [hep-th]]
- G. D’Amico, C. de Rham, S. Dubovsky, G. Gabadadze, D. Pirtskhalava, A.J. Tolley, *Phys. Rev. D* **84**, 124046 (2011). [[arXiv:1108.5231](#) [hep-th]]
- A.E. Gumrukcuoglu, C. Lin, S. Mukohyama, *JCAP* **1111**, 030 (2011). [[arXiv:1109.3845](#) [hep-th]]
- A.E. Gumrukcuoglu, K. Hinterbichler, C. Lin, S. Mukohyama, M. Trodden, *Phys. Rev. D* **88**, 024023 (2013). [[arXiv:1304.0449](#) [hep-th]]
- G. D’Amico, G. Gabadadze, L. Hui, D. Pirtskhalava, *Class. Quant. Grav.* **30**, 184005 (2013). [[arXiv:1304.0723](#) [gr-qc]]
- T. Chullaphan, L. Tannukij, P. Wongjun, *JHEP* **06**, 038 (2015). [[arXiv:1502.08018](#) [gr-qc]]
- A. De Felice, S. Mukohyama, *Phys. Lett. B* **728**, 622 (2014). <https://doi.org/10.1016/j.physletb.2013.12.041>. [[arXiv:1306.5502](#) [hep-th]]
- A. De Felice, A. EmirGumrukcuoglu, S. Mukohyama, *Phys. Rev. D* **88**(12), 124006 (2013). [[arXiv:1309.3162](#) [hep-th]]
- L. Tannukij, P. Wongjun, *Eur. Phys. J. C* **76**(1), 17 (2016). <https://doi.org/10.1140/epjc/s10052-015-3872-0>. [[arXiv:1511.02164](#) [gr-qc]]
- E. Babichev, R. Brito, *Class. Quant. Grav.* **32**, 154001 (2015). <https://doi.org/10.1088/0264-9381/32/15/154001>. [[arXiv:1503.07529](#) [gr-qc]]
- M.S. Volkov, *Class. Quant. Grav.* **30**, 184009 (2013). [[arXiv:1304.0238](#) [hep-th]]
- G. Tasinato, K. Koyama, G. Niz, *Class. Quant. Grav.* **30**, 184002 (2013). [[arXiv:1304.0601](#) [hep-th]]
- S.G. Ghosh, L. Tannukij, P. Wongjun, *Eur. Phys. J. C* **76**(3), 119 (2016). <https://doi.org/10.1140/epjc/s10052-016-3943-x>. [[arXiv:1506.07119](#) [gr-qc]]
- A. Salam, J.A. Strathdee, *Phys. Rev. D* **16**, 2668 (1977)
- D. Zou, R. Yue, M. Zhang, *Eur. Phys. J. C* **77**, 256 (2017). [[arXiv:1612.08056](#) [gr-qc]]
- D. Zou, Y. Liu, R. Yue. [[arXiv:1702.08118](#)]
- S.H. Hendi, R.B. Mann, S. Panahiyan, B.E. Panah, *Phys. Rev. D* **95**, 021501(R) (2017). [[arXiv:1702.00432](#) [gr-qc]]
- S.H. Hendi, G.Q. Li, J.X. Mo, S. Panahiyan, B.E. Panah, *Eur. Phys. J. C* **76**, 571 (2016). [[arXiv:1608.03148](#) [gr-qc]]
- S.H. Hendi, B.E. Panah, S. Panahiyan, *JHEP* **05**, 029 (2016). [[arXiv:1604.00370](#) [hep-th]]
- P. Kanti, T. Pappas, N. Pappas, *Phys. Rev. D* **90**, 124077 (2014). [[arXiv:1409.8664](#) [hep-th]]
- K. Koyama, G. Niz, G. Tasinato, *Phys. Rev. Lett.* **107**, 131101 (2011). [[arXiv:1103.4708](#) [hep-th]]
- K. Koyama, G. Niz, G. Tasinato, *Phys. Rev. D* **84**, 064033 (2011). [[arXiv:1104.2143](#) [hep-th]]
- S.W. Hawking, *Commun. Math. Phys.* **43**, 199 (1975)
- S. Fernando, *Gen. Relativ. Gravit.* **37**, 461 (2005)
- W. Kim, J.J. Oh, *JKPS* **52**, 986 (2008)
- J. Escobedo, “Greybody Factors Hawking Radiation in Disguise”, Masters Thesis, University of Amsterdam (2008)
- M.K. Parikh, F. Wilczek, *Phys. Rev. Lett.* **85**, 5042 (2000). [[arXiv:hep-th/9907001](#)]
- C. H. Fleming, (2005). <http://www.physics.umd.edu/grt/taj/776b/fleming.pdf>
- P. Lange, Calculation of Hawking Radiation as Quantum Mechanical Tunneling. Thesis, Uppsala Universitet (2007)
- M. Visser, *Phys. Rev. A* **59**, 427438 (1999). [[arXiv:quant-ph/9901030](#)]
- P. Boonserm, M. Visser, *Ann. Phys.* **323**, 2779 (2008). [[arXiv:0801.0610](#) [quant-ph]]
- P. Boonserm, Rigorous Bounds on Transmission, Reflection, and Bogoliubov Coefficients. Ph. D. Thesis, Victoria University of Wellington (2009). [[arXiv:0907.0045](#)]
- H. Zhang, X.Z. Li, *Phys. Rev. D* **93**, 124039 (2016)
- S.H. Hendi, R.B. Mann, S. Panahiyan, B.E. Panah, *Phys. Rev. D* **95**, 021501(R) (2017)
- M. Barriola, A. Vilenkin, *Phys. Rev. Lett.* **63**, 341 (1989)
- Q. Huang, J. Chen, Y. Wang, *Int. J. Theor. Phys.* **54**(2), 459 (2015). [[arXiv:1408.6901](#)]
- T. Tamaki, N. Sakai, *Phys. Rev. D* **69**, 044018 (2004). [[gr-qc/0309068](#)]
- H. Kodama, I. Arraut, *Prog. Theor. Exp. Phys.*, 023E02 (2014). [[arXiv:1312.0370](#)]
- A.I. Vainshtein, *Phys. Lett. B* **39**, 393 (1972)
- I. Arraut, *Int. J. Mod. Phys. D* **24**, 1550022 (2015). [[arXiv:1311.0732](#) [gr-qc]]
- T. Ngampitipan, P. Boonserm, P. Wongjun, *AJPA* **4**, 64 (2016)
- T. Ngampitipan, Rigorous Bounds on Greybody Factors for Various Types of Black Holes. Ph. D. Thesis, Chulalongkorn University (2014)
- P. Boonserm, M. Visser, *Phys. Rev. D* **78**, 101502 (2008). [[arXiv:0806.2209](#) [gr-qc]]
- T. Ngampitipan, P. Boonserm, *Int. J. Mod. Phys. D* **22**, 1350058 (2013). [[arXiv:1211.4070](#) [math-ph]]
- P. Boonserm, T. Ngampitipan, M. Visser, *Phys. Rev. D* **88**, 041502 (2013). [[arXiv:1305.1416](#) [gr-qc]]
- P. Boonserm, T. Ngampitipan, M. Visser, *JHEP* **113**, (2014) [[arXiv:1401.0568](#) [gr-qc]]
- P. Boonserm, A. Chatrabhuti, T. Ngampitipan, M. Visser, *J. Math. Phys.* **55**, 112502 (2014). <https://doi.org/10.1063/1.4901127>. [[arXiv:1405.5678](#) [gr-qc]]
- T. Harmark, J. Natario, R. Schiappa, *Adv. Theor. Math. Phys.* **14**, 727 (2010). [[arXiv:1103.4708](#) [hep-th]]
- R. Dong, D. Stojkovic, *Phys. Rev. D* **92**, 084045 (2015). [[arXiv:1505.03145](#) [gr-qc]]

May 27-28, 2016
Hangzhou, China

2016 International Conference on Physics and Physics Education
2016 International Symposium on Materials Science and Engineering

CONFERENCE GUIDE

ICPHY2016

<http://www.icphy.com>

MSCIENG2016

<http://www.mscieng.com>



2016 International Conference on Physics and Physics Education (ICPHY2016)

2016 International Symposium on Materials Science and Engineering (MSCIENG2016)

• Conference Guide •

May 27-28, 2016

Hangzhou, China

Venue: Best Western Hangzhou Meiyuan Hotel

Organizer: Shanghai Laixi Conference Services Co., Ltd.

Contents

Program Committee	1
Conference Schedule.....	2
Detailed Agenda	3
Keynote Speakers	5
Note & Tips	8
Abstracts	9
Call for Papers.....	19
Conference123.net.....	20
Tourism in Hangzhou	21
Conference Venue.....	23

Program Committee

ICPHY2016 and MSCIEENG2016 Program Committee

Wenhong Liu, Professor

School of Electronic and Information, Shanghai Dianji University, China

Kuan-Wei Lee, Professor

Department of Electronic Engineering, I-Shou University, Taiwan

Dr. O. L. Shanmugasundaram, Professor

Department of Textile Technology, KSR College of Technology, India

Ricardo Branco, Professor

Department of Mechanical Engineering, Polytechnic Institute of Coimbra, Portugal

Dr. Hamid Yaghoubi

Iran Maglev Technology (IMT), Iran

Dr. N. ETHIRAJ

Department of Mechanical Engineering, Dr. M.G. R Educational and Research Institute, China

Peng-Sheng Wei, Xi-Wan Chair Professor

Department of Mechanical and Electro-Mechanical Engineering, National Sun Yat-Sen University, Taiwan

Dr. Shimin Mao

Department of Materials Science and Engineering, University of Illinois Urbana Champaign, USA

Oral Presentations

May 27, 2016, 14:00-17:30

Qixia Hall, 2nd Floor (2 楼栖霞厅)

Session Chair: Nyet Moi Siew

Conference	Time	Oral Presenter	Topic
ICPHY2016	14:05-14:25	Olivier Nadeau	University-College Collaborative Program
	14:25-14:45	Petarpa Boonserm	The Modified Tolman-Oppenheimer Volkov (TOV) Equation and the Effect of Charge on the Pressure in Charge Anisotropy
	14:45-15:05	Istok Menkovic	Modeling the 3D Electron Density and Temperature of a Planetary Nebula from Imaging Spectroscopy
	15:05-15:25	Nyet Moi Siew	Fostering Physics Student Teachers' Ability to Generate Productive Questions Using Elstgeest and Alfke's Questioning Model with Manipulatives
	Coffee Break & Photo Taking (25 Minutes)		
	15:50-16:10	Napasorn Jongjittanon	Generating Theorems for Charged Anisotropy in General Relativity
MSCIENG2016	16:10-16:30	Tritos Ngampitipan	Bounding the Greybody Factor, Temperature and Entropy of Black Holes in dRGT Massive Gravity
	16:30-16:50	Shouyun Zhang	The Research on the Production of Bio-based Polyamides 56 Sheath-core Composite Modified Fiber
	16:50-17:10	Hsien Hua Lee	Analysis on a Cast-Iron Pipe Applied to Protection of Underwater Cable
	17:10-17:30	Bee Lyong Yang	Solar Hydrogen Production Achieved Through Single Crystalline and Polycrystalline TiO ₂ Nanostructures

Abstracts

Abstracts Accepted by ICPHY2016

The following are the abstracts of the papers which have been accepted by 2016 International Conference on Physics and Physics Education (ICPHY2016) and the abstracts according to which the authors will make their Oral Presentations at the conference.

[01] **The Modified Tolman-Oppenheimer-Volkov (TOV) Equation and the Effect of Charge on Pressure in Charge Anisotropy (380028)**

Petarpa Boonserm, Napasorn Jongjittanon, Tritos Ngampitipan

Abstract: The Tolman-Oppenheimer-Volkov (TOV) equation describes the interior properties of spherical static perfect fluid object as a relationship between two physical observables - pressure and density. For a fluid sphere object, which contains electric charge, magnetic field, and scalar field, the pressure becomes anisotropic. In the previous article [Phys. Rev. D 76 (2007) 044024; gr-qc/0607001], we deformed TOV in terms of $\delta\rho_c$ and δp_c , and we found a new physical and mathematical interpretation for the TOV equation. In this work, we cannot use the perfect fluid constraints because of the electromagnetic field and the massless scalar field within this object. The TOV equation was thus generalized to involve the electromagnetic and the scalar fields. This model is close to the realistic objects in our universe such as a neutron star. In this paper, we consider the modified TOV equation for Schwarzschild coordinates in a special case. The density is considered as a constant and the scalar field is considered absent. On the general model of the TOV equation, the pressure is expressed in terms of radius. However, this model shows that pressure is affected by electric charge. Moreover, we also calculate the rigorous bound on the transmission probability for the Tolman-Bayin type of charged fluid sphere.

[02] **Generating Theorems for Charged Anisotropy in General Relativity (380025)**

Napasorn Jongjittanon, Petarpa Boonserm, Tritos Ngampitipan

Abstract: For describing the interior of a spherical object in the general relativistic frame, some objects can be considered using the concept of perfect fluid spheres for simplicity. The absence of heat conduction and shear stress, and the presence of isotropic pressure are the characteristics of perfect fluid spheres. Previous works in this field constitute finding solutions for perfect fluid spheres in various coordinates. In this work, we are interested in generating anisotropic solution for fluid spheres. The particular property of anisotropy, which differs from the property of perfect fluid spheres, is that the radial pressure and the transverse pressure are not equal. One cause of anisotropy is the presence of charge inside an object. Anisotropic fluid spheres are models for describing a charged star such as a neutron star. An important tool in studying fluid sphere solutions is the solution generating algorithm. This technique can be used to generate new solution from known solutions without having to solve Einstein's equation directly. The solution generating theorems for anisotropic fluid spheres are constructed in terms of the metric of spacetime. The other purpose is to classify the types of solution into seed and non-seed metrics.

The Modified Tolman-Oppenheimer-Volkov (TOV) Equation and the Effect of Charge on Pressure in Charge Anisotropy

Petarpa Boonserm^{1,*}, Napasorn Jongjittanon², Tritos Ngampitipan³

¹Department of Mathematics and Computer Science, Faculty of Science, Chulalongkorn University, Bangkok, Thailand

²Department of Physics, Faculty of Science, Chulalongkorn University, Bangkok, Thailand

³Faculty of Science, Chandrakasem Rajabhat University, Bangkok, Thailand

Email address:

Petarpa.Boonserm@gmail.com (P. Boonserm), njongjittanon@gmail.com (N. Jongjittanon), tritos.ngampitipan@gmail.com (T. Ngampitipan)

*Corresponding author

To cite this article:

Petarpa Boonserm, Napasorn Jongjittanon, Tritos Ngampitipan. The Modified Tolman-Oppenheimer-Volkov (TOV) Equation and the Effect of Charge on Pressure in Charge Anisotropy. *American Journal of Physics and Applications*. Vol. 4, No. 2, 2016, pp. 57-63.

doi: 10.11648/j.ajpa.20160402.14

Received: February 28, 2016; Accepted: March 18, 2016; Published: March 25, 2016

Abstract: The Tolman-Oppenheimer-Volkov (TOV) equation describes the interior properties of spherical static perfect fluid object as a relationship between two physical observables - pressure and density. For a fluid sphere object, which contains electric charge, magnetic field, and scalar field, the pressure becomes anisotropic. In the previous article [Phys. Rev. D 76 (2007) 044024; gr-qc/0607001], we deformed TOV in terms of $\delta\rho_c$ and δp_c , and we found a new physical and mathematical interpretation for the TOV equation. In this work, we cannot use the perfect fluid constraints because of the electromagnetic field and the massless scalar field within this object. The TOV equation was thus generalized to involve the electromagnetic and the scalar fields. This model is close to the realistic objects in our universe such as a neutron star. In this paper, we consider the modified TOV equation for Schwarzschild coordinates in a special case. The density is considered as a constant and the scalar field is considered absent. On the general model of the TOV equation, the pressure is expressed in terms of radius. However, this model shows that pressure is affected by electric charge. Moreover, we also calculate the rigorous bound on the transmission probability for the Tolman-Bayin type of charged fluid sphere.

Keywords: General Relativity, Modified TOV Equation, Charge Anisotropy, Transmission Probability

1. Introduction

Several general relativistic isotropic stars can be modeled by perfect fluid spheres [1-2]. A perfect fluid is one with no viscosity, shear stresses, or heat conduction. It is one of the exact solutions to the Einstein's field equation, which is the core equation of general relativity established by Einstein in 1915. A perfect fluid, as a solution to the Einstein's field equation, interests physicists because the equation seems impossible to be solved exactly. Therefore, solving for a perfect fluid poses a great challenge. Several perfect fluid sphere solutions have been generated in literature by directly solving Einstein's equation. These known solutions can also, alternatively, be generated by algorithmic techniques [2]. One of the algorithmic techniques is the solution generating theorem [3]. These generating theorems can produce new

solutions for perfect fluid spheres without directly solving the Einstein's field equation. Sometimes, already known solutions are recovered. Sometimes, new (previously unknown) solutions are obtained. Moreover, these theorems can also be used as criteria to classify metrics into seed and non-seed metrics [3]. Furthermore, by rewriting these theorems in terms of pressure and density, we obtain new solutions for the Tolman-Oppenheimer-Volkov (TOV) equation [4]. When charges are added into perfect fluid spheres, new features arise. These charges make the fluid spheres anisotropic. Anisotropic spheres can be used as models for many charged stars [10]. Moreover, the charges can change the pressure and density profile of stars [4]. The scalar field can also make fluid spheres anisotropic [5]. With charge and scalar field, a generalized TOV equation is formed [10]. In this project, generating theorems will be developed for anisotropic spheres. Following

development, the generating theorems will be applied to some known anisotropic spheres. The solution generating theorems for perfect fluid spheres can be found in reference [3]. These theorems facilitate us in terms of not having to solve the Einstein's field equation directly to obtain new solutions.

For the solution generating theorems, the theorem transformations are based on spacetime geometry. But as for physical measurements, an object can more easily be observed in terms of mass and energy rather than the geometry of spacetime around it. Because the object's matter can be expressed by energy-momentum-stress tensor in terms of pressure and density, the solution generating theorems should be applied on the physical observables: pressure and density. In addition, this paper is based on general relativity. One of the exact solutions to Einstein's equation is a perfect fluid sphere. Perfect fluid spheres can be made anisotropic by the existence of charge and scalar field. This consequently results in a more complicated form of the Einstein's equation, which is evidently more difficult to solve.

The relationship between the pressure and density profile is given in the Tolman-Oppenheimer-Volkov [TOV] equation [4];

$$\frac{dp(r)}{dr} = - \frac{[\rho(r)+p(r)][m(r)+4\pi p(r)r^3]}{r^2[1-\frac{2m(r)}{r}]}, \quad (1)$$

$$\frac{dm(r)}{dr} = 4\pi\rho(r)r^2. \quad (2)$$

These equations are inertia solution of static perfect fluid sphere objects, which are derived from the Schwarzschild metric. For the two physical observables, it is also easy to check for physical reasonableness of the quantities. Assuming that we obtain the pressure p_0 and the density ρ_0 , we can transform them to new solutions in terms of $p + \delta p$ and $\rho + \delta \rho$, and take the TOV equation as a Riccati equation.

Referring to the article by P. Boonserm et al. [4], the solution generating theorems for the TOV equation has been developed as follows.

Theorem (P1) [4]. Let $p_0(r)$ and $\rho_0(r)$ solve the TOV equation, and hold $m_0(r) = 4\pi \int \rho_0(r)r^2 dr$ as fixed. Define an auxiliary function $g_0(r)$ by

$$g_0 = \frac{m_0(r)+4\pi p_0(r)r^3}{r^2[1-2m_0(r)/r]}. \quad (3)$$

Then the general solution to the TOV equation is $p(r) = p_0(r) + \delta p(r)$ where

$$\delta p(r) = \frac{\delta p_c \sqrt{1-2m_0(r)/r} \exp\{-2 \int_0^r g_0 dr\}}{1+4\pi\delta p_c \int_0^r \frac{1}{\sqrt{1-2m_0(r)/r}} \exp\{-2 \int_0^r g_0 dr\} r dr}, \quad (4)$$

where δp_c is the shift in the central pressure.

Theorem (P2) [4]. Let $p_0(r)$ and $\rho_0(r)$ solve the TOV equation, and hold g_0 fixed, such that

$$g_0 = \frac{m_0(r)+4\pi p_0(r)r^3}{r^2[1-2m_0(r)/r]} = \frac{m(r)+4\pi p(r)r^3}{r^2[1-2m(r)/r]}. \quad (5)$$

Then the general solution to the TOV equation is given by $p(r) = p_0(r) + \delta p(r)$ and $m(r) = m_0(r) + \delta m(r)$ where

$$\delta m(r) = \frac{4\pi r^3 \delta \rho_c}{3[1+r g_0]^2} \exp\left\{2 \int_0^r g_0 \frac{1-r g_0}{1+r g_0} dr\right\}, \quad (6)$$

and

$$\delta p(r) = - \frac{\delta m}{4\pi r^3} \frac{1+8\pi p_0 r^2}{1-2m_0/r}. \quad (7)$$

Here $\delta \rho_c$ is the shift in the central density. By explicitly combining these formulae we have

$$\delta p(r) = \frac{\delta p_c}{[1+r g_0]^2} \frac{1+8\pi p_0 r^2}{1-\frac{2m_0}{r}} * \exp\left\{2 \int_0^r g_0 \frac{1-r g_0}{1+r g_0} dr\right\},$$

and

$$\delta \rho(r) = - \frac{1}{r^2} \frac{d}{dr} \left(\frac{\delta p(r)r^3}{1+2r g_0(r)} \right).$$

2. Charged Fluid Spheres

2.1. Anisotropic Fluid Spheres and Generalized TOV Equation

The perfect fluid sphere possesses key properties such as the isotropy of pressure with no viscosity, shear stresses, or heat conduction. Using perfect fluid spheres, stars in our universe can be modeled. If charges are added to a perfect fluid sphere, the latter becomes anisotropic. An anisotropic sphere can also be made by a scalar field. Perfect fluid spheres are the first approximation of solution for many objects. However, there are also many other spherical objects that do not fit the properties of perfect fluid spheres. One kind of such object is a neutron star. The radial pressure of the stars differs from the transverse pressure. The applied idea for these stars is referred to as anisotropic fluid spheres.

$$T_{\hat{a}\hat{b}} = \begin{bmatrix} \rho & 0 & 0 & 0 \\ 0 & p_r & 0 & 0 \\ 0 & 0 & p_t & 0 \\ 0 & 0 & 0 & p_t \end{bmatrix}.$$

We define new solution of charged fluid spheres as the metric of spacetime

$$ds^2 = -\zeta_0(r)^2 dt^2 + \frac{dr^2}{B_0(r)} + r^2 d\Omega^2 \quad (8)$$

or with the notation $\{\zeta_0, B_0\}$ by setting

$$G_{\hat{r}\hat{r}} - G_{\hat{\theta}\hat{\theta}} = 8\pi\Delta,$$

where Δ is an arbitrary function in terms of radius r . The Einstein's tensors were written in a non-coordinate form, which represents an observer's view of physical quantities.

2.2. Modeling Static Anisotropy

For describing the inertia properties of anisotropy, we need

to modify the new energy momentum stress tensor for anisotropy. It can be modeled in terms of a linear combination of the “perfect fluid”, “electromagnetic field”, and “massless scalar field”,

From the definition [10], the tensor for perfect fluid spheres is

$$T_f^{ab} = (\rho_f + p_f) V^a V^b + p_f g^{ab}.$$

The tensor for electromagnetic field is

$$T_{em}^{ab} = F^{ac} g_{cd} F^{bd} - \frac{1}{4} g^{ab} (F_{cd} F^{cd}).$$

The tensor for (minimally coupled) massless scalar field is

$$T_s^{ab} = \phi_{;a} \phi_{;b} - \frac{1}{2} g^{ab} (g^{cd} \phi_{;c} \phi_{;d}).$$

Using the covariant conservation of total stress energy, $T^{ab}_{;b} = 0$, we obtain a relation of perfect fluid density with pressure, scalar field, and the field strength tensor of the electromagnetic field

$$(\rho_f + p_f) V^a_{;b} V^b + g^{ab} ([p_f]_{;b} + \sigma_s \phi_{;b}) - F^{ab} (\sigma_{em} V_b) = 0,$$

After we obtain the equation of anisotropy in terms of pressure and density, we have to assume that the equation must be equivalent to the TOV equation.

This is the modified TOV equation [10]

$$\frac{dp_f}{dr} = - \frac{[\rho_f + p_f][m(r) + 4\pi p_f r^3]}{r^2 [1 - \frac{2m(r)}{r}]} - \frac{\sigma_{em} E}{\sqrt{1 - \frac{2m(r)}{r}}} - \sigma_s \frac{d\phi}{dr}, \quad (9)$$

$$\frac{dm}{dr} = 4\pi \rho r^2 = 4\pi (\rho_f + \rho_{em} + \rho_s) r^2, \quad (10)$$

where ρ_f , ρ_{em} , ρ_s , σ_{em} , σ_s , and ϕ represent perfect fluid density, electromagnetic density, electromagnetic charge, and the massless scalar charge and field, respectively.

3. The Effect of Charge on Pressure

3.1. Special Case: When ρ Is Constant and σ_s Is Zero

In this case, the generalized TOV equation becomes

$$\frac{dp_f}{dr} = - \frac{[\rho_f + p_f][m(r) + 4\pi p_f r^3]}{r^2 [1 - \frac{2m(r)}{r}]} - \frac{\sigma_{em} E}{\sqrt{1 - \frac{2m(r)}{r}}} \quad (11)$$

supplemented with

$$\frac{dm}{dr} = 4\pi \rho r^2 = 4\pi (\rho_f + \rho_{em}) r^2. \quad (12)$$

Integrating the above equation, we obtain

$$m(r) = \frac{4}{3} \pi \rho r^3. \quad (13)$$

Substituting $m(r)$ into the generalized TOV equation, we can numerically solve for p_f as shown in Figure 2.

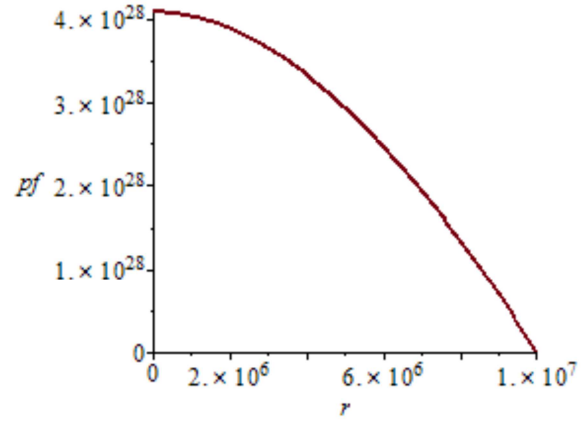


Figure 1. The fluid pressure as a function of radius.

3.2. The Effect Between Charge and Pressure

In this part, we will investigate how the charge affects the pressure in an anisotropic fluid sphere. From equation (11), we set the mass, density, and electric field fixed, and vary the charge density in order to examine how the pressure changes. The effect of charge on pressure is shown in the Table 1.

Table 1. This table shows the effect of charged density on pressure for generalized TOV equation in special case ($\rho = \text{constant}$).

Charge density (C/m ³)	Pressure (N/m ²)
1	4.08×10^{28}
2×10^{11}	7.25×10^{29}
3×10^{11}	1.08×10^{30}
4×10^{11}	2.00×10^{30}
5×10^{11}	1.84×10^{30}

From the table, we can see that when the charge density increases, the pressure also increases. The charge causes the pressure to increase. Anisotropic fluid sphere has a pressure greater than that of perfect fluid sphere for equal mass, density, and electric field. For example, we compare the case of $\sigma_{em} = 10^{11} \text{ kg/m}^3$ with the case of $\sigma_{em} = 5 \times 10^{11} \text{ kg/m}^3$ as shown in Figures 2 and 3, respectively.

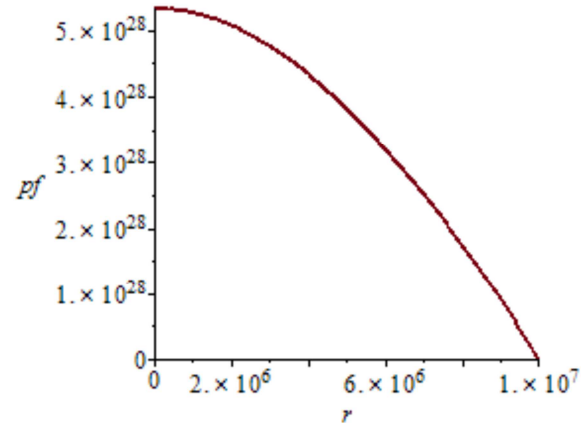


Figure 2. The fluid pressure for $\sigma_{em} = 10^{11} \text{ kg/m}^3$

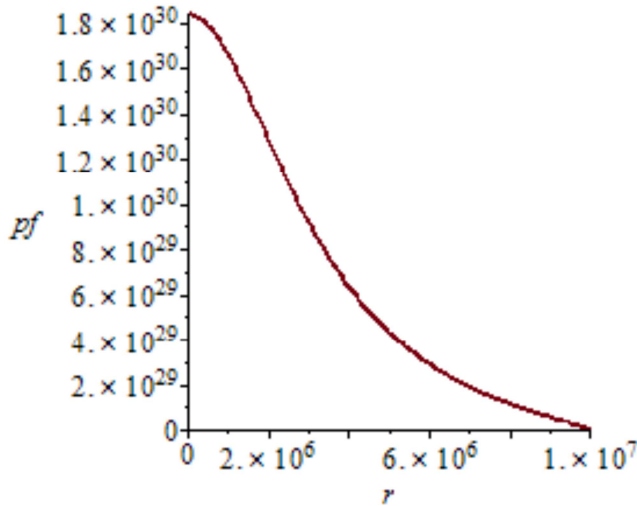


Figure 3. The fluid pressure for $\sigma_{em} = 5 \times 10^{11} \text{ kg/m}^3$.

From these graphs, we can see that when the charge is denser, the fluid pressure increases. In this case, when the charge density increases by 5 times, the pressure can increase by a 100 times. Moreover, the effect of fluid density on pressure is also investigated, as shown in Table 2.

Table 2. This table shows the effect of fluid density on pressure for generalized TOV equation in special case ($\rho = \text{constant}$).

Density (kg/m^3)	Pressure (N/m^2)
1×10^{12}	4.08×10^{28}
1.1×10^{12}	6.28×10^{28}
1.2×10^{12}	1.04×10^{29}
1.3×10^{12}	2.07×10^{29}
1.4×10^{12}	9.47×10^{29}

Similarly, when the fluid density increases, the pressure also increases. This means that the denser charged stars have a pressure greater than the less compact stars.

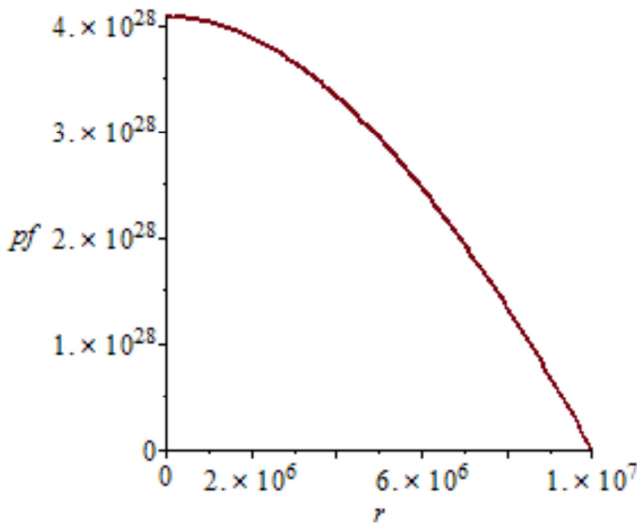


Figure 4. The fluid pressure for $\rho_f = 10^{22} \text{ kg/m}^3$.

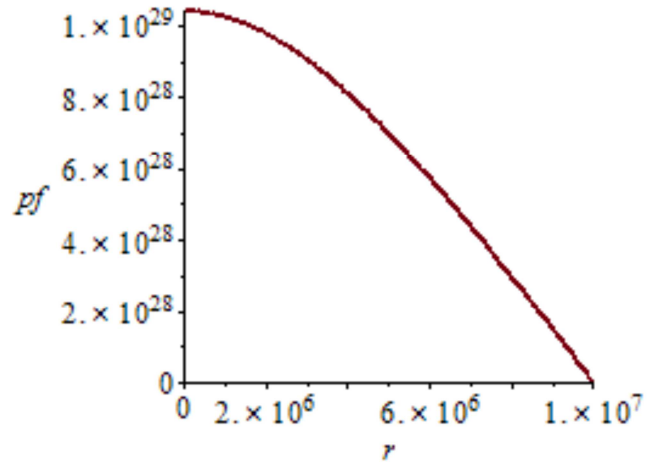


Figure 5. The fluid pressure for $\rho_f = 1.2 \times 10^{22} \text{ kg/m}^3$.

Figures 4 and 5 show the effect of fluid density on pressure. We can see that when the fluid density increases by 1.2 times, the pressure can increase by approximately 100 times. Moreover, when the radius decreases, the pressure increases. That is the center of star has the highest pressure.

4. The Transmission and Reflection Probabilities for Tolman-Bayin Type of Anisotropic Fluid Sphere

4.1. The Transmission Probability

Referring to P. Boonserm, and M Visser [23], we use a similar concept to find the transmission and reflection probabilities for the Tolman-Bayin type of charged fluid sphere.

The wave that can be observed by an observer away from a black hole is the only transmitted wave. The incident wave is a blackbody radiation because a black hole is a blackbody. However, the transmitted wave is no longer a blackbody radiation due to the modification from the curvature of spacetime. We call the transmitted wave as a greybody radiation. The transmission probability is called the greybody factor for black hole systems. The greybody factor is a quantity containing information about the percentage of Hawking radiation that can reach infinity. In addition, we can derive the greybody factor by solving the Schrodinger-like equation. However, we cannot, in general, find the exact solutions [23-25].

For the static, spherically symmetric background, the metric takes the form [10, 26]

$$ds^2 = \zeta_0(r)^2 dt^2 - \frac{dr^2}{B_0(r)} - r^2 d\Omega^2. \quad (14)$$

Substituting in the Einstein's field equation and performing some manipulation, we obtain [26]

$$\frac{dC}{dr} = \left(\frac{\sqrt{B_0}}{r^2} \frac{d}{dr} \left(\frac{1}{\sqrt{B_0}} \right) - \frac{1}{r^3} \right) + \sqrt{B_0} \frac{d}{dr} \left(\frac{1}{\sqrt{B_0}} \right) C - C^2 r + \frac{2q^2}{B_0 r^5}, \quad (15)$$

where

$$C = \frac{\zeta_0'(r)}{r\zeta_0(r)}. \quad (16)$$

Matching this interior solution with the exterior Reissner-Nordstrom at $r = a$, we assume the total charge to be

$$q(a) = Ka^n, \quad (17)$$

where K is constant. Moreover, we can find total gravitational mass

$$m = \frac{na^2(2-n)+2q^2}{2(1+2n-n^2)a}. \quad (18)$$

For simplicity, we are interested in the case $n = 0$. So we obtain

$$\zeta_0^2 = 1 - \frac{2m}{a} + \frac{q^2}{a^2}. \quad (19)$$

$$B_0 = 1 - \frac{2m}{a} + \frac{q^2}{a^2} = 1 - \frac{2q^2}{a^2}. \quad (20)$$

In the presence of a scalar field, it is possible for anisotropic fluid sphere to radiate scalar waves. Therefore, we can find the transmission probability of the scalar waves in propagating to a distant place, or spatial infinity. In [24, 27], the rigorous bound on the transmission probability was calculated for the Myers-Perry black hole. In this paper, we study the Tolman-Bayin type of charged fluid sphere, which takes the form [26]

$$ds^2 = \left(1 - \frac{2m}{a} + \frac{q^2}{a^2}\right)^2 dt^2 - \left(1 + \frac{q^2}{a^2}\right)^{-2} dr^2 - r^2 d\Omega^2. \quad (21)$$

The rigorous bound on the transmission probability is given by [24-25]

$$T \geq \text{sech}^2 \left[\frac{1}{2\omega} \int_{-\infty}^{\infty} V_l(r) dr_* \right]. \quad (22)$$

For the Tolman-Bayin type of charged fluid sphere, the potential takes the form

$$V(r) = \frac{l(l+1)}{r^2} \left(1 - \frac{2m}{a} + \frac{q^2}{a^2}\right)^2 \quad (23)$$

and the tortoise coordinate is given by

$$\frac{dr_*}{dr} = \frac{1}{\left(1 - \frac{2m}{a} + \frac{q^2}{a^2}\right)\left(1 - \frac{2q^2}{a^2}\right)}. \quad (24)$$

Therefore, the rigorous bounds on the transmission probability is

$$\begin{aligned} T &\geq \text{sech}^2 \left[\frac{1}{2\omega} \int_{-\infty}^{\infty} \frac{l(l+1)}{r^2} \left(1 - \frac{2m}{a} + \frac{q^2}{a^2}\right)^2 dr_* \right] \\ &= \text{sech}^2 \left[\frac{1}{2\omega} \int_{r_0}^{\infty} \frac{l(l+1)}{r^2} \frac{1 - \frac{2m}{a} + \frac{q^2}{a^2}}{1 - \frac{2q^2}{a^2}} dr \right] \end{aligned}$$

$$\begin{aligned} &= \text{sech}^2 \left[\frac{1}{2\omega} \int_{r_0}^{\infty} \frac{l(l+1)}{r^2} \frac{a^2 - 2ma + q^2}{a^2 - 2q^2} dr \right] \\ &= \text{sech}^2 \left[\frac{1}{2\omega} l(l+1) \frac{a^2 - 2ma + q^2}{a^2 - 2q^2} \left(-\frac{1}{r}\right)_{r_0}^{\infty} \right] \\ &= \text{sech}^2 \left[\frac{1}{2\omega} l(l+1) \frac{a^2 - 2ma + q^2}{a^2 - 2q^2} \left(\frac{1}{r_0}\right) \right]. \end{aligned} \quad (25)$$

The rigorous bound on the transmission probability is plotted with ω as shown in Figure 6.

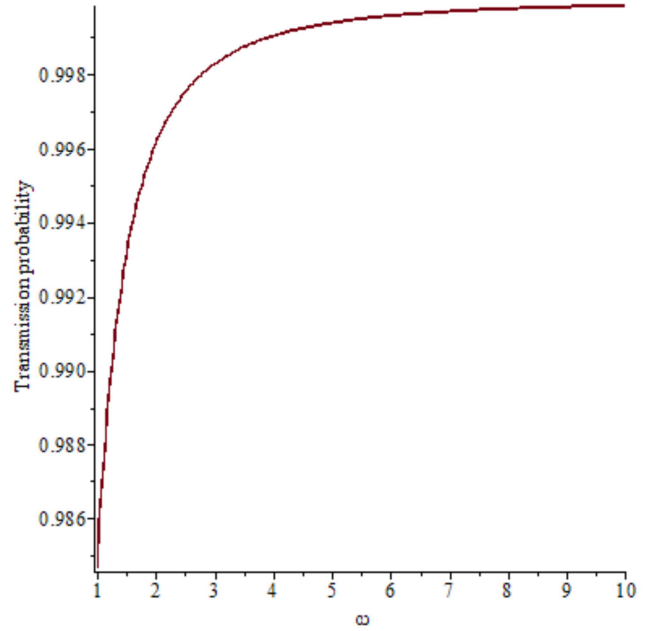


Figure 6. The rigorous bound on the transmission probability as a function of ω .

From the graph, we can see that the rigorous bound on the transmission probability increases as the wave's energy increases. This means that the waves with higher energy can penetrate to spatial infinity with a higher probability than lower energy waves.

4.2. The Reflection Probability

From the law of conservation, the relationship between the reflection probability and the transmission probability satisfies [25]

$$R + T = 1. \quad (26)$$

Therefore, for the given transmission probability, the reflection probability can be obtained

$$R = 1 - T = 1 - \text{sech}^2 \left[\frac{1}{2\omega} l(l+1) \frac{a^2 - 2ma + q^2}{a^2 - 2q^2} \left(\frac{1}{r_0}\right) \right]. \quad (27)$$

The rigorous bound on the reflection probability is plotted with ω as shown in Figure 7.

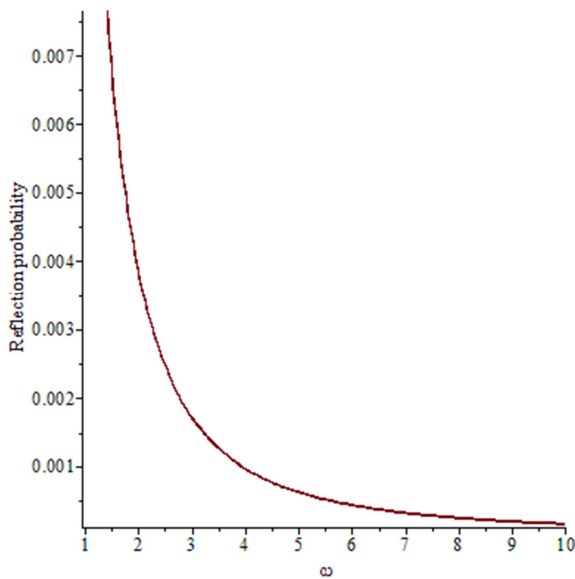


Figure 7. The rigorous bound on the reflection probability as a function of ω .

From Figure 7, we can see that the rigorous bound on reflection probability decreases with increasing wave energy. This relationship is an inverse of the relationship associated with the transmission probability. That is, the increase in the rigorous bound on reflection probability corresponds to the decrease in the rigorous bound on transmission probability, satisfying the law of conservation within the equation (26).

5. Conclusion

In this paper, we derived the generalized TOV equation for anisotropic fluid sphere. We investigated the effect of charge on pressure in the absence of a scalar field, and with a constant charge density. The result shows that the presence of charge can add to the pressure of charged stars. Moreover, a denser star has more pressure than the less compact stars. Finally, we calculated the rigorous bound on the transmission probability and the reflection probability for the Tolman-Bayin type of charged fluid sphere. We found that high energy waves have a higher probability in reaching spatial infinity than low energy waves.

For future work, spherical objects in reality can be more easily observed in terms of pressure and density. Therefore, building a solution generating theorem in terms of pressure and density allows us to gain a clear understanding of star-like object. In this work, the solution generating theorem algorithm is applied to the generalized TOV equation. We can find new solutions from the theorems. Moreover, the type of solutions can also be classified by the theorems. We can also see the interrelationship between the anisotropic solutions.

Acknowledgements

This project was funded by the Ratchadapisek Sompoch Endowment Fund, Chulalongkorn University (Sci-Super 2014-032), by a grant for the professional development of new academic staff from the Ratchadapisek Somphot Fund at

Chulalongkorn University, by the Thailand Research Fund (TRF), and by the Office of the Higher Education Commission (OHEC), Faculty of Science, Chulalongkorn University. PB was additionally supported by a scholarship from the Royal Government of Thailand. TN was also additionally supported by a scholarship from the Development and Promotion of Science and Technology talent project (DPST). NJ was also additional supported by a travel grant from Department of Physics, Faculty of Science, Chulalongkorn University.

References

- [1] M. S. R. Delgaty and K. Lake, "Physical acceptability of isolated, static, spherically symmetric, perfect fluid solutions of Einstein's equations", *Comput. Phys. Commun.* 115 (1998) 395 [arXiv: gr-qc/9809013].
- [2] S. Rahman and M. Visser, "Spacetime geometry of static fluid spheres", *Class. Quant. Grav.* 19 935 2002 [arXiv: gr-qc/0103065].
- [3] P. Boonserm, M. Visser and S. Weinfurter, "Generating perfect fluid spheres in general relativity", *Phys. Rev. D* 71 (2005) 124037 [arXiv: gr-qc/0503007].
- [4] P. Boonserm, M. Visser and S. Weinfurter, "Solution generating theorems for the TOV equation", *Phys. Rev. D* 76 (2007) 044024 [arXiv: gr-qc/0607001].
- [5] D. Martin and M. Visser, "Bounds on the interior geometry and pressure profile of static fluid spheres," *Class. Quant. Grav.* 20 (2003) 3699-3716 [arXiv: gr-qc/ 0306038].
- [6] K. Lake, "All static spherically symmetric perfect fluid solutions of Einstein's Equations," *Phys. Rev. D* 67 (2003) 104015 [arXiv: gr-qc/0209104].
- [7] D. Martin and M. Visser, "Algorithmic construction of static perfect fluid spheres," *Phys. Rev. D* 69 (2004) 104028 [arXiv: gr-qc/0306109].
- [8] S. Ray, A. L. Espíndola, M. Malheiro, J. P. S. Lemos, and V. T. Zanchin, "Electrically charged compact stars and formation of charged black holes", *Phys. Rev. D* 68 084004, 2003 [arXiv: astro-ph/0307262].
- [9] W. Barreto, L. Castillo, and E. Barrios, "Central equation of state in spherical characteristic evolutions", *Phys. Rev. D* 80 084007 2009 [arXiv: 0909.4500 [gr-qc]].
- [10] P. Boonserm, T. Ngampitipan and M. Visser, "Mimicking static anisotropic fluid spheres in general relativity", *International Journal of Modern Physics D* (2015): 1650019 [arXiv: 1501.07044v3 [gr-qc]].
- [11] F. Siebel, J. A. Font, and P. Papadopoulos, "Scalar field induced oscillations of neutron stars and gravitational collapse", *Phys. Rev. D* 65 024021 2001 [arXiv: gr-qc/0108006].
- [12] K. Schwarzschild, "On the gravitational field of a sphere of incompressible fluid according to Einstein's theory", *Sitzungsber. Preuss. Akad. Wiss. Berlin (Math. Phys.)* 1916 (1916) 424 [arXiv: physics/9912033 [physics.hist-ph]].
- [13] S. Carroll, "Spacetime and geometry: an introduction to general relativity", Pearson new international edition, U.S.A., Pearson Education Limited, 2014.

- [14] H. Bondi, "Spherically symmetrical models in general relativity", *Mon. Not. Roy. Astron. Soc.* 107 (1947) 410.
- [15] H. A. Buchdahl, "General relativistic fluid spheres", *Phys. Rev.* 116 (1959) 1027-1034.
- [16] A. Sulaksono, "Anisotropic pressure and hyperon in neutron stars," *Int. J. Mod. Phys. E* 24 (2015) 01, 1550007 [arXiv: 1412.7274 [nucl-th]].
- [17] P. Boonserm, "Some exact solution in general relativity", MSc. Thesis, Victoria University of Wellington, 2006.
- [18] D Kramer, H Stephani, E Herlt, and M MacCallum, "Exact solutions of Einstein's field equations", (Cambridge University Press, England, 1980).
- [19] S. Ray, A. L. Espíndola, M. Malheiro, J. P. S. Lemos, and V. T. Zanchin, "Electrically charged compact stars and formation of charged black holes", *Phys. Rev. D* 68 084004, 2003 [arXiv: astro-ph/0307262].
- [20] W. Barreto, L. Castillo, and E. Barrios, "Central equation of state in spherical characteristic evolutions", *Phys. Rev. D* 80 084007 2009 [arXiv: 0909.4500 [gr-qc]].
- [21] L. Herrera, J. Ospino and A. Di Prisco, "All static spherically symmetric anisotropic solutions of Einstein's equation", *Phys. Rev. D* 77 (2008) 027502 [arXiv: 0712.0713 [gr-qc]].
- [22] Chandrasekhar, S. (1998). *The Mathematical Theory of Black Holes* (Reprinted ed.). Oxford University Press. p. 205. ISBN 0-19850370-9. Retrieved 13 May 2013.
- [23] P. Boonserm, and M. Visser, "Bounding the greybody factors for Schwarzschild black holes." *Phys. Rev. D* 78(10) 101502 2008.
- [24] T. Ngampitipan, "Rigorous bounds on grey body factors for various types of black holes", Ph. D. Thesis, Chulalongkorn University, 2014.
- [25] P. Boonserm, "Rigorous Bounds on Transmission, Reflection, and Bogoliubov Coefficients", Ph. D. Thesis, Victoria University of Wellington (2009) [arXiv: 0907.0045 [math-ph]].
- [26] Ray, Saibal, and Basanti Das, "Tolman-Bayin type static charged fluid spheres in general relativity." *Monthly Notices of the Royal Astronomical Society* 349.4 (2004), 1331-1334.
- [27] P. Boonserm, A. Chatrabhuti, T. Ngampitipan, and M. Visser, "Greybody factors for Myers-Perry black holes", *J. Math. Phys.* 55, 112502 (2014) [arXiv: 1405.5678[gr-qc]].
- [28] K. Komathiraj and S. D. Maharaj, "A class of charged relativistic spheres", *Mathematical and Computational Applications* 15, 665-673, 2010.

The Modified Techniques for Generating Perfect Fluid Sphere in Isotropic Coordinate

Tritos Ngampitipan
Faculty of Science,
Chandrasekhar Rajabhat University
Bangkok 10900, Thailand

Petarpa Boonserm
Department of Mathematics and Computer Science,
Faculty of Science,
Chulalongkorn University
Bangkok 10330, Thailand

Apisit Kinreewong
Department of Mathematics and Computer Science,
Faculty of Science,
Chulalongkorn University
Bangkok 10330, Thailand

Abstract—The Einstein field equation describes the relationship between spacetime geometry and matter (or energy). In general, the equation cannot be solved because of its extreme complexity. Therefore, several related methods have been developed to find the solution. In the article [Phys. J. Vol. 2, No. 2, 2016], the Riccati equation has been used to develop a method to obtain new solutions for perfect fluid spheres in the curvature coordinates. In this paper, we focus on the use of the Riccati equation in finding new solutions for perfect fluid spheres in isotropic coordinates. Moreover, we also present another method, the Fourier transform, to obtain new solutions. The Schwarzschild metric is chosen as the starting metric. The results show that solutions obtained from the Riccati equation and the Fourier transform are both new and different from each other.

Keywords—generating perfect fluid sphere; isotropic coordinate; modified technique; Fourier transform; ordinary differential equation;

I. INTRODUCTION

The general theory of relativity was formulated by Albert Einstein in 1915. It relates the spacetime geometry to matter and the energy within it [1-3]. This characteristic has been expressed in a mathematical form as the equation called the Einstein field equation. It is a fully non-linear partial differential equation which, in general, cannot directly be solved. To reduce the complexity, some assumptions have to be made. One of the assumptions includes a static, spherically symmetric, perfect fluid sphere.

A perfect fluid sphere is one with pressure isotropy, but no viscosity or conduction of heat. Its static and spherical symmetry reduce the Einstein field equation to an ordinary

differential equation that can be solved for an exact solution [4-18].

In this paper, new solutions of perfect fluid sphere in isotropic coordinates [19-22] are obtained using the Riccati equation and the Fourier transform.

II. GENERATING PERFECT FLUID SPHERE

The isotropic coordinates are ones in which the coefficients of radial and angular coordinates are equal. The metric of a static, spherically symmetric, perfect fluid sphere in isotropic coordinates takes the form [23]

$$ds^2 = -\zeta^2(r)dt^2 + \frac{1}{\zeta^2(r)B^2(r)}(dr^2 + r^2 d\Omega^2), \quad (1)$$

where

$$d\Omega^2 = d\theta^2 + \sin^2 \theta d\phi^2. \quad (2)$$

The Einstein field equation is given by

$$G_{\hat{\mu}\hat{\nu}} = 8\pi GT_{\hat{\mu}\hat{\nu}}, \quad (3)$$

where $G_{\hat{\mu}\hat{\nu}}$ is the Einstein tensor and $T_{\hat{\mu}\hat{\nu}}$ is the energy-momentum tensor, which is given by

$$T_{\hat{\mu}\hat{\nu}} = \begin{bmatrix} \rho & 0 & 0 & 0 \\ 0 & p_r & 0 & 0 \\ 0 & 0 & p_t & 0 \\ 0 & 0 & 0 & p_t \end{bmatrix}. \quad (4)$$

The condition for a perfect fluid is $p_r = p_t$. Hence, $T_{\hat{r}\hat{r}} = T_{\hat{\theta}\hat{\theta}}$.
From (3), this gives

$$G_{\hat{r}\hat{r}} = G_{\hat{\theta}\hat{\theta}}. \quad (5)$$

This condition leads to an ordinary differential equation [19-21]

$$\left[\frac{\zeta'(r)}{\zeta(r)} \right]^2 = \frac{B''(r) - B'(r)/r}{2B(r)}. \quad (6)$$

Let

$$g(r) = \frac{\zeta'(r)}{\zeta(r)}, \quad (7)$$

which gives

$$\zeta(r) = \exp\left(\int g(r)dr\right). \quad (8)$$

Then, from (6) we obtain

$$g^2(r) = \frac{B''(r) - B'(r)/r}{2B(r)}. \quad (9)$$

Rearranging the above equation gives

$$B''(r) - \frac{B'(r)}{r} - 2g^2(r)B(r) = 0. \quad (10)$$

Now, we introduce a new function $h(r)$, which is defined by

$$h(r) = \frac{B'(r)}{2B(r)}, \quad (11)$$

which gives

$$B(r) = \exp\left(\int 2h(r)dr\right). \quad (12)$$

Differentiating $h(r)$, we obtain

$$h'(r) = \frac{B''(r)}{2B(r)} - 2h^2(r). \quad (13)$$

Therefore,

$$\frac{B''(r)}{2B(r)} = h'(r) + 2h^2(r). \quad (14)$$

Substituting (11) and (14) into (9) leads to

$$g^2(r) = 2h^2(r) + h'(r) - \frac{h(r)}{r}. \quad (15)$$

The general form of the Riccati equation is given by [24]

$$y'(x) = q_0(x) + q_1(x)y(x) + q_2(x)y^2(x), \quad (16)$$

where $q_0(x)$, $q_1(x)$, and $q_2(x)$ are arbitrary functions. We can write (15) in the Riccati form

$$h'(r) = g^2(r) + \frac{1}{r}h(r) - 2h^2(r), \quad (17)$$

where

$$q_0(r) = g^2(r), q_1(r) = \frac{1}{r} \text{ and } q_2(r) = -2. \quad (18)$$

One property of the Riccati equation is that if we know a particular solution, a general solution can be derived [25]. Let $\{g_0(r), h_0(r)\}$ satisfy (17). Then

$$h'_0(r) = g_0^2(r) + \frac{1}{r}h_0(r) - 2h_0^2(r). \quad (19)$$

We assume that the general solution takes the form

$$h(r) = h_0(r) + \frac{1}{z(r)}. \quad (20)$$

Substituting $h(r)$ in (17), we obtain

$$\begin{aligned} \left[h_0(r) + \frac{1}{z(r)} \right]' &= g^2(r) + \frac{1}{r} \left[h_0(r) + \frac{1}{z(r)} \right] \\ &\quad - 2 \left[h_0(r) + \frac{1}{z(r)} \right]^2. \end{aligned} \quad (21)$$

From (19), we get

$$z'(r) + \left[\frac{1}{r} - 4h_0(r) \right] z(r) = 2. \quad (22)$$

Differentiating (20) gives

$$h'(r) = h_0'(r) - \frac{z'(r)}{z^2(r)}. \quad (23)$$

Substituting $h_0'(r)$ from (19) and $z'(r)$ from (22), we have

$$h'(r) = g_0^2(r) + \frac{1}{r} h(r) - 2h^2(r). \quad (24)$$

Rearranging it gives

$$g_0^2(r) = h'(r) - \frac{1}{r} h(r) + 2h^2(r). \quad (25)$$

Compared to (15), $g(r)$ also satisfies the above equation. Let us investigate the relationship between $g(r)$ and $g_0(r)$ assuming that

$$g(r) = g_0(r) + g^*(r). \quad (26)$$

Substituting $g(r)$ into (15), we get

$$\left[g_0(r) + g^*(r) \right]^2 = h'(r) - \frac{1}{r} h(r) + 2h^2(r). \quad (27)$$

Expanding the complete square leads to

$$g_0^2(r) + 2g_0(r)g^*(r) + g^{*2}(r) = h'(r) - \frac{1}{r} h(r) + 2h^2(r). \quad (28)$$

From (25), the above equation reduces to

$$2g_0(r)g^*(r) + g^{*2}(r) = 0. \quad (29)$$

If $g^*(r) \neq 0$, we get

$$g^*(r) = -2g_0(r). \quad (30)$$

From (26), we obtain

$$g(r) = -g_0(r). \quad (31)$$

That is, if we have $\{g_0(r), h_0(r)\}$ representing a perfect fluid sphere, then

$$\left\{ -g_0(r), h_0(r) + \frac{1}{z(r)} \right\} \quad (32)$$

also represents a perfect fluid sphere.

Next, let us find $z(r)$. We select $h_0(r) = 1$ as an initial solution. Equation (19) gives

$$g_0(r) = \sqrt{2 - \frac{1}{r}}. \quad (33)$$

Substituting $h_0(r) = 1$ into (22), we get

$$z'(r) + \left(\frac{1}{r} - 4 \right) z(r) = 2. \quad (34)$$

The solution is given by

$$z(r) = e^{-(\ln r - 4r)} \int 2e^{(\ln r - 4r)} dr. \quad (35)$$

Integrating it gives

$$z(r) = -\frac{1}{2} - \frac{1}{8r} + c. \quad (36)$$

We choose $c = 0$ as an example. From (20), we obtain

$$h(r) = 1 - \frac{1}{\frac{1}{2} + \frac{1}{8r}} = \frac{1 - 4r}{1 + 4r}. \quad (37)$$

From (31) and (33), we get

$$g(r) = -\sqrt{2 - \frac{1}{r}}. \quad (38)$$

From (8), we are led to

$$\zeta(r) = \exp \left(-\int \sqrt{2 - \frac{1}{r}} dr \right). \quad (39)$$

Integrating by part gives

$$\zeta(r) = C_1 \exp\left(-\sqrt{2r^2 - r} + \frac{1}{2\sqrt{2}} \ln(1 - 4r - 2\sqrt{4r^2 - 2r})\right), \quad (40)$$

where C_1 is a constant of integration. From (12), we get

$$B(r) = \exp\left(2 \int \frac{1-4r}{1+4r} dr\right) = C_2 e^{-2r} (4r+1), \quad (41)$$

where C_2 is a constant of integration.

III. GENERATING SOLUTION USING THE FOURIER TRANSFORM TECHNIQUE

A. Fourier transform applied to differential equation

Suppose we have a differential equation in this form

$$B''(r) - \frac{B'(r)}{r} - 2g^2(r)B(r) = 0. \quad (42)$$

This equation can be solved using the Fourier transform

$$F[B''(r)] - F\left[\frac{B'(r)}{r}\right] - F[2g^2(r)B(r)] = 0. \quad (43)$$

From the formulas of the Fourier transform, we obtain

$$(i\omega)^2 \hat{B}(\omega) - \sqrt{\frac{\pi}{2}} \omega [\hat{B} * \text{sgn}](\omega) - \sqrt{\frac{2}{\pi}} [\hat{g}^2 * \hat{B}](\omega) = 0. \quad (44)$$

We choose

$$g(r) = -\sqrt{2 - \frac{1}{r}} \quad (45)$$

as an example. Then,

$$\begin{aligned} & -\omega^2 \hat{B}(\omega) - \sqrt{\frac{\pi}{2}} \omega \int_{-\infty}^{\infty} \hat{B}(y) \text{sgn}(\omega - y) dy \\ & - \sqrt{\frac{2}{\pi}} \int_{-\infty}^{\infty} \left[2\sqrt{2\pi} \delta(y) + i\sqrt{\frac{\pi}{2}} \text{sgn}(y) \right] \hat{B}(\omega - y) dy = 0. \end{aligned} \quad (46)$$

Using the definition of $\text{sgn}(x)$, we obtain

$$\begin{aligned} & -\omega^2 \hat{B}(\omega) - \sqrt{\frac{\pi}{2}} \omega \left[\int_{-\infty}^{\omega} \hat{B}(y) dy - \int_{\omega}^{\infty} \hat{B}(y) dy \right] \\ & - 4 \int_{-\infty}^{\infty} \delta(y) \hat{B}(\omega - y) dy + i \int_{-\infty}^0 \hat{B}(\omega - y) dy - i \int_0^{\infty} \hat{B}(\omega - y) dy = 0. \end{aligned} \quad (47)$$

The first term in the second line of (47) gives

$$-4 \int_{-\infty}^{\infty} \delta(y) \hat{B}(\omega - y) dy = -4 \hat{B}(\omega). \quad (48)$$

By changing the variable, the second term in the second line of (47) gives

$$i \int_{-\infty}^0 \hat{B}(\omega - y) dy = i \int_{\omega}^{\infty} \hat{B}(y) dy. \quad (49)$$

Similarly, the third term in the second line of (47) gives

$$i \int_0^{\infty} \hat{B}(\omega - y) dy = i \int_{-\infty}^{\omega} \hat{B}(y) dy. \quad (50)$$

Equation (47) becomes

$$\begin{aligned} & -\omega^2 \hat{B}(\omega) - \sqrt{\frac{\pi}{2}} \omega \left[\int_{-\infty}^{\omega} \hat{B}(y) dy - \int_{\omega}^{\infty} \hat{B}(y) dy \right] \\ & - 4 \hat{B}(\omega) - i \left[\int_{-\infty}^{\omega} \hat{B}(y) dy - \int_{\omega}^{\infty} \hat{B}(y) dy \right] = 0. \end{aligned} \quad (51)$$

Rearranging it, we are led to

$$-\frac{\sqrt{2\pi}(\omega^2 + 4)}{\sqrt{2\pi}i + \pi\omega} \hat{B}(\omega) = \int_{-\infty}^{\omega} \hat{B}(y) dy - \int_{\omega}^{\infty} \hat{B}(y) dy. \quad (52)$$

Differentiating both sides with respect to ω and rearranging, we get

$$\hat{B}'(\omega) = -\frac{(2\sqrt{2\pi}i\omega + \pi\omega^2 - 2\sqrt{2\pi})(\sqrt{2\pi} + 1)}{(\sqrt{2\pi}i + \pi\omega)(\omega^2 + 4)} \hat{B}(\omega). \quad (53)$$

By the partial fraction, we obtain

$$\frac{\hat{B}'(\omega)}{\hat{B}(\omega)} = \frac{\pi}{\sqrt{2\pi i + \pi\omega}} - \frac{(\sqrt{2\pi} + 2)\omega + 2i}{\omega^2 + 4}. \quad (54)$$

Integrating both sides over ω gives

$$\ln[\hat{B}(\omega)] = \ln(\sqrt{2\pi i + \pi\omega}) - \frac{\sqrt{2\pi} + 2}{2} \ln(\omega^2 + 4) - i \arctan\left(\frac{\omega}{2}\right). \quad (55)$$

Therefore,

$$\hat{B}(\omega) = C(\sqrt{2\pi i + \pi\omega})(\omega^2 + 4)^{-3/2 - \sqrt{\pi/2}} (2 - i\omega). \quad (56)$$

Finally, by inversing the Fourier transforming, we obtain

$$B(r) = \frac{C}{\sqrt{2\pi}} \int_{-\infty}^{\infty} (\sqrt{2\pi i + \pi\omega})(2 - i\omega)(\omega^2 + 4)^{-3/2 - \sqrt{\pi/2}} e^{i\omega r} d\omega. \quad (57)$$

B. Application to the Schwarzschild metric using the Riccati equation

The Schwarzschild metric in isotropic coordinates takes the form

$$ds^2 = \frac{(1 - M/2r)^2}{(1 + M/2r)^2} dt^2 + \left(1 + \frac{M}{2r}\right)^4 (dr^2 + r^2 d\Omega^2). \quad (58)$$

Comparing to the general form

$$ds^2 = -\zeta^2(r) dt^2 + \frac{1}{\zeta^2(r) B^2(r)} (dr^2 + r^2 d\Omega^2), \quad (59)$$

we obtain

$$\zeta(r) = \frac{1 - M/2r}{1 + M/2r} \text{ and } B(r) = \frac{1}{1 - M^2/4r^2}. \quad (60)$$

From (7) and (11), we get

$$g(r) = \frac{M}{(r + M/2)^2} \text{ and } h(r) = -\frac{M^2}{r(4r^2 - M^2)}. \quad (61)$$

We can take these $g(r)$ and $h(r)$ as the initial solution. That is

$$g_0(r) = \frac{M}{(r + M/2)^2} \text{ and } h_0(r) = -\frac{M^2}{r(4r^2 - M^2)}. \quad (62)$$

Substituting $h_0(r)$ into (22), we get

$$z'(r) + \left[\frac{1}{r} + \frac{4M^2}{r(4r^2 - M^2)} \right] z(r) = 2. \quad (63)$$

The solution is given by

$$z(r) = e^{-p(r)} \int 2e^{p(r)} dr, \quad (64)$$

where

$$p(r) = \int \frac{4r^2 + 3M^2}{r(4r^2 - M^2)} dr. \quad (65)$$

Therefore,

$$h(r) = -\frac{M^2}{r(4r^2 - M^2)} + \frac{1}{e^{-p(r)} \int 2e^{p(r)} dr} \quad (66)$$

and

$$g(r) = -\frac{M}{(r + M/2)^2}. \quad (67)$$

From (8) and (12), we obtain

$$\zeta(r) = \frac{1 + M/2r}{1 - M/2r} \quad (68)$$

and

$$B(r) = \left[\int e^{p(r)} dr \right] \exp \left(\int -\frac{2M^2}{r(4r^2 - M^2)} dr \right). \quad (69)$$

C. Application to the Schwarzschild metric using the Fourier transform

From (61),

$$g(r) = \frac{M}{(r + M/2)^2}, \quad (70)$$

(44) becomes

$$\begin{aligned} -\omega^2 \hat{B}(\omega) - \sqrt{\frac{\pi}{2}} \omega \int_{-\infty}^{\infty} \hat{B}(y) \operatorname{sgn}(\omega - y) dy \\ - \sqrt{\frac{2}{\pi}} \int_{-\infty}^{\infty} \left[M^2 e^{i(M/2)y} (-i) \sqrt{\frac{\pi}{2}} \frac{iy^3}{6} \operatorname{sgn}(y) \right] \hat{B}(\omega - y) dy = 0. \end{aligned} \quad (71)$$

Using the definition of $\operatorname{sgn}(x)$, we obtain

$$\begin{aligned} -\omega^2 \hat{B}(\omega) - \sqrt{\frac{\pi}{2}} \omega \left[\int_{-\infty}^{\omega} \hat{B}(y) dy - \int_{\omega}^{\infty} \hat{B}(y) dy \right] \\ - \frac{M^2}{6} \left[- \int_{-\infty}^0 e^{i(M/2)y} y^3 \hat{B}(\omega - y) dy + \int_0^{\infty} e^{i(M/2)y} y^3 \hat{B}(\omega - y) dy \right] \\ = 0. \end{aligned} \quad (72)$$

By changing the variable, the first term in the second line of (72) gives

$$\int_{-\infty}^0 e^{i(M/2)y} y^3 \hat{B}(\omega - y) dy = \int_{\omega}^{\infty} e^{i(M/2)(\omega - y)} (\omega - y)^3 \hat{B}(y) dy. \quad (73)$$

Similarly, the second term in the second line of (72) gives

$$\int_0^{\infty} e^{i(M/2)y} y^3 \hat{B}(\omega - y) dy = \int_{-\infty}^{\omega} e^{i(M/2)(\omega - y)} (\omega - y)^3 \hat{B}(y) dy. \quad (74)$$

Equation (72) becomes

$$\begin{aligned} -\omega^2 \hat{B}(\omega) - \sqrt{\frac{\pi}{2}} \omega \left[\int_{-\infty}^{\omega} \hat{B}(y) dy - \int_{\omega}^{\infty} \hat{B}(y) dy \right] \\ + \frac{M^2}{6} \int_{\omega}^{\infty} e^{i(M/2)(\omega - y)} (\omega - y)^3 \hat{B}(y) dy \end{aligned}$$

$$- \frac{M^2}{6} \int_{-\infty}^{\omega} e^{i(M/2)(\omega - y)} (\omega - y)^3 \hat{B}(y) dy = 0. \quad (75)$$

Finally, by inverting the Fourier transform, we obtain

$$B(r) = \frac{1}{\sqrt{2\pi}} \int_{-\infty}^{\infty} \hat{B}(\omega) e^{ir\omega} d\omega, \quad (76)$$

where $\hat{B}(\omega)$ is the solution of (75).

CONCLUSION

In this paper, we present two new techniques that can generate new solution for a perfect fluid sphere. The first makes use of the property of the Riccati equation; that is, if we have a particular solution, the general solution can be obtained. In [24], the method of the Riccati equation is developed in curvature coordinates. In this paper, we use the Riccati equation as a focus in isotropic coordinates. These coordinates are highly interesting because the mathematical expressions are relatively simpler than in curvature coordinates. The other method, the Fourier transform, can also generate new solution for perfect fluid sphere. In general, the method of the Riccati equation is simpler than the Fourier transform. However, both methods can be useful in various situations as novel ways to derive new solutions.

ACKNOWLEDGMENT

This project was funded by the Ratchadapisek Sompoch Endowment Fund, Chulalongkorn University (Sci-Super 2014-032), by a grant for the professional development of new academic staff from the Ratchadapisek Somphot Fund at Chulalongkorn University, by the Thailand Research Fund (TRF), and by the Office of the Higher Education Commission (OHEC), Faculty of Science, Chulalongkorn University (RSA5980038). PB was additionally supported by a scholarship from the Royal Government of Thailand. TN was also additionally supported by a scholarship from the Development and Promotion of Science and Technology Talents Project (DPST). AK was also supported by the Science Achievement Scholarship of Thailand (SAST).

REFERENCES

- [1] S. Carroll, Spacetime and Geometry: An Introduction to General Relativity, Pearson new international edition, U.S.A., Pearson Education Limited, 2014.
- [2] B. Piyabut, An Introduction to General Relativity, Danex Inter Corporation Co., Ltd., Bangkok, 2013.
- [3] P. Karndumri, General Relativity, Danex Inter Corporation Co., Ltd., Bangkok, 2015.
- [4] K. Schwarzschild, On the Gravitational Field of a Sphere of Incompressible Fluid according to Einstein's Theory, Sitzungsber. Preuss. Akad. Wiss. Berlin (Math. Phys.), 1916, [arXiv: physics/9912033 [physics.hist-ph]].

- [5] H. Bondi, "Spherically symmetrical models in generalrelativity," Mon. Not. Roy. Astron. Soc. vol. 107, pp.410, 1947.
- [6] H. A. Buchdahl, "General relativistic fluid spheres," Phys. Rev. vol. 116, pp. 1027-1034, 1959.
- [7] D Kramer, H Stephani, E Herlt, and M MacCallum, Exact Solutions of Einstein's Field Equations, Cambridge University Press, England, 1980.
- [8] M. S. R. Delgaty and K. Lake, "Physical acceptability of isolated, static, spherically symmetric, perfect fluid solutions of Einstein's equations," Compute. Phys. Commun. vol. 115, pp. 395, 1998 [arXiv: gr-qc/9809013].
- [9] S. Rahman and M. Visser, "Space-time geometry of static fluid spheres," Class. Quant. Grav. vol. 19, pp. 935, 2002, [arXiv: gr-qc/0103065].
- [10] K. Lake, "All static spherically symmetric perfect fluid solutions of Einstein's equation," Phys. Rev. D vol. 67, pp. 104015, 2003, [arXiv: gr-qc/0209104].
- [11] D. Martin and M. Visser, "Algorithmic construction of static perfect fluid spheres," Phys. Rev. D vol. 69, pp. 104028, 2004, [arXiv: gr-qc/0306109].
- [12] P. Boonserm, M. Visser, and S. Weinfurter, "Generating perfect fluid spheres in general relativity," Phys. Rev. D vol. 71, pp. 124037, 2005, [arXiv: gr-qc/0503007].
- [13] P. Boonserm, Some Exact Solution in General Relativity, MSc. Thesis, Victoria University of Wellington, 2006.
- [14] P. Boonserm, M. Visser, and S. Weinfurter, "Solution generating theorems for the TOV equation," Phys. Rev. D vol. 76, pp. 044024, August 2007, [arXiv:gr-qc/0607001].
- [15] P. Boonserm and M. Visser, "Buchdahl-like transformations for perfect fluid spheres," Int. J. Mod. Phys. D vol.17, pp. 135-163, January 2008, [arXiv:0707.0146 [gr-qc]].
- [16] L. Herrera, J. Ospino and A. DiPrisco, "All static spherically symmetric anisotropic solutions of Einstein's equation," Phys. Rev. D vol. 77, pp. 027502, 2008, [arXiv: 0712.0713 [gr-qc]].
- [17] N. Jongjittanon, Generating Theorems for Charged Anisotropy and Modified Tolman-Oppenheimer-Volkov Equation, M.Sc. Thesis, Chulalongkorn University, 2015.
- [18] P. Boonserm, T. Ngampitipan, and M. Visser, "Mimicking static anisotropic fluid spheres in general relativity," Int. J. Mod. Phys. D vol. 25, pp. 1650019, February 2016, [arXiv:1501.07044 [gr-qc]].
- [19] N. Jongjittanon, P. Boonserm, and T. Ngampitipan, "Generating theorems for charged anisotropy in general relativity," AJP. vol. 4, pp. 50-56, 2016.
- [20] K. Thairatana, Transformation for Perfect Fluid Spheres in Isotropic Coordinates, M.Sc. Thesis, Chulalongkorn University, 2013.
- [21] P. Boonserm, P. Suavansri, and K. Thairatana, "Transformation for perfect fluid spheres in isotropic coordinates," Annual Meeting in Mathematics (AMM2011), Khon Kaen, Thailand, pp. 261-272, 10-11 March, 2011.
- [22] M. R. Finch and J. E. F. Skea, "A review of the relativistic static fluid sphere," Comput. Phys. Commun. vol. 115, pp. 395, 1998, [arXiv: gr-qc/9809013].
- [23] A. Kinreewong, Solution Generating Theorems and Tolman-Oppenheimer-Volkov Equation for Perfect Fluid Spheres in isotropic coordinates, M.Sc. Thesis, Chulalongkorn University, 2015.
- [24] M. A. Kauser and Q. Islam, "Generation of static perfect fluid spheres in general relativity," Phys. J. vol. 2, 2016.
- [25] C. M. Bender and S. A. Orszag, Advanced Mathematical Methods for Scientists and Engineers: Asymptotic Methods and Perturbation Theory", Springer, New York, 1990.

Generating Charged Anisotropy and Modified Tolman-Oppenheimer-Volkov Equation

Petarpa Boonserm

Department of Mathematics and Computer Science,
Faculty of Science,
Chulalongkorn University
Bangkok 10330, Thailand

Tritos Ngampitipan

Faculty of Science,
Chandrasakorn Rajabhat University
Bangkok 10900, Thailand

Napasorn Jongjittanon

Geo-Informatics and Space Technology
Development Agency
Bangkok 10210, Thailand

Abstract—A perfect fluid sphere is one of the established assumptions to reduce the complexity of the Einstein field equation so that an exact solution can possibly be obtained. However, a perfect fluid sphere is not realistic because most stars in the universe are composed of charges. From the perspective of spacetime geometry, the presence of charge makes fluid pressure anisotropic. The condition for charged fluid sphere, in terms of an ordinary differential equation, is different from a perfect fluid sphere. From the perspective of matter, the central equation is the Tolman-Oppenheimer-Volkov (TOV) equation. The presence of charge modifies the TOV equation. In this paper, we develop new generating theorems, both in the view of the spacetime geometry and in the view of matter. For spacetime geometry, we develop two new theorems using the corresponding ordinary differential equation and apply them to the Reissner-Nordström metric. For matter, we develop two new theorems using the corresponding modified TOV equation. Moreover, the effect of charge on fluid density, in case of constant pressure, is also investigated. The results show that the fluid density decreases as the charge density increases, to keep the pressure constant.

Keywords- anisotropy; charged fluid sphere; Einstein-Maxwell field equation; modified TOV equation; solution generating theorem

I. INTRODUCTION

A perfect fluid sphere is one of the exact solutions to the Einstein field equation [1-8]. It is usually used to ideally model a star such as a white dwarf and a neutron star. One of the properties of a perfect fluid sphere is the isotropy of pressure. However, in the real world, most stars and planets are anisotropic in pressure. The anisotropy of pressure possibly arises from the presence of charge and scalar field [9-16]. Therefore, the use of a charged fluid sphere as the model of a star is more realistic than the use of a perfect fluid sphere.

In the context of spacetime geometry, a perfect fluid sphere is obtained by solving the Einstein field equation. In the presence of charge, in the context of a charged fluid sphere, we have to solve the Einstein-Maxwell field equation instead. In general, the Einstein or the Einstein-Maxwell field equation is highly complicated that the exact solutions cannot be derived. Thus, approximation methods are needed. Furthermore, we can find the solutions to the Einstein or the Einstein-Maxwell field equation by what is called as a solution generating theorem [17-23]. The theorem generates the solutions by not having to directly solve the Einstein or the Einstein-Maxwell field equation.

In the context of matter, the relationship between fluid pressure and density can be described by the Tolman-Oppenheimer-Volkov (TOV) equation [24-25]. In the presence of charge, the TOV equation is modified [26]. Similar to the Einstein or the Einstein-Maxwell field equation, the TOV or the modified TOV is not exactly solved. Therefore, we also develop solution generating theorems for the modified TOV equation in the same manner as the Einstein-Maxwell field equation.

In this paper, we develop two new generating theorems in terms of spacetime geometry using an ordinary differential equation to which the Einstein-Maxwell field equation reduces and then apply them to the Reissner-Nordström metric. We also develop two new generating theorems in terms of fluid pressure and density using the modified TOV equation. Moreover, the effect of charge on fluid density, in case of constant pressure, is also investigated.

icmss2018

Gmail

Move to Inbox

More

COMPOSE

Fwd: ICMSS2018: Decision on Manuscript #DE-9121

Inbox x

Inbox

Starred

Important

Sent Mail

Drafts

Categories

[Gmail]Trash

Notes

Personal

Travel

More

Tritos Ngampitipan <tritos.ngampitipan@gmail.com>

to me

----- Forwarded message -----

From: **ICMSS2018 / UPM** <icmss2018@upm.edu.my>

Date: 2018-03-01 9:34 GMT+07:00

Subject: ICMSS2018: Decision on Manuscript #DE-9121

To: tritos.ngampitipan@gmail.com

Dear Dr. Tritos Ngampitipan,

Greetings from ICMSS2018!

We are pleased to inform you that your manuscript **#DE-9121**, entitled

has been accepted by our reviewers and scientific committee, provided **minor revision** of the manuscript are mac your manuscript.

We look forward to receiving the revised manuscript, together with a letter of response to each modification made,

Regards,
SECRETARIAT OF ICMSS2018
Department of Mathematics
Faculty of Science
Universiti Putra Malaysia

icmss2018@upm.edu.my
<http://einspem.upm.edu.my/icmss2018>

2 Attachments

INTERNATIONAL CONFERENCE
ON MATHEMATICAL SCIENCES
AND STATISTICS 2018

UPM ICMSS2018
AN INTERNATIONAL CONFERENCE
ON MATHEMATICAL SCIENCES
AND STATISTICS 2018
PUTRAJAYA, MALAYSIA

Manuscript ID : 08-0021
Manuscript Title : The various techniques for generating perfect fluid sphere
Reviewer ID :
Date Sent : 29 January 2018
Date Due : 12 February 2018

Dear Reviewer:
Please review the attached manuscript that has been submitted to the 8th International Conference on Mathematical Sciences and Statistics (ICMSS2018). This is a double blind review, neither your identity nor the author's is revealed. Please return only the completed evaluation form to the scientific committee via email.

Section 1: General Observation (Please use in the relevant box)

PDF MEF_DE-9121_R..

INTERNATIONAL CONFERENCE
ON MATHEMATICAL SCIENCES
AND STATISTICS 2018

UPM ICMSS2018
AN INTERNATIONAL CONFERENCE
ON MATHEMATICAL SCIENCES
AND STATISTICS 2018
PUTRAJAYA, MALAYSIA

Manuscript ID : 08-0021
Manuscript Title : The various techniques for generating perfect fluid sphere
Reviewer ID :
Date Sent : 29 January 2018
Date Due : 12 February 2018

Dear Reviewer:
Please review the attached manuscript that has been submitted to the 8th International Conference on Mathematical Sciences and Statistics (ICMSS2018). This is a double blind review, neither your identity nor the author's is revealed. Please return only the completed evaluation form to the scientific committee via email.

Section 1: General Observation (Please use in the relevant box)

PDF MEF_DE-9121_R..

Tritos Ngampitipan <tritos.ngampitipan@gmail.com>

to ICMSS2018, me

The two techniques for generating perfect fluid sphere

Tritos Ngampitipan¹ and Petarpa Boonserm²

¹ Faculty of Science, Chandrakasem Rajabhat University, Bangkok 10900, Thailand,
tritos.ngampitipan@gmail.com

² Department of Mathematics and Computer Science, Faculty of Science,
Chulalongkorn University, Bangkok 10330, Thailand,
petarpa.boonserm@gmail.com

Abstract. The Einstein field equation is the second order partial differential equation. It relates spacetime curvature to matter. In general, the exact solutions cannot be obtained because the equation is so complicated. One of the popular assumptions to reduce the complexity of the equation is that matter is a static, spherically symmetric, perfect fluid. In this way, the Einstein field equation is transformed to a second order differential equation with variable coefficients. In this paper, we are interested in solutions about regular singular points. Therefore, the method of Frobenius can be applied. Moreover, the reduced Einstein equation is of the Riccati form. With the property of the Riccati equation, we can find the general solutions if the particular solutions are specified.

Keywords: differential equation with variable coefficients, Einstein field equation, method of Frobenius, perfect fluid, Riccati equation

1 Introduction

The Einstein field equations describe how spacetime curves by the presence of matter and energy. They are the central equations in the general theory of relativity. Mathematically, the Einstein field equations are the second order partial differential equations. In fact, they are a set of 16 equations in our $(3 + 1)$ -dimensional real world. Without any assumption or symmetry, the Einstein field equations cannot exactly be solved. To look for an exact solution, some assumptions have to be imposed to reduce the complexity of the Einstein field equations. An example of such assumptions is to model matter as a static and spherically symmetric perfect fluid. This assumption leads to the first two exact solutions to the Einstein field equations, which are known as the (exterior) Schwarzschild solution and the interior Schwarzschild solution [1]. After this discovery, a static perfect fluid sphere became more popular, after which many exact solutions were found [2–12].

Exact solutions can be obtained in many different ways. Some tried to solve the Einstein field equations directly with the aid of some assumptions. Some used special techniques to obtain exact solutions without solving the Einstein

field equations [13–16]. Some generated new solutions from previously known solutions using the property of the Riccati equation [17–20]. Some applied the Frobenius method [21, 22] to solve the Klein-Gordon equation on a curved background given by the Einstein field equation [23] and the generalized Einstein field equation in higher derivative gravity theories [24]. In this paper, we will use the Frobenius method and the properties of the Riccati equation to obtain exact solutions.

This paper is organized as follows. The assumption of perfect fluid spheres is imposed in section 2. The solutions to the Einstein field equations obtained by the Frobenius method and the properties of the Riccati equation are given in sections 3 and 4, respectively. A comparison between the two methods is made in section 5. Finally, a concluding remark is provided in section 6.

2 Perfect fluid spheres

The curvature of spacetime is described by the Einstein equations

$$G^\mu_\nu = 8\pi GT^\mu_\nu, \quad (1)$$

where G^μ_ν is the Einstein tensor and T^μ_ν is the energy-momentum tensor, which takes the form

$$T^\mu_\nu = \text{diag}(-\rho, p_r, p_t, p_t). \quad (2)$$

We are interested in perfect fluid as the source of the energy-momentum tensor. One of the properties of being a perfect fluid is its pressures in all directions are the same. That is $p_r = p_t$ or, in terms of the components of the energy-momentum tensor,

$$T^1_1 = T^2_2. \quad (3)$$

From (1), the above condition leads to

$$G^1_1 = G^2_2. \quad (4)$$

The metric of the spacetime is given by

$$ds^2 = \zeta^2(r)dt^2 + \frac{dr^2}{B(r)} + r^2(d\theta^2 + \sin^2\theta d\phi^2). \quad (5)$$

Applying this metric to (4), we obtain

$$2r^2B(r)\zeta''(r) + [r^2B'(r) - 2rB(r)]\zeta'(r) + [rB'(r) - 2B(r) + 2]\zeta(r) = 0. \quad (6)$$

This is a second order linear ordinary differential equation. Moreover, this equation must be satisfied when the condition of perfect fluid spheres is imposed.

3 Frobenius Method

To apply the Frobenius method, equation (6) is rewritten as

$$r^2 \zeta''(r) + \frac{rB'(r) - 2B(r)}{2B(r)} r \zeta'(r) + \frac{rB'(r) - 2B(r) + 2}{2B(r)} \zeta(r) = 0. \quad (7)$$

Dividing the above equation by r^2 gives

$$\zeta''(r) + \frac{rB'(r) - 2B(r)}{2rB(r)} \zeta'(r) + \frac{rB'(r) - 2B(r) + 2}{2r^2B(r)} \zeta(r) = 0. \quad (8)$$

We see that the coefficients of $\zeta'(r)$ and $\zeta(r)$ are not analytic at $r = 0$. Thus, the Frobenius method can be applied to find a power series of the form

$$\zeta(r) = \sum_{k=0}^{\infty} A_k r^{k+n}, \quad (9)$$

where $A_0 \neq 0$. Differentiating the above solution gives

$$\zeta'(r) = \sum_{k=0}^{\infty} (k+n) A_k r^{k+n-1} \quad (10)$$

and

$$\zeta''(r) = \sum_{k=0}^{\infty} (k+n-1)(k+n) A_k r^{k+n-2}. \quad (11)$$

Moreover, expanding the coefficients of $r\zeta'(r)$ and $\zeta(r)$ in (7) in a power series gives

$$\frac{rB'(r) - 2B(r)}{2B(r)} = -1 + \sum_{i=1}^{\infty} p_i r^i \quad (12)$$

and

$$\frac{rB'(r) - 2B(r) + 2}{2B(r)} = \frac{1 - B(0)}{B(0)} + \sum_{i=1}^{\infty} q_i r^i. \quad (13)$$

Substituting (9) - (13) into (7), we obtain

$$\begin{aligned} & \left[n(n-1) - n + \frac{1 - B(0)}{B(0)} \right] A_0 r^n + \\ & \sum_{k=1}^{\infty} \left[(k+n-1)(k+n) - (k+n) + \frac{1 - B(0)}{B(0)} \right] A_k r^{k+n} + \\ & \left(\sum_{i=1}^{\infty} p_i r^i \right) \left[\sum_{k=0}^{\infty} (k+n) A_k r^{k+n} \right] + \left(\sum_{i=1}^{\infty} q_i r^i \right) \left(\sum_{k=0}^{\infty} A_k r^{k+n} \right) = 0. \end{aligned} \quad (14)$$

The indicial equation is given by

$$n(n-1) - n + \frac{1 - B(0)}{B(0)} = 0. \quad (15)$$

The roots of the above indicial equation is given by

$$n = \frac{2 \pm \sqrt{4 - 4[1 - B(0)]/B(0)}}{2} = 1 \pm \sqrt{1 - \frac{1 - B(0)}{B(0)}} = 1 \pm \sqrt{\frac{2B(0) - 1}{B(0)}}. \quad (16)$$

We choose $B(r) = -1/2 - br^2$, where b is constant. Substituting in equations (12) and (13), we obtain

$$\frac{rB'(r) - 2B(r)}{2B(r)} = -\frac{1}{1 + 2br^2} = -1 - \sum_{i=1}^{\infty} (-2b)^i r^{2i} \quad (17)$$

and

$$\frac{rB'(r) - 2B(r) + 2}{2B(r)} = -\frac{3}{1 + 2br^2} = -3 - 3 \sum_{i=1}^{\infty} (-2b)^i r^{2i}. \quad (18)$$

From the chosen $B(r)$, we obtain $B(0) = -1/2$. Equation (16) becomes

$$n = -1, 3. \quad (19)$$

The two roots are separated by an integer. Consider the smaller root $n = -1$. Substituting in (14) gives

$$\sum_{k=1}^{\infty} [(k-2)(k-1) - (k-1) - 3] A_k r^{k-1} - \left[\sum_{i=1}^{\infty} (-2b)^i r^{2i} \right] \left[\sum_{k=0}^{\infty} (k-1) A_k r^{k-1} \right] - \left[3 \sum_{i=1}^{\infty} (-2b)^i r^{2i} \right] \left(\sum_{k=0}^{\infty} A_k r^{k-1} \right) = 0.$$

Rearranging the above equation, we obtain

$$\sum_{k=1}^{\infty} k(k-4) A_k r^{k-1} - \left[\sum_{i=1}^{\infty} (-2b)^i r^{2i} \right] \left[\sum_{k=0}^{\infty} (k+2) A_k r^{k-1} \right] = 0. \quad (20)$$

Rearranging the above equation, we obtain

$$\begin{aligned} & -3A_1 + (-4A_2 + 4bA_0)r + (-3A_3 + 6bA_1)r^2 + \\ & (-8b^2A_0 + 8bA_2)r^3 + (5A_5 - 12b^2A_1 + 10bA_3)r^4 + \\ & (12A_6 + 16b^3A_0 - 16b^2A_2 + 12bA_4)r^5 + \dots = 0. \end{aligned} \quad (21)$$

The coefficients of any power of r must be zero. We find that

$$A_1 = A_3 = A_5 = \dots = 0 \quad (22)$$

and

$$\begin{aligned} A_2 &= bA_0 \\ A_6 &= -bA_4. \end{aligned} \quad (23)$$

Substituting in (9), we obtain

$$\begin{aligned}\zeta(r) &= \frac{A_0}{r} + bA_0r + A_4r^3 - bA_4r^5 + \dots \\ &= A_0 \left(\frac{1}{r} + br \right) + A_4r^3 (1 - br^2 + \dots),\end{aligned}\quad (24)$$

where A_0 and A_4 are arbitrary constants. This is the general solution to equation (7).

4 Riccati Equation

To transform equation (8) into the Riccati equation, we start by defining a new function

$$h(r) = \frac{\zeta'(r)}{\zeta(r)}.\quad (25)$$

Its first derivative is given by

$$h'(r) = \frac{\zeta''(r)}{\zeta(r)} - h^2(r).\quad (26)$$

Thus,

$$\frac{\zeta''(r)}{\zeta(r)} = h'(r) + h^2(r).\quad (27)$$

Substituting (25) and (27) into (8), we get

$$h'(r) + h^2(r) + \frac{rB'(r) - 2B(r)}{2rB(r)}h(r) + \frac{rB'(r) - 2B(r) + 2}{2r^2B(r)} = 0.\quad (28)$$

Rearranging the above equation gives

$$h'(r) = -\frac{rB'(r) - 2B(r) + 2}{2r^2B(r)} - \frac{rB'(r) - 2B(r)}{2rB(r)}h(r) - h^2(r).\quad (29)$$

From the chosen $B(r)$, the above equation becomes

$$h'(r) = \frac{3}{r^2 + 2br^4} + \frac{1}{r + 2br^3}h(r) - h^2(r).\quad (30)$$

This is the Riccati equation of which the general form is

$$A'(r) = q_0(r) + q_1(r)A(r) + q_2(r)A^2(r),\quad (31)$$

where $q_0(r) \neq 0$ and $q_2(r) \neq 0$. Comparing (31) with (30), we obtain

$$q_0(r) = \frac{3}{r^2 + 2br^4}, q_1(r) = \frac{1}{r + 2br^3}, q_2(r) = -1.\quad (32)$$

Let $h_0(r)$ satisfy (30). Then,

$$h'_0(r) = \frac{3}{r^2 + 2br^4} + \frac{1}{r + 2br^3}h_0(r) - h_0^2(r). \quad (33)$$

By the property of the Riccati equation, the other solution is given by

$$h(r) = h_0(r) + \frac{1}{z(r)}, \quad (34)$$

where $z(r)$ satisfies

$$z'(r) - \left[-\frac{1}{r + 2br^3} + 2h_0(r) \right] z(r) = 1. \quad (35)$$

The solution is given by

$$z(r) = \frac{1}{e^{\int P(r)dr}} \int e^{\int P(r)dr} dr, \quad (36)$$

where

$$P(r) = - \left[-\frac{1}{r + 2br^3} + 2h_0(r) \right]. \quad (37)$$

Thus,

$$z(r) = \sqrt{\frac{1 + 2br^2}{2br^2}} e^{\int 2h_0(r)dr} \int \sqrt{\frac{2br^2}{1 + 2br^2}} e^{-\int 2h_0(r)dr} dr. \quad (38)$$

From (34), we obtain

$$h(r) = h_0(r) + \sqrt{\frac{2br^2}{1 + 2br^2}} e^{-\int 2h_0(r)dr} \left[\int \sqrt{\frac{2br^2}{1 + 2br^2}} e^{-\int 2h_0(r)dr} dr \right]^{-1}. \quad (39)$$

From (25), $\zeta(r)$ is given by

$$\zeta(r) = ce^{\int h(r)dr}, \quad (40)$$

where c is an arbitrary constant. This is the other solution to equation (30). After knowing $h_0(r)$, we can know the explicit form of (40).

5 Comparing the Two Methods

From section 3, we can see that the general solution can be obtained using the Frobenius method. However, the method of Frobenius can be applied to a second order linear ordinary differential equation with some specific form.

On the other hand, the method of Riccati in section 4 can be applied to a first order nonlinear ordinary differential equation with any form. However, only knowing one solution, we can find the other solution. In fact, any second order linear ordinary differential equation can be transformed into the Riccati equation and vice versa. A single known solution to the Riccati equation can therefore be obtained through many methods for a second order linear ordinary differential equation including the Frobenius method.

6 Conclusion

The Einstein field equation is a second order nonlinear partial differential equation. When imposing the condition of perfect fluid spheres, the Einstein field equation can be transformed into a second order linear ordinary differential equation. After rearranging this equation, we can obtain the general solution by the method of Frobenius. Moreover, this second order linear ordinary differential equation can be transformed to the Riccati equation. After knowing one solution, we can obtain the other solution.

It is not obvious to conclude which of the two methods is more preferable. Sometimes, it is necessary to combine the two methods to obtain the general solution to a second order linear ordinary differential equation.

7 Acknowledgement

This project was funded by the Ratchadapisek Somphot Fund, Chulalongkorn University, for the professional development of new academic staff, by the Thailand Research Fund (TRF), and by the Office of the Higher Education Commission (OHEC), Faculty of Science, Chulalongkorn University (RSA5980038). PB was additionally supported by a scholarship from the Royal Government of Thailand. TN was also additionally supported by a scholarship from the Development and Promotion of Science and Technology Talents Project (DPST).

References

1. Schwarzschild, K.: On the gravitational field of a sphere of incompressible fluid according to Einsteins theory. *Sitzungsber. Preuss. Akad. Wiss. Berlin (Math. Phys.)* (1916), [arXiv: physics/9912033 [physics.hist-ph]].
2. Bondi, H.: Spherically symmetrical models in general relativity. *Mon. Not. Roy. Astron. Soc.* 107, 410 (1947).
3. Buchdahl, H. A.: General relativistic fluid spheres. *Phys. Rev.* 116, 1027-1034 (1959).
4. Kramer, D., Stephani, H., Herlt, E., MacCallum M.: *Exact solutions of Einsteins field equations*, Cambridge University Press, England, 1980.
5. Delgaty, M. S. R., Lake, K.: Physical acceptability of isolated, static, spherically symmetric, perfect fluid solutions of Einsteins equations. *Comput. Phys. Commun.* 115, 395 (1998) [arXiv: gr-qc/9809013].
6. Rahman, S., Visser, M.: Space-time geometry of static fluid spheres. *Class. Quant. Grav.* 19, 935 (2002) [arXiv: gr-qc/0103065].
7. Lake, K.: All static spherically symmetric perfect fluid solutions of Einsteins equation. *Phys. Rev. D* 67, 104015 (2003) [arXiv: gr-qc/0209104].
8. Martin, D., Visser, M.: Algorithmic construction of static perfect fluid spheres. *Phys. Rev. D* 69, 104028 (2004) [arXiv: gr-qc/0306109].
9. Boonserm, P., Visser, M., Weinfurtner, S.: Generating perfect fluid spheres in general relativity. *Phys. Rev. D* 71, 124037 (2005), [arXiv: gr-qc/0503007].
10. Boonserm, P.: *Some Exact Solution in General Relativity*. MSc. Thesis, Victoria University of Wellington (2006).

11. Boonserm, P., Visser, M.: Buchdahl-like transformations for perfect fluid spheres. *Int. J. Mod. Phys. D* 17, 135-163 (2008), [arXiv:0707.0146 [gr-qc]].
12. Herrera, L., Ospino, J., Prisco, A. Di.: All static spherically symmetric anisotropic solutions of Einsteins equation. *Phys. Rev. D* 77, 027502 (2008) [arXiv: 0712.0713 [gr-qc]].
13. Boonserm, P., Ngampitipan, T., Visser, M.: Mimicking static anisotropic fluid spheres in general relativity. *Int. J. Mod. Phys. D* 25, 1650019 (2016) [arXiv:1501.07044 [gr-qc]].
14. Jongjittanon, N., Boonserm, P., Ngampitipan, T.: Generating theorems for charged anisotropy in general relativity. *AJPA*. 4, 50-56 (2016).
15. Thairatana, K.: Transformation for perfect fluid spheres in isotropic coordinates. M.Sc. Thesis, Chulalongkorn University (2013).
16. Boonserm, P., Suavansri, P., Thairatana, K.: Transformation for perfect fluid spheres in isotropic coordinates. *Annual Meeting in Mathematics (AMM2011)*, Khon Kaen, Thailand, 261-272 (2011).
17. Boonserm, P., Visser, M., Weinfurtnr, S.: Solution generating theorems for the TOV equation. *Phys. Rev. D* 76, 044024 (2007), [arXiv: gr-qc/0607001].
18. Jongjittanon, N.: Generating theorems for charged anisotropy and modified Tolman-Oppenheimer-Volkov equation. M.Sc. Thesis, Chulalongkorn University (2015).
19. Kinreewong, A.: Solution generating theorems and Tolman-Oppenheimer-Volkov equation for perfect fluid spheres in isotropic coordinates. M.Sc. Thesis, Chulalongkorn University (2015).
20. Kauser, M. A., Islam, Q.: Generation of static perfect fluid spheres in general relativity. *Phys. J.* 2 (2016).
21. Riley, K. F., Hobson, M. P., Bence, S. J.: *Mathematical Methods for Physics and Engineering: A Comprehensive Guide*, Cambridge University Press, England, 2006.
22. Piaggio, H. T. H.: *Differential Equations*, Read Books, 2008.
23. Konoplya, R. A., Zhidenko, A.: Quasinormal modes of black holes: from astrophysics to string theory. *Rev. Mod. Phys.* 83, 793-836 (2011) [arXiv:1102.4014 [gr-qc]].
24. Perkins, A.: Static spherically symmetric solutions in higher derivative gravity. PhD Thesis, Imperial College London (2016).

Article

Near-Horizon Geodesics for Astrophysical and Idealised Black Holes: Coordinate Velocity and Coordinate Acceleration

Petarpa Boonserm ¹ , Tritos Ngampitipan ² and Matt Visser ^{3,*} 

¹ Department of Mathematics and Computer Science, Faculty of Science, Chulalongkorn University, Bangkok 10330, Thailand; petarpa.boonserm@gmail.com

² Faculty of Science, Chandrakasem Rajabhat University, Bangkok 10900, Thailand; tritos.ngampitipan@gmail.com

³ School of Mathematics and Statistics, Victoria University of Wellington, P.O. Box 600, Wellington 6140, New Zealand

* Correspondence: matt.visser@sms.vuw.ac.nz

Received: 1 April 2018; Accepted: 24 May 2018; Published: 28 May 2018



Abstract: Geodesics (by definition) have an intrinsic 4-acceleration zero. However, when expressed in terms of coordinates, the *coordinate acceleration* d^2x^i/dt^2 can very easily be non-zero, and the *coordinate velocity* dx^i/dt can behave unexpectedly. The situation becomes extremely delicate in the near-horizon limit—for both astrophysical and idealised black holes—where an inappropriate choice of coordinates can quite easily lead to significant confusion. We shall carefully explore the relative merits of horizon-penetrating *versus* horizon-non-penetrating coordinates, arguing that in the near-horizon limit the coordinate acceleration d^2x^i/dt^2 is best interpreted in terms of horizon-penetrating coordinates.

Keywords: geodesic equation; coordinate velocity; coordinate acceleration; horizon-penetrating coordinates; horizon-non-penetrating coordinates

PACS: 04.20.-q; 04.70.-s; 04.70.Bw; 02.40.Hw

1. Introduction

Coordinate dependence in general relativity is a topic that continues to cause confusion to this day, despite over 100 years of work on this issue. (For a variety of articles, both pro and con, both published and unpublished, see [1–14]. For two recent overviews, see [15,16]). The situation is particularly acute in the immediate vicinity of any horizon that might be present, whether it be for an astrophysical or an idealised (mathematical) black hole, where an inappropriate choice of coordinates can needlessly add to the confusion. Indeed, while horizons are often associated with coordinate singularities, these coordinate singularities are a property of the coordinate patch, not the spacetime geometry, and these coordinate singularities can quite easily go away with a different choice of coordinates. For astrophysical black holes, as opposed to maximally analytically extended idealised black holes, one still trusts the usual Einstein equations in the domain of outer communication—and down to any inner horizon that might be present. Similarly for the black holes arising from numerical simulations, which are key to modelling the astrophysical black holes of direct observational interest, one typically calculates down to some region inside the outer horizon, but well above the singular region, relying on the usual idealised picture for near-(outer)-horizon physics. Finally, for semi-classical black holes, as long as the quantum fields are in the Unruh vacuum state, the near-horizon geometry in the vicinity of the future horizon is qualitatively similar to that in classical general relativity.

In short, the black holes of observational interest in astronomy and cosmology can be adequately represented, at least in the domain of outer communication and down to any inner horizon that might be present, by the idealised Schwarzschild and Kerr spacetimes—and analysis of the near-horizon physics can adequately be performed using the classical Schwarzschild and Kerr spacetimes. In fact, it is very useful to distinguish:

- Horizon-penetrating coordinates—these coordinate systems are regular as one crosses the horizon (for example, Painlevé–Gullstrand coordinates, Kerr–Schild coordinates, and variants thereof).
- Horizon-non-penetrating coordinates—these coordinate systems are singular as one crosses the horizon (for example, the Schwarzschild curvature coordinates, isotropic coordinates, and variants thereof).

The horizon-non-penetrating coordinates are simpler for some purposes (the metric is typically diagonal), but are ill-behaved in the immediate vicinity of the horizon. In contrast horizon-penetrating coordinates are better behaved in the immediate vicinity of the horizon, but the metric is typically non-diagonal, and the asymptotic behaviour may sometimes be more subtle than expected. We shall work through a number of examples illustrating the dangers and the pitfalls.

Consider for instance the Schwarzschild geometry—this is a very well-known spacetime since it was the first known exact solution to the (vacuum) Einstein field equations [17]. It is certainly of direct physical relevance—the spacetime geometry exterior to the sun and that exterior to slowly-rotating astrophysical black holes can be well-approximated by the Schwarzschild geometry. Perhaps the simplest form of the Schwarzschild spacetime is the Hilbert form expressed in terms of (what are now known as) Schwarzschild curvature coordinates [18–20]

$$ds^2 = - \left(1 - \frac{2m}{r}\right) dt^2 + \left(1 - \frac{2m}{r}\right)^{-1} dr^2 + r^2 (d\theta^2 + \sin^2 \theta d\phi^2). \quad (1)$$

There is a coordinate singularity at $r = 2m$, see for instance [21–30], making this representation horizon-non-penetrating [31]. It is easy to see that in these coordinates the radial geodesics “pile up” at $r = 2m$, never (in these coordinates) crossing the horizon. In fact, for any radial incoming geodesic, $\dot{r} \rightarrow 0$ as one approaches the horizon.

Taking into account the Killing conservation law for the energy, we shall soon see that, even for infalling particles, $\dot{r} \rightarrow$ (something positive) sufficiently close to the horizon, though not at the horizon itself. However, this near-horizon $\dot{r} > 0$ phenomenon is a coordinate artefact; the behaviour can be very different in other coordinates. Despite this, some researchers are now (even in 2018) completely misinterpreting this coordinate artefact and asserting that “gravity becomes repulsive near the horizon”. This claim is, at best, a gross misinterpretation of the actual situation. (For specific examples of this particular confusion, see particularly [1,3–6,9–13]. For partial antidotes, see [7,8,14]. For a somewhat different sort of coordinate confusion, mistaking white holes for black holes, see [2].)

Below, we shall show that the coordinate acceleration near horizons is, in horizon-penetrating coordinates, (such as the Painlevé–Gullstrand [32–40] or Kerr–Schild [21,24,27–29,40] coordinates), much easier to understand. We shall then wrap up with some generic comments regarding arbitrary horizon-penetrating coordinate systems [41–44].

We shall use letters from the beginning of the Roman alphabet (a, b, c, d, \dots) for spacetime indices, (see for instance Wald [22], or Hobson–Efstathiou–Lasenby [23]). Whenever there is a clearly defined time coordinate t , we shall use letters from the middle of the Roman alphabet (i, j, k, l, \dots) for the remaining spatial indices. We reserve the notation \dot{x} and \ddot{x} for derivatives with respect to the time coordinate t .

2. Geodesic Equation

Consider the geodesic equation in non-affine-parameterised form:

$$\frac{d^2 x^a}{d\lambda^2} + \Gamma^a_{bc} \frac{dx^b}{d\lambda} \frac{dx^c}{d\lambda} = f(\lambda) \frac{dx^a}{d\lambda}. \quad (2)$$

This part of the analysis works equally well for timelike or null geodesics. Assume the zero'th coordinate is timelike, at least outside any horizon that might be present. That is, take $x^a = (t, x^i)$. We can then choose the coordinate t to be a non-affine parameter for the geodesic. The geodesic equation separates into

$$\frac{d^2 t}{dt^2} + \Gamma^t_{bc} \frac{dx^b}{dt} \frac{dx^c}{dt} = f(t) \frac{dt}{dt}; \quad (3)$$

$$\frac{d^2 x^i}{dt^2} + \Gamma^i_{bc} \frac{dx^b}{dt} \frac{dx^c}{dt} = f(t) \frac{dx^i}{dt}. \quad (4)$$

The first of these equations implies

$$f(t) = \Gamma^t_{bc} \frac{dx^b}{dt} \frac{dx^c}{dt}. \quad (5)$$

The second equation then becomes

$$\frac{d^2 x^i}{dt^2} = -\Gamma^i_{bc} \frac{dx^b}{dt} \frac{dx^c}{dt} + \left(\Gamma^t_{bc} \frac{dx^b}{dt} \frac{dx^c}{dt} \right) \frac{dx^i}{dt}. \quad (6)$$

This is still very general. Let us now specialize to spherical symmetry, taking

$$g_{ab} = \left[\begin{array}{cc|cc} g_{tt} & g_{tr} & 0 & 0 \\ g_{tr} & g_{rr} & 0 & 0 \\ \hline 0 & 0 & g_{\theta\theta} & 0 \\ 0 & 0 & 0 & g_{\phi\phi} \end{array} \right]. \quad (7)$$

Then the radial geodesics are given by

$$\frac{d^2 r}{dt^2} = -\Gamma^r_{bc} \frac{dx^b}{dt} \frac{dx^c}{dt} + \left(\Gamma^t_{bc} \frac{dx^b}{dt} \frac{dx^c}{dt} \right) \frac{dr}{dt}. \quad (8)$$

That is,

$$\ddot{r} = - \left[\Gamma^r_{tt} + 2\Gamma^r_{rt} \dot{r} + \Gamma^r_{rr} \dot{r}^2 \right] + \left[\Gamma^t_{tt} + 2\Gamma^t_{rt} \dot{r} + \Gamma^t_{rr} \dot{r}^2 \right] \dot{r}. \quad (9)$$

Finally, regrouping, we see

$$\ddot{r} = -\Gamma^r_{tt} + (\Gamma^t_{tt} - 2\Gamma^r_{rt}) \dot{r} + (2\Gamma^t_{rt} - \Gamma^r_{rr}) \dot{r}^2 + \Gamma^t_{rr} \dot{r}^3. \quad (10)$$

Note that the “coordinate acceleration” \ddot{r} is *cubic* in the “coordinate velocity” \dot{r} . This effect is certainly real if perhaps naively unexpected. (This effect is also manifestly coordinate-dependent.)

3. Killing Conservation Law for Energy: Coordinate Velocity

In all the situations we will be interested in, there is a timelike Killing vector (timelike outside any horizon that may be present), and there is no real loss of generality in taking the t coordinate to be compatible with that Killing vector; so $K^a = (\partial_t)^a$. (That is, we choose coordinates to *manifestly* respect the time-translation Killing symmetry.) However, then any timelike geodesic with 4-velocity V^a is subject to the energy conservation law

$$g_{ab} K^a V^b = -\epsilon \quad (11)$$

where ϵ is a constant, effectively the energy per unit rest mass. Observe that $\epsilon = 1$ corresponds to dropping a particle at rest from spatial infinity; $\epsilon > 1$ corresponds to dropping a moving particle

from spatial infinity; $\epsilon < 1$ corresponds to a gravitationally bound particle, dropped at rest from some finite radius. In fact, in an asymptotically flat spacetime, $\epsilon = 1/\sqrt{1 - \beta_\infty^2}$, where β_∞ is the “coordinate velocity at infinity.” In spherical symmetry, this Killing conservation law can be written as

$$g_{tb} \frac{(1, \dot{r}, 0, 0)^b}{\|(1, \dot{r}, 0, 0)\|} = -\epsilon. \quad (12)$$

That is,

$$(g_{tt} + g_{tr} \dot{r}) = -\epsilon \sqrt{-(g_{tt} + 2g_{tr} \dot{r} + g_{rr} \dot{r}^2)}. \quad (13)$$

Even more explicitly,

$$(g_{tt} + g_{tr} \dot{r})^2 = -\epsilon^2 (g_{tt} + 2g_{tr} \dot{r} + g_{rr} \dot{r}^2). \quad (14)$$

This is *quadratic* in \dot{r} , with a general solution

$$\dot{r} = \frac{-g_{tr}(1 + \epsilon^{-2}g_{tt}) \pm \sqrt{(1 + \epsilon^{-2}g_{tt})(g_{tr}^2 - g_{tt}g_{rr})}}{g_{rr} + \epsilon^{-2}g_{tr}^2}. \quad (15)$$

Physically, the situation is this: If one drops a particle from some initial position r_0 with initial coordinate velocity \dot{r}_0 , then one can calculate the energy ϵ from Equation (11) and subsequently extract \dot{r} at general positions r from Equation (15).

Formally, null geodesics can be viewed as the $\epsilon \rightarrow \infty$ limit of this formalism. This is most easily seen from Equations (13) or (14), which in the $\epsilon \rightarrow \infty$ limit imply

$$g_{tt} + 2g_{tr} \dot{r} + g_{rr} \dot{r}^2 = 0. \quad (16)$$

However, this is exactly the condition that the radial curve is a null curve. In this null limit, one sees that the Killing conservation law becomes

$$\dot{r} = \frac{-g_{tr} \pm \sqrt{g_{tr}^2 - g_{tt}g_{rr}}}{g_{rr}}. \quad (17)$$

Two special cases are of particular interest:

- In coordinate charts where the metric is diagonal, (for example, the Schwarzschild curvature coordinates or isotropic coordinates), we have $g_{tr} = 0$. Therefore, for timelike geodesics,

$$\dot{r} = \pm \frac{\sqrt{(1 + \epsilon^{-2}g_{tt})(-g_{tt}g_{rr})}}{g_{rr}}. \quad (18)$$

As long as we are primarily interested in dropping (infalling) particles, we must choose the negative root and set

$$\dot{r} = - \frac{\sqrt{(1 + \epsilon^{-2}g_{tt})(-g_{tt}g_{rr})}}{g_{rr}}. \quad (19)$$

In the null limit ($\epsilon \rightarrow \infty$), this simplifies considerably and becomes

$$\dot{r} = - \sqrt{\frac{-g_{tt}}{g_{rr}}}. \quad (20)$$

- In contrast, in coordinate charts where the metric satisfies $g_{tt}g_{rr} - g_{tr}^2 = -1$, (for example, the Painlevé–Gullstrand coordinates or Kerr–Schild coordinates), for timelike geodesics, we have

$$\dot{r} = \frac{-g_{tr}(1 + \epsilon^{-2}g_{tt}) \pm \sqrt{1 + \epsilon^{-2}g_{tt}}}{g_{rr} + \epsilon^{-2}g_{tr}^2}. \quad (21)$$

As long as we are primarily interested in dropping (infalling) particles, we can safely choose the negative root and set

$$\dot{r} = \frac{-g_{tr}(1 + \epsilon^{-2}g_{tt}) - \sqrt{1 + \epsilon^{-2}g_{tt}}}{g_{rr} + \epsilon^{-2}g_{tr}^2} = -\sqrt{1 + \epsilon^{-2}g_{tt}} \left\{ \frac{1 + g_{tr}\sqrt{1 + \epsilon^{-2}g_{tt}}}{g_{rr} + \epsilon^{-2}g_{tr}^2} \right\}. \quad (22)$$

Note that $1 + \epsilon^{-2}g_{tt} \geq 0$ in order to keep \dot{r} real, while $g_{rr} + \epsilon^{-2}g_{tr}^2 > 0$ always, so choosing the negative root selects the ingoing geodesic.

In the null limit ($\epsilon \rightarrow \infty$), this simplifies considerably and becomes

$$\dot{r} = -\left\{ \frac{1 + g_{tr}}{g_{rr}} \right\}. \quad (23)$$

Let us now apply these quite general considerations to study the fixed-energy coordinate acceleration.

4. Coordinate Acceleration

For a dropped (timelike trajectory) particle, the coordinate acceleration at arbitrary radius is thus an interplay between the geodesic equation

$$\ddot{r} = -\Gamma_{tt}^r + (\Gamma_{tt}^t - 2\Gamma_{rt}^r) \dot{r} + (2\Gamma_{rt}^t - \Gamma_{rr}^r) \dot{r}^2 + \Gamma_{rr}^t \dot{r}^3, \quad (24)$$

and the Killing-induced coordinate velocity equation

$$\dot{r} = \frac{-g_{tr}(1 + \epsilon^{-2}g_{tt}) \pm \sqrt{(1 + \epsilon^{-2}g_{tt})(g_{tr}^2 - g_{tt}g_{rr})}}{g_{rr} + \epsilon^{-2}g_{tr}^2}. \quad (25)$$

Combining these results, we would get something of the general form

$$\ddot{r} = f(\epsilon, r) \quad (26)$$

where $f(\epsilon, r)$ is some explicit *but coordinate-dependent* function. Note that we could always use the chain rule to write $\ddot{r} = \frac{d\dot{r}}{dr} \frac{dr}{dt} = \frac{d\dot{r}}{dr} \dot{r} = \frac{1}{2} \frac{d(\dot{r}^2)}{dr}$. This serves as a consistency check, and side-steps the geodesic equation, but when doing so, one loses information regarding the coordinate velocity dependence of the coordinate acceleration. We shall now give a few examples of this phenomenon, focusing particularly on near-horizon behaviour.

5. Example: Schwarzschild Geometry

The Schwarzschild spacetime geometry is perhaps the pre-eminent example of an exact solution in general relativity [17–21,24–27]. As specific examples of near-horizon behaviour for the coordinate velocity \dot{r} and coordinate acceleration \ddot{r} , let us consider the Schwarzschild spacetime in four commonly occurring coordinate systems [28–30,32–36]: Schwarzschild curvature coordinates, isotropic coordinates, Painlevé–Gullstrand coordinates, and Kerr–Schild coordinates.

5.1. Schwarzschild Curvature Coordinates

The Schwarzschild geometry in Schwarzschild curvature coordinates is described by

$$ds^2 = - \left(1 - \frac{2m}{r}\right) dt^2 + \left(1 - \frac{2m}{r}\right)^{-1} dr^2 + r^2 (d\theta^2 + \sin^2 \theta d\phi^2). \quad (27)$$

It is easy to calculate the Christoffel symbols and to verify that the geodesic equation implies

$$\ddot{r} = -\frac{m(1 - 2m/r)}{r^2} + \left[\frac{3m}{r^2(1 - 2m/r)} \right] \dot{r}^2. \quad (28)$$

This can be rewritten as

$$\ddot{r} = -\frac{m}{r^2} \left\{ \left(1 - \frac{2m}{r}\right) - \frac{3\dot{r}^2}{(1 - 2m/r)} \right\}. \quad (29)$$

This gives the coordinate acceleration \ddot{r} in terms of the Newtonian value $-m/r^2$, modified by relativistic corrections—due to both spacetime geometry and the local coordinate velocity. Furthermore, this already demonstrates (working in terms of r and \dot{r}) that \ddot{r} changes sign at the critical coordinate velocities given by

$$(\dot{r})_*^2 = \frac{1}{3} \left(1 - \frac{2m}{r}\right)^2. \quad (30)$$

At large r (that is, weak fields), this sign flip takes place at $\dot{r}^2 \approx 1/3$; this is mildly relativistic but certainly not ultra-relativistic. (In fact, this sign flip takes place for both ingoing and outgoing geodesics.) Furthermore, from the Killing conservation equation, we deduce

$$\dot{r} = \pm \left(1 - \frac{2m}{r}\right) \sqrt{1 - \epsilon^{-2} \left(1 - \frac{2m}{r}\right)}. \quad (31)$$

In particular at the horizon $(\dot{r})_H = 0$, and at spatial infinity, we see $\lim_{r \rightarrow \infty} \dot{r} = \sqrt{1 - \epsilon^{-2}}$ for fixed ϵ . Combining these geodesic and Killing results

$$\ddot{r} = -\frac{m}{r^2} \left(1 - \frac{2m}{r}\right) \left(1 - \frac{3(\epsilon^2 - 1 + 2m/r)}{\epsilon^2}\right). \quad (32)$$

Note that (for fixed ϵ), the coordinate acceleration \ddot{r} goes through zero and changes sign at the critical values of r given by

$$r_* = \frac{6m}{3 - 2\epsilon^2}; \quad \text{and} \quad r_* = 2m. \quad (33)$$

(In fact, this sign flip takes place for both ingoing and outgoing geodesics.) In particular, at the horizon $(\ddot{r})_H = 0$ for fixed ϵ .

For a time-like particle dropped at rest from spatial infinity ($\epsilon = 1$), this simplifies to

$$\dot{r} = -\left(1 - \frac{2m}{r}\right) \sqrt{\frac{2m}{r}}; \quad \ddot{r} = -\frac{m}{r^2} \left(1 - \frac{2m}{r}\right) \left(1 - \frac{6m}{r}\right); \quad r_* \in \{6m, 2m\}. \quad (34)$$

(Note that asymptotically $\dot{r} \rightarrow \sqrt{2m/r}$, and $\ddot{r} \rightarrow -m/r^2$, as expected from the Newtonian limit.)

Oddly enough (in this particular coordinate system), the coordinate acceleration switches sign at $r_* = 6m$, the location of the innermost stable circular orbit (ISCO); this is a coincidence, not anything fundamental.

For a light-like particle ($\epsilon \rightarrow \infty$), this simplifies to

$$\dot{r} = -\left(1 - \frac{2m}{r}\right); \quad \ddot{r} = +2\frac{m}{r^2} \left(1 - \frac{2m}{r}\right); \quad r_* = 2m. \quad (35)$$

(Note that a photon can have non-trivial coordinate velocity and non-zero coordinate acceleration even if its physical speed is always exactly equal to c . This is one of the reasons that the concepts of coordinate velocity and coordinate acceleration must be used with care and discretion.)

Now these particular observations are not new, dating back (at least) to Hilbert in 1915 and the mid-1920s [18–20]. (It must be emphasised that Hilbert’s comments have subsequently been grossly misinterpreted by some of the later commentators on this topic.) (See particularly [1,3–6,9–13]. For partial antidotes, see [7,8,14]. For a different sort of coordinate confusion (mistaking white holes for black holes) see [2].) What is new in the current discussion is that we will now put these issues into a wider context emphasising the extent to which these results are simply coordinate artefacts.

The radial coordinate velocity and radial coordinate acceleration for timelike geodesics are plotted as shown in Figures 1 and 2. For null geodesics, see Figures 3 and 4.

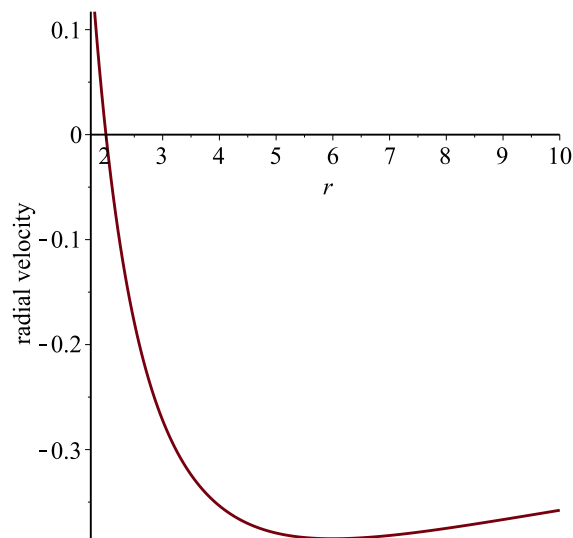


Figure 1. Behaviour of \dot{r} in the Schwarzschild geometry when using Schwarzschild curvature coordinates for $m = 1$ and $\epsilon = 1$. Note the curve crosses the r axis only at $r = 2$, and the coordinate velocity is negative all the way from the horizon to spatial infinity.

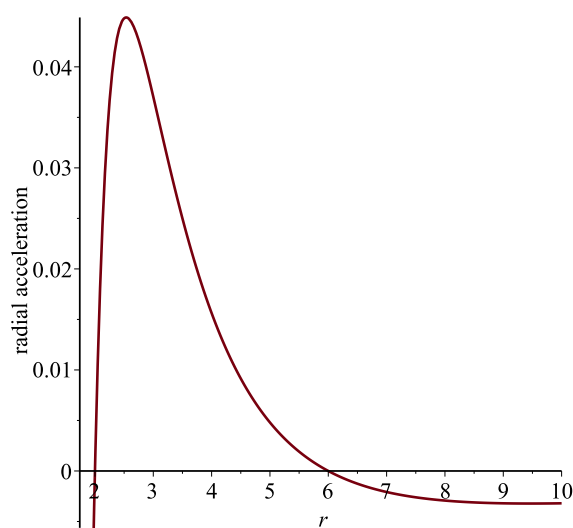


Figure 2. Behaviour of \ddot{r} in the Schwarzschild geometry when using Schwarzschild curvature coordinates for $m = 1$ and $\epsilon = 1$. Note the curve crosses the r axis at both $r = 2$ and $r = 6$; the coordinate acceleration is positive between the horizon and the ISCO.

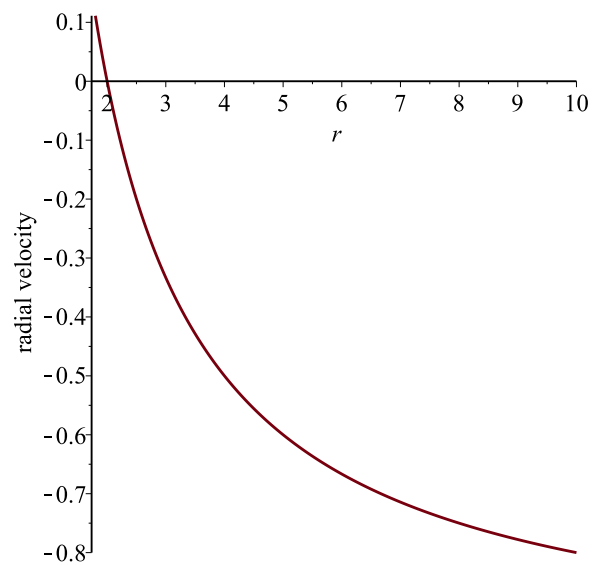


Figure 3. Behaviour of \dot{r} for null geodesics in the Schwarzschild geometry when using Schwarzschild curvature coordinates for $m = 1$ and $\epsilon \rightarrow \infty$. Note the curve crosses the r axis only at $r = 2$, and the coordinate velocity is negative all the way from the horizon to spatial infinity.

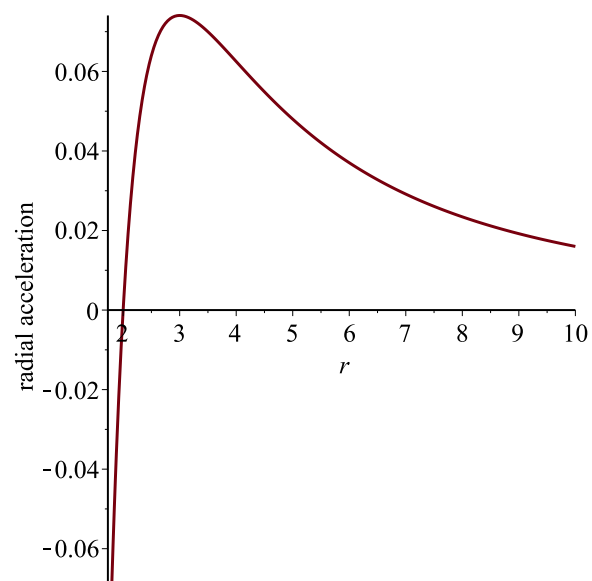


Figure 4. Behaviour of \ddot{r} for null geodesics in the Schwarzschild geometry when using Schwarzschild curvature coordinates for $m = 1$ and $\epsilon \rightarrow \infty$. Note the curve crosses the r axis only at $r = 2$, and the coordinate acceleration is positive all the way from the horizon to spatial infinity.

5.2. Isotropic Coordinates

The Schwarzschild geometry in isotropic coordinates is described by [21]

$$ds^2 = -\frac{\left(1 - \frac{m}{2r}\right)^2}{\left(1 + \frac{m}{2r}\right)^2} dt^2 + \left(1 + \frac{m}{2r}\right)^4 \left[dr^2 + r^2 (d\theta^2 + \sin^2 \theta d\phi^2) \right]. \quad (36)$$

Compared to Schwarzschild curvature coordinates, only the meaning of the r coordinate has changed. Indeed,

$$r_{\text{Schwarzschild}} = r_{\text{isotropic}} \left(1 + \frac{m}{2r_{\text{isotropic}}} \right)^2. \quad (37)$$

(In these isotropic coordinates, the horizon is now at $r = \frac{m}{2}$.)

The Christoffel symbols are easily calculated and the geodesic equation becomes

$$\ddot{r} = -\frac{m}{r^2} \frac{(1 - \frac{m}{2r})}{(1 + \frac{m}{2r})^7} + 3 \frac{m}{r^2} \frac{(1 - \frac{m}{6r})}{(1 - \frac{m}{2r})(1 + \frac{m}{2r})} \dot{r}^2. \quad (38)$$

This can also be recast as

$$\ddot{r} = -\frac{m}{r^2} \left\{ \frac{(1 - \frac{m}{2r})}{(1 + \frac{m}{2r})^7} - 3 \frac{(1 - \frac{m}{6r})}{(1 - \frac{m}{2r})(1 + \frac{m}{2r})} \dot{r}^2 \right\}. \quad (39)$$

This already demonstrates (working in terms of r and \dot{r}) that \ddot{r} changes sign at the critical coordinate velocities

$$(\dot{r})_*^2 = \frac{1}{3} \frac{(1 - \frac{m}{2r})^2}{(1 + \frac{m}{2r})^6 (1 - \frac{m}{6r})}. \quad (40)$$

At large r , (i.e., weak fields), this sign flip takes place at $\dot{r}^2 \approx 1/3$; this is mildly relativistic but certainly not ultra-relativistic. (In the weak-field limit, the Schwarzschild curvature coordinates and the isotropic coordinates asymptotically approach each other.)

From the Killing conservation equation, since the metric in isotropic coordinates is diagonal, we deduce

$$\dot{r} = \pm \frac{\sqrt{(\epsilon^2 + g_{tt})(-g_{tt}g_{rr})}}{\epsilon g_{rr}} = \pm \frac{\sqrt{(1 + \epsilon^{-2}g_{tt})(-g_{tt}g_{rr})}}{g_{rr}}. \quad (41)$$

This implies

$$\dot{r} = \pm \frac{1}{\epsilon} \sqrt{\epsilon^2 - \left(\frac{1 - \frac{m}{2r}}{1 + \frac{m}{2r}} \right)^2} \frac{(1 - \frac{m}{2r})}{(1 + \frac{m}{2r})^3}. \quad (42)$$

Note that, at the horizon, now located at $r = m/2$, we again have $\dot{r} \rightarrow 0$, while at spatial infinity we again see $\dot{r} \rightarrow \sqrt{1 - \epsilon^{-2}}$ at fixed energy. Combining these results, for a dropped particle (of fixed energy ϵ), we have

$$\ddot{r} = -\frac{m}{r^2} \frac{(1 - \frac{m}{2r})}{(1 + \frac{m}{2r})^7} \left(1 - \frac{3(1 - \frac{m}{6r})}{\epsilon^2} \left[\epsilon^2 - \left(\frac{1 - \frac{m}{2r}}{1 + \frac{m}{2r}} \right)^2 \right] \right). \quad (43)$$

Note that the coordinate acceleration \ddot{r} goes through zero and (apart from the trivial zero at $r_* = m/2$) changes sign at the critical values r_* of r given by solving the cubic equation

$$r_* : \quad 1 - \frac{3(1 - \frac{m}{6r})}{\epsilon^2} \left[\epsilon^2 - \left(\frac{1 - \frac{m}{2r}}{1 + \frac{m}{2r}} \right)^2 \right] = 0. \quad (44)$$

For a particle dropped at rest from spatial infinity ($\epsilon = 1$), this simplifies to

$$\dot{r} = -\sqrt{1 - \left(\frac{1 - \frac{m}{2r}}{1 + \frac{m}{2r}} \right)^2} \frac{(1 - \frac{m}{2r})}{(1 + \frac{m}{2r})^3} \quad (45)$$

$$\ddot{r} = -\frac{m}{r^2} \frac{(1 - \frac{m}{2r})}{(1 + \frac{m}{2r})^7} \left(1 - 3 \left(1 - \frac{m}{6r} \right) \left[1 - \left(\frac{1 - \frac{m}{2r}}{1 + \frac{m}{2r}} \right)^2 \right] \right), \quad (46)$$

with the (non-trivial) zeros of coordinate acceleration determined by

$$1 - 3 \left(1 - \frac{m}{6r}\right) \left[1 - \left(\frac{1 - \frac{m}{2r}}{1 + \frac{m}{2r}}\right)^2\right] = 0 \quad r_* = (5 \pm 2\sqrt{5}) \frac{m}{2}. \quad (47)$$

(Though not entirely obvious, it is easy to check that, at large distances $\dot{r} \rightarrow \sqrt{2m/r}$, as expected from the Newtonian limit. It is more obvious that at large distances $\ddot{r} \rightarrow -m/r^2$. In isotropic coordinates, the ISCO is at $(\frac{5}{2} + \sqrt{6})m$, which is not where $\dot{r} \rightarrow 0$; that these two locations coincided in curvature coordinates is merely a coincidence.)

For null geodesics ($\epsilon \rightarrow \infty$), we have

$$\dot{r} = -\frac{(1 - \frac{m}{2r})}{(1 + \frac{m}{2r})^3} \quad \ddot{r} = \frac{2m}{r^2} \frac{(1 - \frac{m}{2r})(1 - \frac{m}{4r})}{(1 + \frac{m}{2r})^7}. \quad (48)$$

The radial coordinate velocity and radial coordinate acceleration for timelike geodesics are plotted as shown in Figures 5 and 6. For null geodesics, see Figures 7 and 8. Note the similarities *and differences* compared to what we saw for Schwarzschild curvature coordinates.

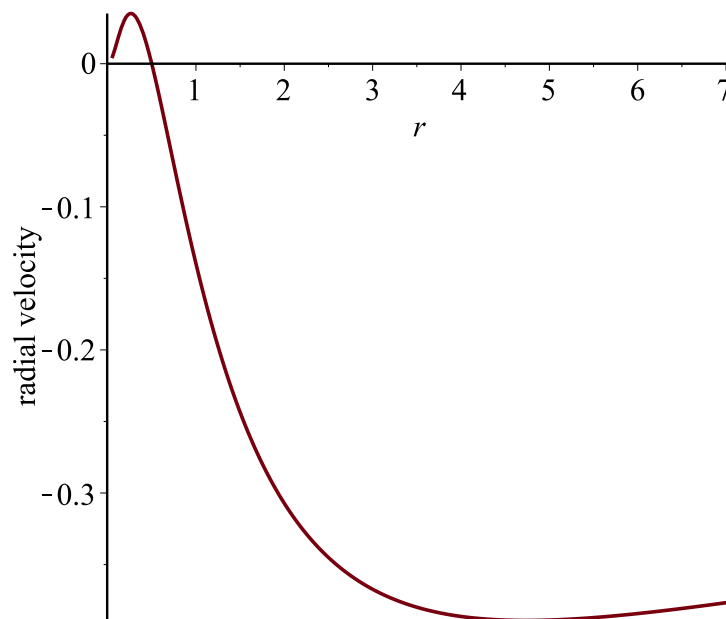


Figure 5. Behaviour of \dot{r} in the Schwarzschild geometry using isotropic coordinates for $m = 1$ and $\epsilon = 1$. Note the coordinate velocity is negative all the way from the horizon (now at $m/2$) to spatial infinity.

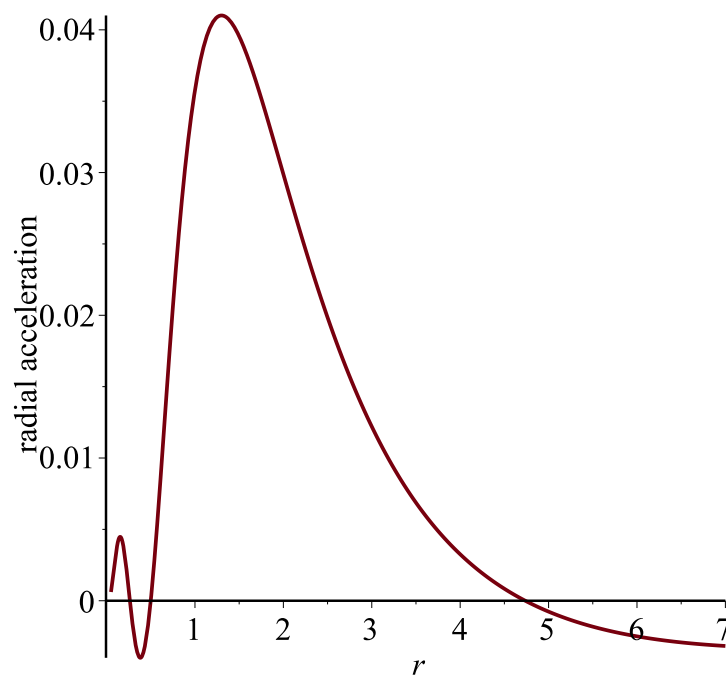


Figure 6. Behaviour of \ddot{r} in the Schwarzschild geometry using isotropic coordinates for $m = 1$ and $\epsilon = 1$. Note that the curve crosses the r axis both at $r = 1/2$ and $r = \frac{5+2\sqrt{5}}{2} \approx 4.736067977$; there is a third unphysical root at $r = \frac{5-2\sqrt{5}}{2} \approx 0.263932023$.

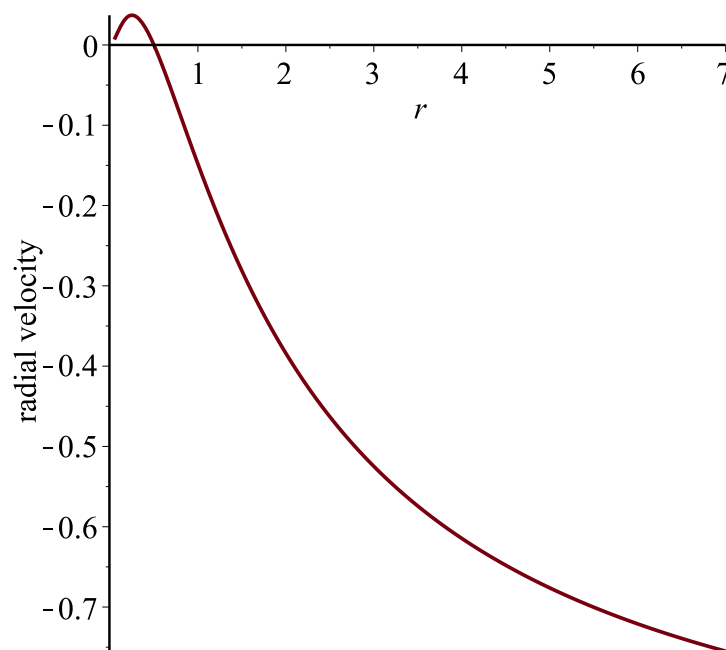


Figure 7. Behaviour of \dot{r} for null geodesics in the Schwarzschild geometry using isotropic coordinates for $m = 1$ and $\epsilon \rightarrow \infty$. Note the coordinate velocity is negative all the way from the horizon (now at $m/2$) to spatial infinity.

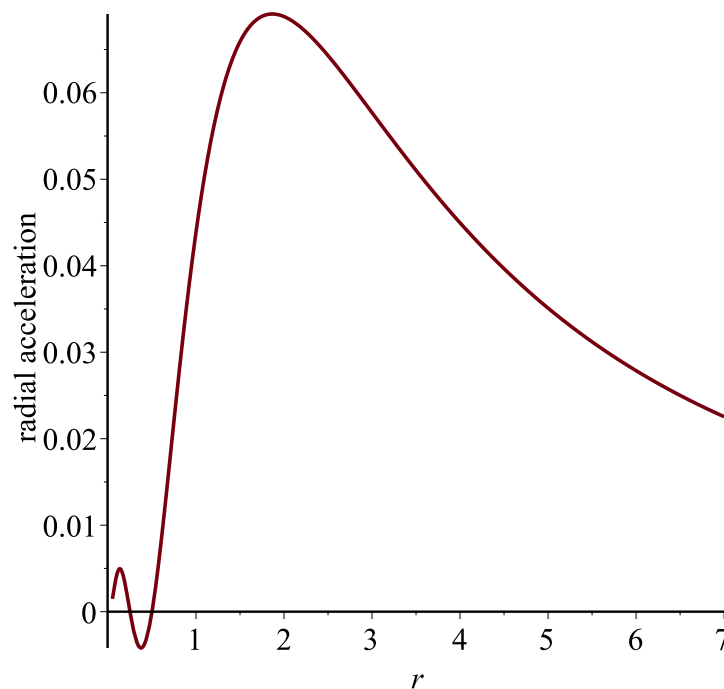


Figure 8. Behaviour of \ddot{r} for null geodesics in the Schwarzschild geometry using isotropic coordinates for $m = 1$ and $\epsilon \rightarrow \infty$. Note the horizon is now at $m/2$; there is an extra zero at $m/4$. Note the coordinate acceleration is positive all the way from the horizon to spatial infinity.

5.3. Painleve–Gullstrand Coordinates

The Schwarzschild geometry in Painleve–Gullstrand coordinates is described by [32–36]

$$ds^2 = -\left(1 - \frac{2m}{r}\right) dt_{PG}^2 + 2\sqrt{\frac{2m}{r}} dt_{PG} dr + dr^2 + r^2 (d\theta^2 + \sin^2 \theta d\phi^2) \quad (49)$$

where the Painleve–Gullstrand time coordinate is given in terms of the Schwarzschild time coordinate by

$$t_{PG} = t_{Schwarzschild} - 2m \left[2\sqrt{\frac{r}{2m}} - \ln \left(\frac{1 + \sqrt{2m/r}}{1 - \sqrt{2m/r}} \right) \right]. \quad (50)$$

Note in particular that $g_{tt} g_{rr} - g_{tr}^2 = -1$.

It is easy to calculate the Christoffel symbols and verify that, in these coordinates, the radial geodesic equation becomes

$$\ddot{r} = -\frac{m}{r^2} \left(1 - \frac{2m}{r}\right) + \frac{3m}{r^2} \sqrt{\frac{2m}{r}} \dot{r} + \frac{3m}{r^2} \dot{r}^2 + \frac{\sqrt{2m/r}}{2r} \dot{r}^3. \quad (51)$$

We can rewrite this as

$$\ddot{r} = -\frac{m}{r^2} \left\{ \left(1 - \frac{2m}{r}\right) - 3\sqrt{\frac{2m}{r}} \dot{r} - 3\dot{r}^2 \right\} + \frac{\sqrt{2m/r}}{2r} \dot{r}^3. \quad (52)$$

Viewed as a function of \dot{r} , this flips sign at the critical coordinate velocity

$$(\dot{r})_* = \sqrt[6]{\frac{2m}{r}} - \sqrt{\frac{2m}{r}}, \quad (53)$$

which is always positive outside the horizon. (This actually implies that \dot{r} factorizes as follows: $\dot{r} = (\dot{r} - [\sqrt[6]{2m/r} - \sqrt{2m/r}]) \times (\text{quadratic in } \dot{r})$, where the quadratic has no real zeroes. Unfortunately, the specific form of the quadratic is too messy to be illuminating.)

In view of the fact that, in these coordinates $-g_{tt}g_{rr} + g_{tr}^2 = 1$, the general Killing-induced result for the coordinate velocity simplifies to

$$\dot{r} = \frac{-g_{tr}(\epsilon^2 + g_{tt}) \pm \epsilon \sqrt{(\epsilon^2 + g_{tt})}}{\epsilon^2 g_{rr} + g_{tr}^2}. \quad (54)$$

Thence

$$\dot{r} = \frac{-\sqrt{2m/r}(\epsilon^2 - 1 + 2m/r) \pm \epsilon \sqrt{(\epsilon^2 - 1 + 2m/r)}}{\epsilon^2 + 2m/r}. \quad (55)$$

This can also be written as

$$\dot{r} = -\sqrt{\frac{2m}{r}} + \frac{\sqrt{2m/r} \pm \epsilon \sqrt{(\epsilon^2 - 1 + 2m/r)}}{\epsilon^2 + 2m/r}. \quad (56)$$

At the horizon, $r = 2m$, we have

$$(\dot{r})_H \in \left\{ 0, \frac{-2\epsilon^2}{\epsilon^2 + 1} \right\}. \quad (57)$$

Therefore, we see that the ingoing geodesic crosses the horizon with finite coordinate velocity

$$(\dot{r})_H = -\frac{2\epsilon^2}{\epsilon^2 + 1} = -\frac{2}{1 + \epsilon^{-2}} \in (-2, 0), \quad (58)$$

while the outgoing geodesic crosses the horizon with coordinate velocity zero. (Note that $|\dot{r}|$ can easily exceed unity; this is just a coordinate speed, not a physical speed.) This makes it clear that, for a dropped particle, we should take the negative root in \dot{r} so that

$$\dot{r} = -\sqrt{1 - \epsilon^{-2}(1 - 2m/r)} \frac{1 + \sqrt{2m/r} \sqrt{1 - \epsilon^{-2}(1 - 2m/r)}}{1 + \epsilon^{-2}(2m/r)}. \quad (59)$$

Combining these results, for a dropped particle (fixed energy ϵ), we have

$$\begin{aligned} \ddot{r} = & -\frac{m}{r^2} \left(1 - \frac{2m}{r} \right) \\ & + \frac{3m}{r^2} \sqrt{\frac{2m}{r}} \left[\frac{-\sqrt{2m/r}(\epsilon^2 - 1 + 2m/r) - \epsilon \sqrt{(\epsilon^2 - 1 + 2m/r)}}{\epsilon^2 + 2m/r} \right] \\ & + \frac{3m}{r^2} \left[\frac{-\sqrt{2m/r}(\epsilon^2 - 1 + 2m/r) - \epsilon \sqrt{(\epsilon^2 - 1 + 2m/r)}}{\epsilon^2 + 2m/r} \right]^2 \\ & + \frac{\sqrt{2m/r}}{2r} \left[\frac{-\sqrt{2m/r}(\epsilon^2 - 1 + 2m/r) - \epsilon \sqrt{(\epsilon^2 - 1 + 2m/r)}}{\epsilon^2 + 2m/r} \right]^3. \end{aligned} \quad (60)$$

For a timelike particle dropped at rest from spatial infinity ($\epsilon = 1$), this simplifies quite drastically to yield

$$\dot{r} = -\sqrt{\frac{2m}{r}}; \quad \ddot{r} = -\frac{m}{r^2}. \quad (61)$$

(The fact that in this particular situation the Painleve–Gullstrand coordinate system exactly reproduces the Newtonian result is one of the many reasons that the Painleve–Gullstrand coordinate system is so useful.)

Note that for $\epsilon = 1$ the (ingoing) coordinate acceleration \ddot{r} is extremely simple, and always negative. In fact, the coordinate acceleration is finite at horizon crossing $(\ddot{r})_H = -1/(4m)$.

For an infalling light-like particle ($\epsilon \rightarrow \infty$), this again simplifies quite drastically to yield

$$\dot{r} = -1 - \sqrt{\frac{2m}{r}}; \quad \ddot{r} = -\frac{1}{2r} \sqrt{\frac{2m}{r}} \left(1 + \sqrt{\frac{2m}{r}} \right). \quad (62)$$

Note that for $\epsilon \rightarrow \infty$ the (ingoing) coordinate acceleration \ddot{r} is relatively simple, and always negative. In fact, the coordinate acceleration is finite at horizon crossing $(\ddot{r})_H = -1/(2m)$. (The situation for Painlevé–Gullstrand coordinates is ultimately so simple that graphs are not needed.)

5.4. Kerr–Schild Coordinates

The Schwarzschild geometry in Kerr–Schild coordinates is described by [24,42]

$$ds^2 = -dt^2 + dr^2 + r^2 (d\theta^2 + \sin^2 \theta d\phi^2) + \frac{2m}{r} (dt + dr)^2. \quad (63)$$

That is,

$$ds^2 = -\left(1 - \frac{2m}{r}\right) dt^2 + \frac{4m}{r} dt dr + \left(1 + \frac{2m}{r}\right) dr^2 + r^2 (d\theta^2 + \sin^2 \theta d\phi^2). \quad (64)$$

Note in particular that $g_{tt} g_{rr} - g_{tr}^2 = -1$.

The Christoffel symbols are easily calculated and in these coordinates the radial geodesic equation becomes

$$\ddot{r} = -\frac{m}{r^2} \left(1 - \frac{2m}{r}\right) + \frac{6m^2}{r^3} \dot{r} + \frac{3m}{r^2} \left(1 + \frac{2m}{r}\right) \dot{r}^2 + \frac{2m}{r^2} \left(1 + \frac{m}{r}\right) \dot{r}^3. \quad (65)$$

It may be better to rewrite this as follows:

$$\ddot{r} = -\frac{m}{r^2} \left\{ \left(1 - \frac{2m}{r}\right) - \frac{6m}{r} \dot{r} - 3 \left(1 + \frac{2m}{r}\right) \dot{r}^2 - 2 \left(1 + \frac{m}{r}\right) \dot{r}^3 \right\}. \quad (66)$$

This factorizes

$$\ddot{r} = -\frac{m}{r^2} (1 + \dot{r})^2 \left\{ \left(1 - \frac{2m}{r}\right) - 2 \left(1 + \frac{m}{r}\right) \dot{r} \right\}. \quad (67)$$

As a function of \dot{r} , we see that \ddot{r} flips sign at the critical coordinate velocity

$$(\dot{r})_* = \frac{1 - 2m/r}{2(1 + m/r)}. \quad (68)$$

This is always positive, and less than 1/2, outside the horizon.

In view of the fact that in these coordinates $-g_{tt} g_{rr} + g_{tr}^2 = 1$, the general Killing-induced result for the coordinate velocity simplifies to

$$\dot{r} = \pm \sqrt{(1 + \epsilon^{-2} g_{tt})} \frac{1 \mp g_{tr} \sqrt{1 + \epsilon^{-2} g_{tt}}}{g_{rr} + \epsilon^{-2} g_{tr}^2}. \quad (69)$$

Thence

$$\dot{r} = \pm \sqrt{1 - \epsilon^{-2} (1 - 2m/r)} \frac{1 \mp (2m/r) \sqrt{1 - \epsilon^{-2} (1 - 2m/r)}}{(1 + 2m/r) + \epsilon^{-2} (2m/r)^2}. \quad (70)$$

At the horizon

$$(\dot{r})_H \in \left\{ 0, -\frac{2\epsilon^2}{2\epsilon^2 + 1} \right\}. \quad (71)$$

Therefore, the ingoing geodesic crosses the horizon with finite coordinate velocity

$$(\dot{r})_H = -\frac{2\epsilon^2}{2\epsilon^2 + 1} \in \left(-1, -\frac{2}{3}\right), \quad (72)$$

while the outgoing geodesic crosses the horizon with coordinate velocity zero. This makes it clear that, for a dropped particle, we should take the negative root in \dot{r} .

Combining these results, for a dropped (ingoing) particle (fixed energy ϵ), we have

$$\dot{r} = -\sqrt{1 - \epsilon^{-2}(1 - 2m/r)} \frac{1 + (2m/r)\sqrt{1 - \epsilon^{-2}(1 - 2m/r)}}{(1 + 2m/r) + \epsilon^{-2}(2m/r)^2}. \quad (73)$$

For unbound particles ($\epsilon \geq 1$), this is negative real everywhere, both outside and inside the horizon—in fact, all the way down to $r = 0$. For the coordinate acceleration,

$$\begin{aligned} \ddot{r} = & -\frac{m}{r^2} \left\{ \left(1 - \frac{2m}{r}\right) \right. \\ & -\frac{6m}{r} \left[\frac{-(2m/r)(\epsilon^2 - 1 + 2m/r) - \epsilon\sqrt{(\epsilon^2 - 1 + 2m/r)}}{\epsilon^2(1 + 2m/r) + (2m/r)^2} \right] \\ & -3 \left(1 + \frac{2m}{r}\right) \left[\frac{-(2m/r)(\epsilon^2 - 1 + 2m/r) - \epsilon\sqrt{(\epsilon^2 - 1 + 2m/r)}}{\epsilon^2(1 + 2m/r) + (2m/r)^2} \right]^2 \\ & \left. -2 \left(1 + \frac{m}{r}\right) \left[\frac{-(2m/r)(\epsilon^2 - 1 + 2m/r) - \epsilon\sqrt{(\epsilon^2 - 1 + 2m/r)}}{\epsilon^2(1 + 2m/r) + (2m/r)^2} \right]^3 \right\}. \end{aligned} \quad (74)$$

At the horizon, $r = 2m$, we have

$$(\ddot{r})_H = -\frac{3}{2} \frac{\epsilon^2}{(2\epsilon^2 + 1)^3 m}, \quad (75)$$

a finite inward coordinate acceleration.

For a timelike particle dropped at rest from spatial infinity ($\epsilon = 1$), this simplifies to

$$\dot{r} = -\left[\frac{(2m/r)^2 + \sqrt{2m/r}}{(1 + 2m/r) + (2m/r)^2} \right] = -\sqrt{\frac{2m}{r}} \left[\frac{1 + (2m/r)^{3/2}}{1 + 2m/r + (2m/r)^2} \right]. \quad (76)$$

(Note that asymptotically $\dot{r} \rightarrow -\sqrt{2m/r}$, as expected from the Newtonian limit.) Furthermore,

$$\begin{aligned} \ddot{r} = & -\frac{m}{r^2} \left\{ \left(1 - \frac{2m}{r}\right) + \frac{6m}{r} \left[\frac{(2m/r)^2 + \sqrt{(2m/r)}}{(1 + 2m/r) + (2m/r)^2} \right] \right. \\ & -3 \left(1 + \frac{2m}{r}\right) \left[\frac{(2m/r)^2 + \sqrt{(2m/r)}}{(1 + 2m/r) + (2m/r)^2} \right]^2 \\ & \left. +2 \left(1 + \frac{m}{r}\right) \left[\frac{(2m/r)^2 + \sqrt{(2m/r)}}{(1 + 2m/r) + (2m/r)^2} \right]^3 \right\}. \end{aligned} \quad (77)$$

Note that the coordinate acceleration \ddot{r} and the coordinate velocity \dot{r} are both always negative. We can also factorize this as

$$\ddot{r} = -\frac{m}{r^2} \left[1 - \sqrt{\frac{2m}{r}} \left\{ \frac{1 + (2m/r)^{3/2}}{1 + 2m/r + (2m/r)^2} \right\} \right]^2 \times \left\{ \left(1 - \frac{2m}{r} \right) + 2\sqrt{\frac{2m}{r}} \left(1 + \frac{m}{r} \right) \left[\frac{1 + (2m/r)^{3/2}}{1 + 2m/r + (2m/r)^2} \right] \right\}. \quad (78)$$

We can see that when approaching the horizon, at fixed $\epsilon = 1$, we have

$$(\dot{r})_H = -\frac{2}{3}; \quad (\ddot{r})_H = -\frac{1}{18m}. \quad (79)$$

The radial coordinate velocity and radial coordinate acceleration are plotted as shown in Figures 9 and 10, respectively.

Finally, note that for a light-like particle ($\epsilon \rightarrow \infty$) in Kerr–Schild coordinates, we have the very drastic simplification

$$\dot{r} = -1; \quad \ddot{r} = 0. \quad (80)$$

(Therefore, in Kerr–Schild coordinates, ingoing photons happen to have coordinate acceleration zero. This is one reason Kerr–Schild coordinates are popular. For this particular case, a figure would be entirely superfluous.)

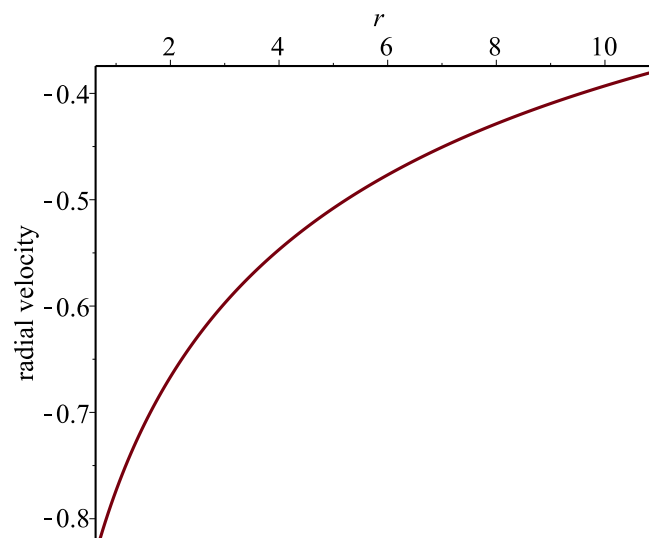


Figure 9. Behaviour of \dot{r} for the Schwarzschild geometry in Kerr–Schild coordinates for $m = 1$ and $\epsilon = 1$. Note that the coordinate velocity at the horizon is $-2/3$ and that the coordinate velocity remains negative between the horizon and spatial infinity.

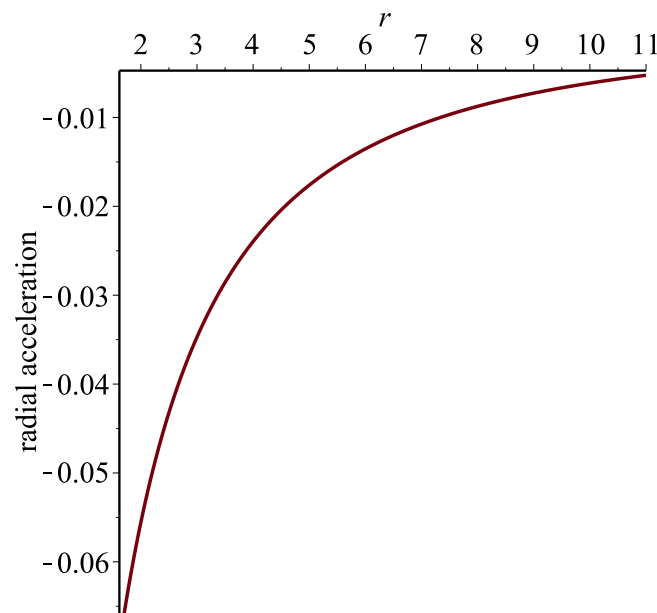


Figure 10. Behaviour of \ddot{r} for the Schwarzschild geometry in Kerr-Schild coordinates for $m = 1$ and $\epsilon = 1$. Note the coordinate acceleration remains negative between the horizon and spatial infinity.

6. Conclusions

Now that we have seen some examples of what happens to near-horizon geodesics in various coordinate systems, let us attempt to draw some general inferences. While the specific computations in this article have been carried out for the Schwarzschild geometry, this is known to be a good approximation for slowly rotating astrophysical black holes, and for numerical simulations of black holes, and even for semi-classical black holes in the Unruh quantum vacuum—so the overall conclusions are generic to a wide class of physically and observationally interesting black holes.

The most obvious conclusion we can draw is that the coordinate velocity, and coordinate acceleration, are (quite naturally) extremely coordinate-dependent, and that no general physical conclusions can be drawn from the magnitude of the coordinate velocity (\dot{r} can easily exceed unity) or the *sign* of the coordinate acceleration \ddot{r} . Claims that gravity in general relativity is “repulsive” at high speeds and/or near the horizon are at best disingenuous—they are merely misinterpretations of coordinate artefacts. For a fixed spacetime, by suitably choosing the coordinate system we can easily make $(\dot{r})_H = 0$ or $(\dot{r})_H = (\text{finite negative})$ at horizon crossing. For a fixed spacetime, by suitably choosing the coordinate system we can easily make the coordinate acceleration \ddot{r} *either positive or negative* just prior to horizon crossing. Indiscriminately mixing general relativistic and Newtonian concepts is dangerous and misleading.

The major distinction we have seen in the specific examples we explored was in the difference between horizon-penetrating and horizon-non-penetrating coordinates. There are good physical and mathematical reasons for this. In horizon-non-penetrating coordinates geodesics (essentially by definition) pile up at the horizon and do not cross it—in coordinates of this type $|\dot{r}|$ first increases as one falls inwards, but then has to go to zero at the horizon. This implies that $|\dot{r}|$ must have a maximum where $\partial_r \dot{r} = 0$ and hence $\ddot{r} = 0$. Thence, regions where the coordinate acceleration is positive $\ddot{r} > 0$ are *unavoidable* in horizon-non-penetrating coordinates. In contrast, horizon-penetrating coordinates are much better behaved when studying near horizon physics, with the coordinate velocity and coordinate acceleration being non-zero and finite at horizon crossing.

Author Contributions: All three authors contributed equally to this work.

Funding: This project was funded by the Ratchadapisek Sompoch Endowment Fund, Chulalongkorn University (Sci-Super 2014-032), by a grant for the professional development of new academic staff from the Ratchadapisek Sompoch Fund at Chulalongkorn University, by the Thailand Research Fund (TRF), and by the Office of the Higher Education Commission (OHEC), Faculty of Science, Chulalongkorn University (RSA5980038). PB was additionally supported by a scholarship from the Royal Government of Thailand. TN was also additionally supported by a scholarship from the Development and Promotion of Science and Technology talent project (DPST). MV was supported by the Marsden Fund, via a grant administered by the Royal Society of New Zealand.

Conflicts of Interest: The authors declare no conflicts of interest.

References

- McGruder, C.H. Acceleration of particles to high energy via gravitational repulsion in the Schwarzschild field. *Astropart. Phys.* **2017**, *86*, 18–20. [[CrossRef](#)]
- Guerreiro, T.; Monteiro, F. Light geodesics near an evaporating black hole. *Phys. Lett. A* **2015**, *379*, 2441–2444. [[CrossRef](#)]
- Felber, F. Test of relativistic gravity for propulsion at the Large Hadron Collider. *AIP Conf. Proc.* **2010**, *1208*, 247–260.
- Felber, F.S. Exact relativistic ‘antigravity’ propulsion. *AIP Conf. Proc.* **2006**, *813*, 1374–1381.
- Mashhoon, B. Beyond gravito-electro-magnetism: Critical speed in gravitational motion. *Int. J. Mod. Phys. D* **2005**, *14*, 2025–2037. [[CrossRef](#)]
- Krori, K.D.; Barua, M. Gravitational Repulsion by Kerr and Kerr–Newman Black Holes. *Phys. Rev. D* **1985**, *31*, 3135–3139. [[CrossRef](#)]
- Spallicci, A.D.A.M. Comment on “Acceleration of particles to high energy via gravitational repulsion in the Schwarzschild field” [Astropart. Phys. 86 (2017) 18–20]. *Astropart. Phys.* **2017**, *94*, 42–43. [[CrossRef](#)]
- Spallicci, A.D.A.M.; Ritter, P. A fully relativistic radial fall. *Int. J. Geom. Meth. Mod. Phys.* **2014**, *11*, 1450090. [[CrossRef](#)]
- Berkahn, D.L.; Chappell, J.M.; Abbott, D. Velocity dependence of point masses, moving on timelike geodesics, in weak gravitational fields. *arXiv* **2017**, arXiv:1708.09725.
- Berkahn, D.L.; Chappell, J.M.; Abbott, D. Hilbert’s forgotten equation of velocity dependent acceleration in a gravitational field. *arXiv* **2017**, arXiv:1708.0143.
- Célérier, M.-N.; Santos, N.O.; Satheeshkumar, V.H. Can gravity be repulsive? *arXiv* **2016**, arXiv:1606.08300.
- Felber, F. Comment on “Reversed gravitational acceleration...”, arXiv:1102.2870v2. *arXiv* **2011**, arXiv:1111.6564.
- Loinger, A.; Marsico, T. On Hilbert’s gravitational repulsion (A historical Note). *arXiv* **2009**, arXiv:0904.1578.
- Ohanian, H.C. Reversed Gravitational Acceleration for High-speed Particles. *arXiv* **2011**, arXiv:1102.2870.
- Iorio, L. 100 Years of Chronogeometrodynamics: The Status of the Einstein’s Theory of Gravitation in Its Centennial Year. *Universe* **2015**, *1*, 38–81. [[CrossRef](#)]
- Debono, I.; Smoot, G.F. General Relativity and Cosmology: Unsolved Questions and Future Directions. *Universe* **2016**, *2*, 23. [[CrossRef](#)]
- Schwarzschild, K. On the gravitational field of a mass point according to Einstein’s theory. *Sitzungsber. Preuss. Akad. Wiss. Phys. Math.* **1916**, *1916*, 189–196, arXiv:physics/9905030.
- Hilbert, D. Die Grundlagen der Physik. (Erste Mitteilung.). *Nachrichten von der Gesellschaft der Wissenschaften zu Göttingen, Mathematisch-Physikalische Klasse* **1915**, *1915*, 395–408.
- Hilbert, D. Die Grundlagen der Physik. (Zweite Mitteilung). *Nachrichten von der Gesellschaft der Wissenschaften zu Göttingen, Mathematisch-Physikalische Klasse* **1917**, *1917*, 53–76.
- Hilbert, D. Die Grundlagen der Physik. *Math. Ann.* **1924**, *92*, 1–32. [[CrossRef](#)]
- Misner, C.W.; Thorne, K.S.; Wheeler, J.A. *Gravitation*; W. H. Freeman and Company: San Francisco, CA, USA, 1973.
- Wald, R.M. *General Relativity*; University of Chicago Press: Chicago, IL, USA, 1984.
- Hobson, M.P.; Efstathiou, G.P.; Lasenby, A.N. *General Relativity: An Introduction for Physicists*; Cambridge University Press: Cambridge, UK, 2006.
- Stephani, H.; Kramer, D.; MacCallum, M.; Hoenselaers, C.; Herlt, E. *Exact Solutions of Einstein’s Field Equations*; Cambridge University Press: Cambridge, UK, 2002.
- Parry, A.R. A Survey of Spherically Symmetric Spacetimes. *Anal. Math. Phys.* **2014**, *4*, 333–375. [[CrossRef](#)]

26. Muller, T.; Grave, F. Catalogue of Spacetimes. *arXiv* **2009**, arXiv:0904.4184.
27. Visser, M. *Lorentzian Wormholes: From Einstein to Hawking*; Springer: Woodbury, NY, USA, 1995.
28. Martel, K.; Poisson, E. Regular coordinate systems for Schwarzschild and other spherical spacetimes. *Am. J. Phys.* **2001**, *69*, 476–480. [[CrossRef](#)]
29. Lake, K. A Class of quasi-stationary regular line elements for the Schwarzschild geometry. *arXiv* **1994**, arXiv:gr-qc/9407005.
30. Czerniawski, J. What is wrong with Schwarzschild's coordinates? *Concepts Phys.* **2006**, *3*, 307–318.
31. Fromholz, P.; Poisson, E.; Will, C.M. The Schwarzschild metric: It's the coordinates, stupid. *Am. J. Phys.* **2014**, *82*, 295–300. [[CrossRef](#)]
32. Painlevé, P. La mécanique classique et la theorie de la relativité. *C. R. Acad. Sci.* **1921**, *173*, 677–680.
33. Gullstrand, A. Allgemeine Lösung des statischen Einkörper-problems in der Einsteinschen Gravitationstheorie. *Ark. Mat. Astron. Fys.* **1922**, *16*, 1–15.
34. Visser, M. Acoustic propagation in fluids: An unexpected example of Lorentzian geometry. *arXiv* **1993**, arXiv:gr-qc/9311028.
35. Visser, M. Acoustic black holes: Horizons, ergospheres, and Hawking radiation. *Class. Quant. Gravity* **1998**, *15*, 1767–1791. [[CrossRef](#)]
36. Barceló, C.; Liberati, S.; Visser, M. Analogue gravity. *Living Rev. Relativ.* **2005**, *8*, 12. [[CrossRef](#)] [[PubMed](#)]
37. Hamilton, A.J.S.; Lisle, J.P. The River model of black holes. *Am. J. Phys.* **2008**, *76*, 519–532. [[CrossRef](#)]
38. Visser, M. Heuristic approach to the Schwarzschild geometry. *Int. J. Mod. Phys. D* **2005**, *14*, 2051–2067. [[CrossRef](#)]
39. Finch, T.K. Coordinate families for the Schwarzschild geometry based on radial timelike geodesics. *Gen. Relativ. Gravit.* **2015**, *47*, 56. [[CrossRef](#)]
40. Rosquist, K. A moving medium simulation of Schwarzschild black hole optics. *Gen. Relativ. Gravit.* **2004**, *36*, 1977–1982. [[CrossRef](#)]
41. Wiltshire, D.L.; Visser, M.; Scott, S.M. (Eds.) *The Kerr Spacetime: Rotating Black Holes in General Relativity*; Cambridge University Press: Cambridge, UK, 2005.
42. Visser, M. The Kerr spacetime: A brief introduction. *arXiv* **2007**, arXiv:0706.0622.
43. Rosquist, K. A unifying coordinate family for the Kerr–Newman metric. *Gen. Relativ. Gravit.* **2009**, *41*, 2619–2632. [[CrossRef](#)]
44. Rajan, D.; Visser, M. Cartesian Kerr–Schild variation on the Newman–Janis ansatz. *Int. J. Mod. Phys. D* **2017**, *26*, 1750167. [[CrossRef](#)]



© 2018 by the authors. Licensee MDPI, Basel, Switzerland. This article is an open access article distributed under the terms and conditions of the Creative Commons Attribution (CC BY) license (<http://creativecommons.org/licenses/by/4.0/>).